

Distilling heterogeneous treatment effects: Stable subgroup estimation in causal inference[†]

Melody Huang^{1,*}, Tiffany M. Tang^{2,*}, Ana M. Kenney³

February 12, 2025

ABSTRACT

Recent methodological developments have introduced new black-box approaches to better estimate heterogeneous treatment effects; however, these methods fall short of providing interpretable characterizations of the underlying individuals who may be most at risk or benefit most from receiving the treatment, thereby limiting their practical utility. In this work, we introduce a novel method, *causal distillation trees* (CDT), to estimate interpretable subgroups. CDT allows researchers to fit *any* machine learning model of their choice to estimate the individual-level treatment effect, and then leverages a simple, second-stage tree-based model to “distill” the estimated treatment effect into meaningful subgroups. As a result, CDT inherits the improvements in predictive performance from black-box machine learning models while preserving the interpretability of a simple decision tree. We derive theoretical guarantees for the consistency of the estimated subgroups using CDT, and introduce stability-driven diagnostics for researchers to evaluate the quality of the estimated subgroups. We illustrate our proposed method on a randomized controlled trial of antiretroviral treatment for HIV from the AIDS Clinical Trials Group Study 175 and show that CDT out-performs state-of-the-art approaches in constructing stable, clinically relevant subgroups.

[†]The authors would like to thank participants at the American Causal Inference Conference, Johns Hopkins Biostatistics Causal Inference Seminar, UNC Chapel Hill Biostatistics Seminar for their feedback and comments.

*Denotes equal contribution.

¹Yale University. Email: melody.huang@yale.edu, URL: www.melodyyhuang.com

²University of Notre Dame. Email: ttang4@nd.edu, URL: <https://tiffanymtang.github.io/>

³University of California Irvine. Email: anamaria.kenney@uci.edu

1 Introduction

While much of the causal inference literature has focused on estimating an average treatment effect for a specific intervention, researchers are often interested in understanding the underlying treatment effect heterogeneity for a given intervention. For example, in medical settings, researchers are often concerned about potential subsets of units who may be harmed by a particular drug or medical intervention. Similarly, in the social sciences, being able to understand who will benefit or could be potentially harmed by a specific intervention is crucial for evaluating the cost-benefit associated with a specific intervention. While different approaches have been proposed to consider how to better estimate treatment effect heterogeneity across individuals, being able to *characterize* subgroups of individuals in a study in an interpretable way remains challenging.

In its simplest form, many existing subgroup analyses in causal inference focus on subgroups *a priori* specified by researchers, which relies on substantive knowledge. In the absence of such prior knowledge, many tree-based approaches have been proposed to discover new subgroups with heterogeneous treatment effects (e.g., [Su et al., 2009](#); [Lipkovich et al., 2011](#); [Loh et al., 2015](#); [Seibold et al., 2016](#)), of which causal trees ([Athey and Imbens, 2016](#)) are arguably the most popular.¹ Similar to decision trees ([Breiman et al., 1984](#)), causal trees partition the underlying into groups by finding clusters of individuals who have similar treatment effects together. Moreover, unlike linear regression approaches, causal trees output a readily-interpretable partition of subgroups while also accounting for potential high-order interactions.

A drawback to causal trees, however, is that they can be highly unstable and overfit in the presence of even small amounts of noise (e.g., [Cattaneo et al., 2022](#)). Recent literature has proposed alternatives to better model heterogeneous treatment effects with ‘metalearners’—e.g., *T*-learners (e.g., [Foster et al., 2011](#)), *S*-learners (e.g., [Hill, 2011](#)), *X*-learner ([Künzel et al., 2019](#)), *R*-learner ([Nie and Wager, 2021](#)), *B*-learner ([Oprescu et al., 2023](#)), *DR*-learner ([Kennedy, 2023](#)), *lp-R*-learner ([Kennedy et al., 2022](#)). These black-box metalearners provide theoretical guarantees in the form of quasi-oracle properties in recovering the *individual*-level treatment effect; however, they no longer produce a tree-like output and thus cannot be directly used to identify interpretable subgroups.

¹Citation count was used as a proxy for popularity. In comparing the citation count of the different papers, as of 2025, the original causal tree paper by [Athey and Imbens \(2016\)](#) has over 2,000 citations, while the alternative methods have anywhere from 100-500 citations.

In the following paper, we propose *causal distillation trees* (CDT) to stably estimate interpretable subgroups. CDT allows researchers to leverage the power of black-box meta learners, while preserving the interpretability of a simple tree output. At a high level, CDT is a two-stage learner. The first stage estimates a heterogeneous treatment effect model using a flexible meta-learner to generate a predicted individual-level treatment effect for each unit. The second stage then *distills* the information from the predicted individual-level treatment effect through a decision tree to estimate interpretable subgroups. The first step serves as a de-noising step to help mitigate the instabilities that decision trees traditionally suffer from. The second step of ‘distillation’ draws upon existing ideas in machine learning (Hinton, 2015; Furlanello et al., 2018; Menon et al., 2021), which uses the distillation step to improve prediction accuracy in certain settings. However, unlike typical machine learning settings, where the primary goal is to improve the second stage learner’s predictive ability, we leverage distillation to improve our ability to estimate interpretable subgroups using the second stage decision tree learner.

Our paper provides several key theoretical and methodological contributions. First, while recent papers have similarly proposed the use of a two-stage learner to estimate subgroups (e.g., Foster et al., 2011; Bargagli Stoffi and Gnecco, 2020; Zhang et al., 2021; Rehill, 2024), CDT is agnostic to what first-stage learner researchers use, allowing for a large degree of flexibility in choosing an informative teacher model. Second, unlike previous work, which has largely relied on simulated evidence, we derive theoretical guarantees, proving the consistency of CDT in recovering the optimal partitioning into subgroups. To our knowledge, we are the first paper to prove the theoretical properties in recovering subgroups from using distillation. Our theoretical results highlight that distillation can actually offset the instabilities incurred from using causal trees (or other tree-based approaches) in low signal-to-noise regimes, while preserving the interpretability of these methods.

Finally, we propose a novel model selection procedure to help researchers select a teacher model in CDT. Unlike existing model selection procedures, which compare the goodness-of-fit of different models, our selection procedure is explicitly tailored for estimating subgroups. We introduce a new measure, which we call the *Jaccard Subgroup Similarity Index* (SSI), that quantifies the similarity of subgroups. Researchers can use the subgroup similarity index to select the teacher model that recovers the most stable subgroups.

The paper is structured as follows. Section 2 presents notation and formalizes the notion of

a subgroup in causal inference. In Section 3, we introduce causal distillation trees and derive the theoretical properties of CDT. In Section 4, we propose a model selection procedure for researchers to select a teacher model that will maximize stability of subgroup recovery.

We demonstrate the effectiveness of CDT across extensive simulation settings (Section 5), and an AIDS clinical trial case study (Section 6). Section 7 concludes.

2 Setup and Notation

Throughout the paper, we will use the potential outcomes framework, where $Y_i(1), Y_i(0) \in \mathbb{R}$ denote the potential outcome under treatment and control, respectively. Let $Z_i \in \{0, 1\}$ denote the treatment assignment indicator. We assume consistency of treatment assignment across the study and no interference (i.e., the stable unit treatment value assumption). Let $Y_i := Y_i(1)Z_i + Y_i(0)(1 - Z_i)$ be the observed outcomes. Finally, we assume that researchers have access to a set of pre-treatment covariates $X_i \in \mathbb{R}^p$ for each unit in their study, and $\{Y_i(1), Y_i(0), X_i, Z_i\}$ are drawn independently and identically distributed from an arbitrary joint distribution for $i = 1, \dots, n$.

A common estimand of interest is the *average treatment effect* for a given study sample:

$$\tau_{\text{ATE}} = \frac{1}{n} \sum_{i=1}^n \{Y_i(1) - Y_i(0)\}.$$

In practice, a more policy-relevant quantity is the conditional average treatment effect, which considers the average treatment effect across subsets of individuals in the study population. Existing literature has recommended researchers leverage their substantive expertise to posit what characteristics could potentially moderate the treatment effect.

Informally, we consider a *subgroup* as a subset of individuals, defined by a discrete partition in the space of X , where the partitions in the space correspond to substantively different treatment effects. In particular, we are interested in characterizing different groups of individuals in a study that have different effects from receiving the same treatment.

We formally define a *subgroup* $\mathcal{G}_g : \mathcal{X} \rightarrow \{0, 1\}$ as

$$\mathcal{G}_g(X) = \prod_{j=1}^p \mathbb{1} \{X^{(j)} \in R_g^{(j)}\}, \quad (1)$$

where $X^{(j)}$ denotes the j^{th} covariate, and $R_g^{(j)} \subseteq \text{supp}(X^{(j)})$. Here, $\mathcal{G}_g(X)$ represents a collection of binary decision *rules* that characterize a subset of individuals in the study (Lipkovich et al., 2017). For example, if $\mathcal{G}_g(X) = \mathbb{1}\{X^{\text{gender}} = \text{Female}\} \cdot \mathbb{1}\{X^{\text{age}} < 35\}$, then $\mathcal{G}_g(X)$ corresponds to the subset of female-identifying individuals who are under the age of 35. A collection of subgroups $\{\mathcal{G}_1(X_i), \dots, \mathcal{G}_G(X_i)\}$ is said to be a discrete *partition* of the covariate space of X if $\sum_{g=1}^G \mathcal{G}_g(X_i) = 1$ for all units $i = 1, \dots, n$. (i.e., each unit belongs to exactly one subgroup and cannot belong to multiple subgroups).

Finally, given a subgroup $\mathcal{G}_g(X)$, we define $\tau^{(g)}$ as the *subgroup average treatment effect*:

$$\tau^{(g)} := \frac{1}{n_g} \sum_{i=1}^n \mathcal{G}_g(X_i) \cdot \{Y_i(1) - Y_i(0)\}, \quad (2)$$

where n_g is the number of samples in subgroup g .

The primary focus of the paper will be on estimating an *optimal partition*, which maximizes treatment effect heterogeneity across subgroups using the most parsimonious set of rules. Specifically, we aim to construct the most parsimonious partition that minimizes the squared loss between the true individual-level treatment effects and the associated subgroup average treatment effects:

$$\{\mathcal{G}_g(X)\}_{g=1}^G = \arg \min_{\{\mathcal{G}'_g(X)\}_{g \in \Omega}} \mathbb{E} \left[\left\{ \tau_i - \sum_g \mathcal{G}'_g(X_i) \cdot \tau^{(g)} \right\}^2 \right], \quad (3)$$

where Ω denotes the space of all possible partitions of the covariate space of X . Under squared loss, the optimal partition corresponds to a subset in the covariate space of X that maximizes the difference in treatment effect heterogeneity across subgroups. In other words, *within* a partitioned group, the treatment effect heterogeneity is minimized, thereby *maximizing* the variance in treatment effects *across* groups. In practice, researchers can choose alternative loss functions that correspond to what are substantively meaningful partitions in the covariate space. However, the theoretical guarantees we derive utilize the squared loss, and generalizing the results for other loss functions is an open avenue of future research.

Our work is distinct from existing literature in considering subgroup average treatment effects. For example, alternative quantities considered in the literature include the sorted group average treatment effect (GATES), which considers the average treatment effect, across subsets formed

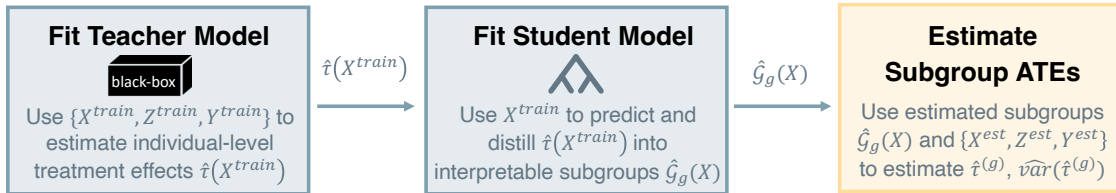


Figure 1: Overview of Causal Distillation Trees (CDT). CDT leverages a two-stage procedure, which first fits a teacher model (e.g., a black-box metalearner) to estimate individual-level treatment effects and secondly fits a student model (e.g., a decision tree) to predict the estimated individual-level treatment effects, in effect distilling the estimated individual-level treatment effects and producing interpretable subgroups. This two-stage learner is learned using the training data (blue-gray boxes). Finally, using the estimated subgroups, the subgroup average treatment effects are honestly estimated with a held-out estimation set (yellow box).

based on the magnitude of the estimated effect (i.e., the ATE, across individuals who would most benefit) (e.g., Imai and Li, 2024; Chernozhukov et al., 2018; Dwivedi et al., 2020). GATES relies on using a machine learning model to generate predictions of the CATE. Then, grouping the predicted CATEs by highest to lowest, it estimates the ATE across each group. While quantities like GATE provide a way for researchers to evaluate the range of possible treatment effects within a study, it falls short of providing interpretability for the *characteristics* of the units within each group.

3 Causal distillation trees

3.1 Overview

We propose a method, *causal distillation trees* (CDT), which stably estimates interpretable subgroups. CDT is a two-stage learner (Figure 1). The first stage learner, referred to as the *teacher* model, learns an informative model for the individual-level treatment effect using the observed data $\{Y, Z, X\}$. Using this teacher model, we generate a prediction for the individual-level treatment effect for all units (i.e., $\hat{\tau}(X_i)$). In the second stage, we *distill* the predicted $\hat{\tau}(X_i)$'s into interpretable subgroups by fitting a decision tree, called the *student* model, to predict the $\hat{\tau}(X_i)$'s from the covariates X . The estimated decision rules from the decision tree define a discrete partition, which naturally maps to the collection of subgroups $\{\hat{\mathcal{G}}_1(X), \dots, \hat{\mathcal{G}}_G(X)\}$ (see Figure 2 for illustration). Finally, using these estimated partitions, we estimate the subgroup average treatment effect for each subgroup.

Informally, we can think of the first stage learner as smoothing the individual-level treatment effects by projecting τ_i into the basis space of the covariates X . By using the projected version

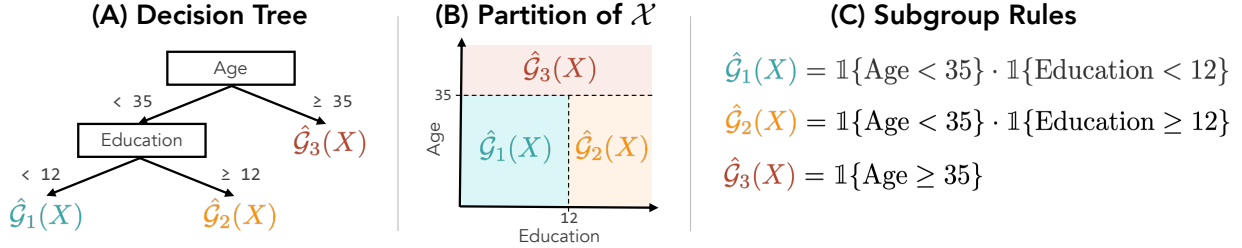


Figure 2: Given a decision tree (A), its decision splits correspond to binary cuts that partition the covariate space \mathcal{X} , shown in (B). Furthermore, the decision splits leading to each terminal node map to the collection of rules that define a subgroup, shown in (C).

of the individual-level treatment effect instead of τ_i , the second stage learner will be able to more stably estimate the subgroups, as the teacher model will have de-noised the outcomes.

Throughout the paper, we use a decision tree—specifically, a classification and regression tree (CART) (Breiman et al., 1984)—as the second-stage learner. While researchers can in theory swap out the second-stage learner for alternative rule-based approaches (e.g., Bargagli-Stoffi et al., 2020; Wang and Rudin, 2022; Wan et al., 2023), we focus on decision trees because the output of the decision tree maps intuitively to a standard interpretation of a subgroup as a discrete partition of the covariate space.

To avoid post-selection bias, we recommend researchers use sample splitting. Specifically, researchers should randomly split the data into a training and a hold-out estimation set. The training set will be used to estimate the subgroups $\{\hat{\mathcal{G}}_1(X), \dots, \hat{\mathcal{G}}_G(X)\}$ while the hold-out estimation set is reserved to estimate the subgroup average treatment effects $\hat{\tau}^{(1)}, \dots, \hat{\tau}^{(G)}$. This provides an honest estimate of the subgroup average treatment effect (Athey and Imbens, 2016).

In addition, to avoid overfitting to the teacher model, researchers should estimate the $\hat{\tau}(X_i)$'s using out-of-sample procedures in the first stage. In particular, if the teacher model comes with a built-in out-of-sample estimation procedure (e.g., causal forests can estimate $\hat{\tau}(X_i)$ via out-of-bag samples), we estimate $\hat{\tau}(X_i)$ using these model-specific out-of-sample estimates. Otherwise, we perform repeated cross-fitting (Chernozhukov et al., 2018) to learn the $\hat{\tau}(X_i)$'s. We detail this sample splitting procedure and CDT in Algorithm 2.

3.2 Consistency of subgroup estimation: Single rule setting

We now investigate the theoretical properties of CDT. We will show that under a set of regularity assumptions, CDT consistently recovers the optimal subgroups, and can improve the rate of convergence in estimating subgroups over standard decision trees. We show that the rate of convergence will depend on (1) the smoothness in the outcomes, and (2) how much noise there is in the underlying process. We focus our discussion on settings in which researchers are using standard greedy tree algorithms, such as CART, to estimate the second-stage decision tree. We note that in settings when researchers employ alternative algorithms to construct decision trees, some of the assumptions for consistency can be potentially relaxed.

Throughout, we denote $\mathbb{E}_n(A_i)$ as the expectation of a variable A_i over the observed sample (i.e., $\mathbb{E}_n(A_i) := \frac{1}{n} \sum_{i=1}^n A_i$), while $\mathbb{E}(A_i)$ refers to the population-level expectation. Furthermore, for each unit i and candidate split k , we define $\tau(X_i, k)$ as the prediction generated from a decision tree, constructed with the true individual-level treatment effects τ_i and a single split at threshold k (i.e., $\tau(X_i, k) := \mathbb{1}\{X_i \leq k\}\mathbb{E}(\tau_i | X_i \leq k) + \mathbb{1}\{X_i > k\}\mathbb{E}(\tau_i | X_i > k)$). Similarly, we define $\tau^d(X_i, k)$ as the prediction generated from a decision tree, constructed with the distilled individual-level treatment effects $\hat{\tau}_i^d$ and a single split at threshold k (i.e., $\tau^d(X_i, k) := \mathbb{1}\{X_i \leq k\}\mathbb{E}(\hat{\tau}_i^d | X_i \leq k) + \mathbb{1}\{X_i > k\}\mathbb{E}(\hat{\tau}_i^d | X_i > k)$).

In this section, we will consider the simplest univariate setting, in which we observe a single covariate and the underlying subgroups are defined by a single rule. Section 3.3 will then generalize the results to show consistency of the estimated subgroups, comprised of multiple rules in the multivariate setting. More formally, let $X \in \mathcal{X} \subseteq \mathbb{R}$, with the underlying subgroups defined as $\mathcal{G}_1(X) = \mathbb{1}\{X \leq s\}$ and $\mathcal{G}_2(X) = \mathbb{1}\{X > s\}$ for some optimal split threshold $s \in \mathbb{R}$. We define an *optimal split* under the squared loss as follows.

Definition 3.1 (Optimal Split) *An optimal split $s \in \mathcal{X}$ satisfies*

$$s := \arg \min_{s' \in \mathcal{X}} \mathbb{E} [\ell(\tau_i; X_i, s')], \tag{4}$$

where ℓ is defined as the squared loss function: $\ell(\tau_i; X_i, s') := (\tau_i - \tau(X_i, s'))^2$.

To ensure that there exists an optimal split, we must assume the following.

Assumption 1 Define F_X to be the cumulative distribution function of the covariate X . Define the points s_l and s_u such that $0 < F_X(s_l) < F_X(s_u) < 1$. Let s be an optimal split as defined in Definition 3.1.

- (a) Assume F_X is absolutely continuous with a density dF_X that is bounded away from zero and is continuous in a neighborhood of s .
- (b) Assume that s is unique.

Assumption (1) guarantees that there exists subgroups of interest to estimate. Intuitively, Assumption (1)-(a) ensures that the squared loss function will attain a minimum value for $s \in [s_l, s_u]$. Assumption (1)-(b) rules out the possibility that there could be more than one potential split point. Furthermore, we are implicitly ruling out the setting considered in Cattaneo et al. (2022), in which the true optimal split does not exist.

Given that the subgroups exist, we will now show that the estimated subgroups $\hat{\mathcal{G}}(X)$ from CDT converge to the true subgroups $\mathcal{G}(X)$. Greedy search guarantees that within a given sample of size n , the estimated split point, denoted \hat{s}_n , minimizes the within-sample loss (i.e., $\hat{s}_n := \min_{s' \in \text{supp}_n(X)} \mathbb{E}_n[\ell(\tau_i; X, s')]$). As such, in a hypothetical setting that researchers had access to τ_i , the estimated subgroups $\hat{\mathcal{G}}(X)$ from a decision tree would give the optimal partitioning of the covariate space of X , *within a given sample*. Thus, to establish the consistency of CDT, we must consider two gaps. First, CDT uses the distilled treatment effects $\hat{\tau}_i^d$ in lieu of the individual-level treatment effect τ_i . As such, we must constrain the differences that can arise from distilling the raw treatment effects with the teacher model. Second, we must show that the within-sample optimal partitioning will asymptotically recover the population-level optimal partitioning.

To address the first gap, we restrict our focus to *valid* teacher models, whose distilled treatment effects result in the same population-level optimal subgroups as the original treatment effects.

Assumption 2 (Valid Teacher Model) Let s denote the population-level optimal split according to (4), and define s^d as

$$s^d := \arg \min_{s' \in \mathcal{X}} \mathbb{E} \left[\ell(\hat{\tau}_i^d; X_i, s') \right]. \quad (5)$$

Assume that the teacher model \mathcal{M} used to distill the treatment effects into $\hat{\tau}_i^d$ satisfies $s^d = s$. In this case, we say that the teacher model is valid.

Under validity of teacher model, the optimal partitioning of the covariate space of X cannot change after distilling the individual-level treatment effects. In other words, the *optimal* population splits from the distilled individual-level treatment effects $\hat{\tau}_i^d$ will be equivalent to the optimal split with the true individual-level treatment effects τ_i . A sufficient, though not necessary, condition for a valid teacher model is a correctly-specified teacher model, such that the residual noise that cannot be explained by the model must be uncorrelated with the covariates X (i.e., exogeneity). In the context of a randomized control trial, we expect this to be true if the teacher model is flexible enough and the sample size is sufficiently large (details in Appendix A).

We further assume that the amount that $\tau^d(X; s')$ changes as the split point s' changes within a neighborhood of s is bounded.

Assumption 3 Let $\tau_0 = \frac{1}{2} \{ \mathbb{E}(\hat{\tau}_i^d | X_i < s) + \mathbb{E}(\hat{\tau}_i^d | X_i \geq s) \}$. Define $M(s) = \mathbb{E} [(\hat{\tau}_i^d - \tau_0) \mathbb{1}\{X_i \leq s\}]$. Let \mathcal{N} be a neighborhood around s , where $\mathcal{N} := (l, u) \subset [s_l, s_u]$. Then, assume the following:

- $\tau(x)$ is continuous in (l, s) and (s, u) , where:

$$\lim_{x \rightarrow s^-} \tau(x) = \tau(s^-) \text{ and } \lim_{x \rightarrow s^+} \tau(x) = \tau(s^+)$$

- For $\epsilon > 0$, there exists an $1 < \alpha < 2$ where:

$$\inf_{|s' - s| < \epsilon, s' \neq s} \frac{|M(s) - M(s')|}{|s - s'|^\alpha} > 0$$

- There exists an $0 < \eta \leq 1$ such that for all $\epsilon > 0$:

$$\mathbb{E} [(\hat{\tau}_i^d - \tau_0)^2 \mathbb{1}\{s - \epsilon \leq X_i \leq s + \epsilon\}] \leq C\epsilon^{2\eta}.$$

Assumption (3) is a standard assumption in establishing consistency of M -estimators (e.g., Van der Vaart, 2000, Theorem 5.52). Informally, we can think of α and η as parameters that control the smoothness of the underlying function around the optimal split point s . The assumption rules

out settings in which $\hat{\tau}_i^d$ can take on values of infinity close to the optimal split point s . In practice, we expect Assumption (3) to generally hold across a large class of data generating processes. For example, in settings when $\tau^d(X; s')$ is continuously differentiable in the neighborhood \mathcal{N} and bounded in s , then $\alpha = 2$ and $\eta = 1/2$. Assumption (3) also allows for discontinuities at the split point s , so long as $\tau^d(X_i; s)$ is continuous within the neighborhood around the split point.

Finally, we must assume bounded moments on the distilled treatment effects.

Assumption 4 (Bounded Moments) *Assume there exists constants $M_2 < \infty$ and $M_4 < \infty$ such that $\mathbb{E} \{(\hat{\tau}_i^d)^2\} \leq M_2$ and $\mathbb{E} \{(\hat{\tau}_i^d)^4\} \leq M_4$.*

With Assumptions (1)-(4), we can establish convergence.

Proposition 3.1 (Convergence in Subgroup Recovery, for Single Covariate Setting) *Let $\hat{\mathcal{G}}_1(X_i) := \mathbb{1}\{X_i \leq \hat{s}_n\}$ denote the subgroup estimated by CDT. Then, under Assumptions (1)-(4), CDT will consistently recover the subgroups:*

$$\mathbb{E} \left[\left| \hat{\mathcal{G}}_1(X_i) - \mathcal{G}_1(X_i) \right| \right] \lesssim |\hat{s}_n - s| = O_p(n^{-1/2(\alpha-\eta)})$$

Proposition 3.1 formalizes that the rate of convergence depends directly on how smooth the underlying data generating process is. The rate of convergence in the estimated subgroups inherits a characteristic highlighted in Escanciano (2020), which bridged the gap in convergence rate of the estimated split in a decision tree \hat{s}_n between a fully continuous setting (considered in Banerjee and McKeague, 2007; Buhlmann and Yu, 2002), and discontinuous settings, as considered in Chan (1993) and Kosorok (2008).

Consider the setting in which $\tau^d(X; s')$ is continuously differentiable. This would imply a rate of convergence of $O_p(n^{-2/3})$. On the other hand, in the setting when $\tau(X)$ is discontinuous at $X = s$, then $\hat{s} - s = O_p(n^{-1})$. Intuitively, as the underlying data generating process becomes more discontinuous at the split point s , the faster the estimated split \hat{s}_n will converge to the true split s . While these results have been studied in the decision tree and change point estimation literature (see, for example, Banerjee and McKeague, 2007; Buhlmann and Yu, 2002; Escanciano, 2020), we are, to the best of our knowledge, the first to formally connect the notion of split consistency to subgroup recovery.

Proposition 3.1 provides practical guidance in considering what suitable teacher models should be used to best improve the rate of convergence using distillation. In standard decision tree settings, α and η are something inherent to the underlying data generating process. In contrast, under distillation, we are considering the underlying smoothness of not the original outcomes τ_i , but the distilled $\hat{\tau}_i^d$, which are constructed from a teacher model. This implies that in settings when the underlying $\tau(X)$ is smooth around the optimal split point, but the teacher model correctly constructs piecewise functions around the partitioning points, then this can improve the rate of convergence from $O_p(n^{-2/3})$ to the much faster rate of $O_p(n^{-1})$.

In addition to consistently recovering the subgroups, CDT can further improve the stability of the split estimation by de-noising the individual-level treatment effect and increasing the signal strength in the individual-level treatment effect. To illustrate, in the following example we consider a setting in which researchers have access to the true individual-level treatment effect τ_i and estimate a decision tree using the covariates X_i . In practice, this is infeasible, as researchers can never observe τ_i , but this comparison serves as a helpful benchmark to compare the potential improvements from distillation.

Example 3.1 (Improving stability of splits with distillation) *Consider a setting where $\tau(X)$ is continuously differentiable and bounded in a neighborhood around s . Furthermore, assume we can write the individual-level treatment effect and the distilled treatment effects as a function of $\tau(X_i)$ and a noise term:*

$$\tau_i = \tau(X_i) + v_i, \text{ and } \hat{\tau}_i^d = \tau(X_i) + v_i^d.$$

Assume that $\mathbb{E}(v_i) = \mathbb{E}(v_i^d) = 0$, both $\text{var}(v_i)$ and $\text{var}(v_i^d)$ are finite, and $\text{var}(\tau(X_i)) > 0$. Then, under squared loss and mild regularity assumptions (i.e., Assumption (B.3)), the relative asymptotic variance of the estimated splits without distillation \hat{s}_n and with distillation \hat{s}_n^d is a function of the relative signal-to-noise ratio between the individual-level treatment effect and the distilled individual-level treatment effects:

$$\frac{\text{asyvar}(\hat{s}_n)}{\text{asyvar}(\hat{s}_n^d)} = \left(\frac{\text{SNR}_{\text{distil}}}{\text{SNR}_{\text{original}}} \right)^{2+4/3},$$

where $\text{SNR}_{\text{distil}} = \text{var}(\tau(X))/\text{var}(v^d)$ and $\text{SNR}_{\text{original}} = \text{var}(\tau(X))/\text{var}(v)$.

The results from Example 3.1 follow from noting that the asymptotic distribution of the estimated

splits in a linear setting follow Chernoff’s distribution (Buhlmann and Yu, 2002; Groeneboom, 1989). While the variance itself is not straightforward to interpret and depends on an Airy function, the *ratio* of variances simplifies into a function of the signal-to-noise ratios. See Appendix B for the full derivation.

Example 3.1 formalizes the intuition that as the first-stage learner more closely approximates $\tau(X)$ (i.e., the conditional expectation function of τ , given X), the stability of the estimated splits under distillation also improves. In particular, we can view the first-stage learner as a denoising, or smoothing, step that filters the original individual-level treatment effect τ_i to a less noisy representation, in the space of X .

3.3 Consistency of subgroup estimation: General setting with multiple rules

We next extend the consistency results from the previous subsection to the general multivariate setting, in which we observe p total covariates (i.e., $X \in \mathbb{R}^p$) and the optimal subgroups, satisfying (3), consist of an arbitrary number of rules with different covariates and different split points. Throughout, we will denote the total number of binary decision rules for a subgroup as r_g . In this setting, we can rewrite the optimal subgroups in terms of their binary decision rules. For example, without loss of generality, the first subgroup $\mathcal{G}_1(X)$ would be written as $\mathcal{G}_1(X) = \prod_{k=1}^{r_1} \mathbb{1} \{X^{(j_k)} \leq s^{(j_k)}\}$, where $s^{(j_k)} \in \text{supp}(X^{(j_k)})$, and $j_1, \dots, j_{r_1} \in \{1, \dots, p\}$. Under this setting, estimating consistent subgroups requires not only consistently recovering the correct split points, but also selecting the right covariates to split on.

To show this consistency, we must introduce an additional separability condition, which states that conditional on the previously selected binary decision rules, the differences in loss from constructing a relevant and irrelevant rule must be greater than zero (i.e., separable).

Assumption 5 (Separability Condition) *For each subgroup index $g \in \{1, \dots, G\}$ and rule index $r \in \{1, \dots, r_g\}$, without loss of generality, write the subgroup defined by the $r - 1$ previously selected binary decision rules as $\mathcal{G}_g^{(r-1)}(X) = \prod_{k=1}^{r-1} \mathbb{1} \{X^{(j_k)} \leq s^{(j_k)}\}$. We assume that there is separability, conditional on the previously selected binary decision rules:*

$$\min_{a \in A_r, b \in B_r} \left\{ \mathbb{E} \left[\ell(\tau_i; X^{(a)}, s^{(a)}) \mid \mathcal{G}_g^{(r-1)}(X) = 1 \right] - \mathbb{E} \left[\ell(\tau_i; X^{(b)}, s^{(b)}) \mid \mathcal{G}_g^{(r-1)}(X) = 1 \right] \right\} = \delta > 0,$$

where $B_r = \{j_r, \dots, j_{r_g}\}$ denotes the set of remaining relevant subgroup feature indices, $A_r = \{1, \dots, p\} \setminus B_r$ denotes the set of irrelevant subgroup feature indices, $s^{(a)}$ and $s^{(b)}$ correspond to the optimal split points, conditional on $\mathcal{G}_g^{(r-1)}(X) = 1$, for $X^{(a)}$ and $X^{(b)}$ respectively, and $\mathcal{G}_g^{(0)}(X) \equiv 1$.

Informally, Assumption (5) states that given the previously constructed rules, whether a rule is relevant or not must be distinguishable through the loss function. Moreover, δ represents the minimum difference at the population-level of the loss associated with splitting on a relevant and irrelevant covariate, conditional on the previous splits. This is intuitively similar to the irrepre-sentable condition for the LASSO (Zhao and Yu, 2006; Meinshausen and Bühlmann, 2006; Zou, 2006) or its variants (Javanmard and Montanari, 2013), which states that irrelevant features cannot be too correlated with relevant ones to achieve model selection consistency. If the losses between relevant and irrelevant rules are tied, then this means the tree will be unable to distinguish between what are relevant and irrelevant rules.

Assumption (5) ensures that the subgroups follow a problem with optimal substructure, such that a greedy search approach to constructing the second-stage decision tree learner is valid. In settings where Assumption (5) is not met, standard greedy tree algorithms such as CART can fail to recover the optimal partitioning even with infinite amounts of data (see Tan et al., 2024 for a formal discussion). Recent work has introduced alternative algorithms to construct optimal trees under weaker assumptions, but at a much higher computational cost (e.g., Hu et al., 2019; Lin et al., 2020), and are often restricted to specific settings such as binary features. Moreover, several studies have demonstrated the out-of-sample performance gains of optimal trees is only 1-2%, and the expected depth of greedy trees remains close to that of optimal trees (e.g., van der Linden et al., 2024). Given the popularity of greedy search approaches and the computational burden of many optimal tree construction approaches, we focus our discussion on settings in which greedy search algorithms can feasibly construct optimal subgroups.

With separability, we can now extend the results from Proposition 3.1.

Theorem 3.1 (Consistency of subgroup estimation with decision trees) *Let Assumptions (1)-(3) hold for all relevant covariates, conditional on the previously select decision rules. Additionally, assume bounded moments (Assumption (4)) and separability (Assumption (5)). Then, the difference between the estimated subgroup $\hat{\mathcal{G}}_g(X_i)$ using CDT and the true subgroup $\mathcal{G}_g(X_i)$ is upper*

bounded by the following:

$$\mathbb{E} \left(\left| \hat{\mathcal{G}}_g(X_i) - \mathcal{G}_g(X_i) \right| \right) \leq \frac{2r_g(C_\tau + M\delta)}{\delta} \left| \hat{s}_n^{(k)} - s^{(k)} \right| + \frac{2r_g}{\delta} \left\{ \mathbb{E}_n \left[\ell(\hat{\tau}_i^d; X^{(k)}, s^{(k)}) \right] - \mathbb{E} \left[\ell(\hat{\tau}_i^d; X^{(k)}, s^{(k)}) \right] \right\},$$

for all groups $g \in \{1, \dots, G\}$, where r_g corresponds to the number of rules in the g^{th} subgroup, $k = \arg \max_{k'} \left\{ \left| \hat{s}_n^{(k')} - s^{(k')} \right| + \mathbb{E}_n \left[\ell(\hat{\tau}_i^d; X^{(k')}, s^{(k')}) \right] - \mathbb{E} \left[\ell(\hat{\tau}_i^d; X^{(k')}, s^{(k')}) \right] \right\}$, M is a finite positive constant, and δ corresponds to the constant in the separability condition. Applying Proposition 3.1:

$$\hat{\mathcal{G}}_g(X_i) \xrightarrow{P} \mathcal{G}_g(X_i).$$

The results of Theorem 3.1 follow from first noting that the estimated splits will converge in probability to the optimal split (i.e., Lemma 3.1), and then showing that the within-sample loss will converge in probability to the true population-level loss. (See Appendix B for proof.) In particular, the rate of convergence of $\hat{\mathcal{G}}_g(X_i)$ to $\mathcal{G}_g(X_i)$ is dependent on (1) the degree of separability in the losses between relevant and irrelevant rules (i.e., δ), and (2) the underlying convergence rate of the sample splits to the true optimal splits (i.e., the rate at which $\left| \hat{s}_n^{(k)} - s^{(k)} \right| \rightarrow 0$). An immediate implication of Theorem 3.1 is that not only will the tree consistently split at the correct cutoff points, but it will also correctly select the important features that should be used in the splitting criteria.

To help illustrate the benefits of CDT, we provide a numerical example that compares the performance of CDT with a standard causal tree.

Example 3.2 (Numerical comparison of CDT with causal trees) Consider a simple data generating process, in which $X_i \stackrel{iid}{\sim} MVN(0, I)$ and $\tau_i = 2 \cdot \mathbf{1} \{X_i^{(1)} > 0\} - \mathbf{1} \{X_i^{(2)} < -0.5\} + \epsilon_i$, where $\epsilon_i \sim N(0, \sigma_\tau^2)$ (details in Section 5). For both CDT and causal trees, we calculate the total number of subgroups estimated, the number of true positive features (i.e., correctly estimated subgroup features), and number of false positive features (i.e., incorrectly estimated subgroup features). The number of estimated subgroups using causal tree increases linearly as a function of the sample size, while CDT correctly recovers the true underlying subgroups. Figure 3 visualizes the results.

To summarize, we have shown that under a set of regularity assumptions and a well-specified

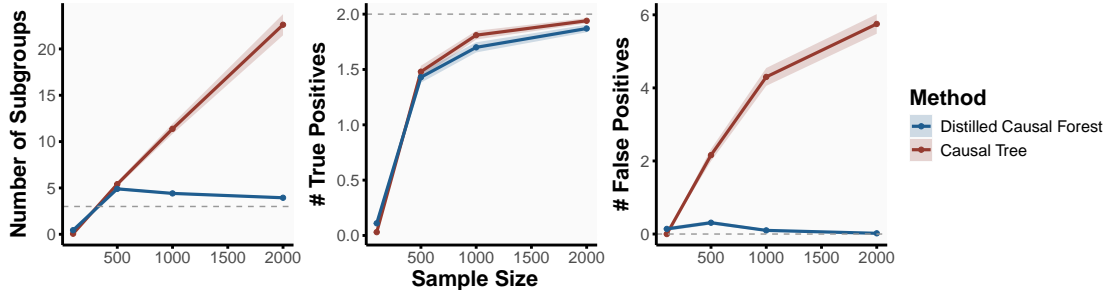


Figure 3: Performance of causal trees and CDT (using causal forests as the teacher model), measured via the (A) number of estimated subgroups as well as (B) the number of true positive and (C) number of false positive features used in the estimated subgroups, under the additive subgroup data-generating process with linear covariates simulation (detailed in Section 5). The oracle number of subgroups, true positives, and false positives are shown as dashed gray lines. Results are averaged across 100 simulation replicates with ribbons denoting $\pm 1SE$.

teacher model, CDT is able to consistently recover the set of optimal subgroups. Furthermore, CDT improves the efficiency of subgroup recovery over existing tree-based approaches by first denoising the underlying data using the teacher model. The act of distilling thus allows researchers to leverage the interpretable outputs of decision trees in constructing subgroups, while offsetting the instabilities that usually adversarially impact tree estimation.

3.4 Estimating subgroup average treatment effects

In the following subsection, we consider how to estimate the subgroup average treatment effects. For simplicity, we will focus on an experimental setting, with extensions for estimating the subgroup average treatment effect in observational settings in Appendix A.4.

More formally, we assume that there is random treatment assignment in the study, such that the treatment indicator Z is independent of $Y(1), Y(0)$, and X .

Assumption 6 (Random Treatment Assignment)

$$\{Y(1), Y(0), X\} \perp\!\!\!\perp Z$$

Furthermore, we assume positivity, such that all units have a non-zero probability of receiving treatment.

Assumption 7 (Positivity) *There exists some constant $0 < \eta \leq 0.5$ such that:*

$$\eta < \Pr(Z = 1 \mid X) \leq 1 - \eta.$$

Finally, we define a subgroup difference-in-means estimator $\hat{\tau}^{(g)}$ for $g = 1, \dots, G$ as

$$\hat{\tau}^{(g)} := \frac{1}{\sum_{i=1}^n Z_i \cdot \hat{\mathcal{G}}_g(X_i)} \sum_{i=1}^n Z_i Y_i \hat{\mathcal{G}}_g(X_i) - \frac{1}{\sum_{i=1}^n (1 - Z_i) \cdot \hat{\mathcal{G}}_g(X_i)} \sum_{i=1}^n (1 - Z_i) Y_i \hat{\mathcal{G}}_g(X_i). \quad (6)$$

We will take a finite-sample perspective, where we consider only the variation that arises from the treatment assignment process. Following existing literature, we condition on a set of valid randomizations—i.e., the set of random treatment allocations, such that there are treatment and control units in each subgroup $g \in \{1, \dots, G\}$.² With some abuse of notation, we suppress the explicit conditioning in the results presented in the following section.

Because we are using sample splitting and honest estimation to estimate the subgroups, the estimated subgroups can be treated as *a priori* defined strata within the study. As such, under Theorem 3.1, the subgroup difference-in-means estimator, defined in Equation (6), provides a consistent estimate of the true subgroup average treatment effects.

Theorem 3.2 (Bias and Variance of Subgroup Difference-in-Means Estimator) *Under Assumptions (1)-(7), the bias of the difference-in-means across the units in the estimated subgroup $\hat{\mathcal{G}}_g(X_i)$ (i.e., $\hat{\tau}^{(g)}$), as defined in Equation (6) is upper bounded by the following:*

$$|\mathbb{E}(\hat{\tau}^{(g)}) - \tau^{(g)}| \leq \frac{1}{n_g} \sum_{i=1}^n \left| \hat{\mathcal{G}}_g(X_i) - \mathcal{G}_g(X_i) \right| \left| Y_i(1) - Y_i(0) \right|,$$

where n_g is the number of samples in subgroup g . Moreover, the variance of $\hat{\tau}^{(g)}$ is

$$\text{var}(\hat{\tau}^{(g)}) = \frac{1}{n_g} \{ \beta_g(1) \text{var}_g(Y_i(1)) + \beta_g(0) \text{var}_g(Y_i(0)) - \text{var}_g(\tau_i) \}$$

where $\beta_g(z) = \mathbb{E}\{1 / \sum_{i=1}^n \hat{\mathcal{G}}_g(X_i) \mathbb{1}\{Z_i = z\}\}$ and $\text{var}_g\{Y(z)\} := \mathbb{E}\left\{ \frac{1}{n_g - 1} \sum_{i=1}^n \hat{\mathcal{G}}_g(X_i) (Y_i(z) - \overline{Y_g(z)})^2 \right\}$ for $z \in \{0, 1\}$.

²Because of the sparsity induced by the causal distillation trees, we expect that the total number of subgroups G should be small, relative to the sample size n . As such, we anticipate this restriction will have little impact on the results in practice. See Schochet (2024) and Miratrix et al. (2013) for more discussion.

There are several takeaways to highlight from Theorem 3.2. First, we see that there is finite-sample bias that arises from slippage between the estimated subgroups and the true subgroups. The rate of convergence in $\hat{\tau}^{(g)}$ to $\tau^{(g)}$ will depend on how quickly $\hat{\mathcal{G}}_g(X_i)$ converges to $\mathcal{G}_g(X_i)$.

Second, from Theorem 3.2, we can construct a conservative variance estimator using the sample analogs for $\text{var}_g(Y_i(z))$ for $z \in \{0, 1\}$:

$$\widehat{\text{var}}(\tau^{(g)}) = \frac{1}{n_g} \left\{ \hat{\beta}_g(1) \widehat{\text{var}}_g(Y_i(1)) + \hat{\beta}_g(0) \widehat{\text{var}}_g(Y_i(0)) \right\},$$

where $\hat{\beta}_g(z) = \left(\frac{1}{n_g} \sum_{i=1}^n \hat{\mathcal{G}}_g(X_i) \mathbb{1}\{Z_i = z\} \right)^{-1}$ (i.e., the inverse of the proportion of units with treatment $Z_i = z$ in the g -th subgroup). Miratrix et al. (2013) show that the gap between $\hat{\beta}_g(z)$ and $\beta_g(z)$ can be upper bounded as a function of $1/n$. Asymptotically, this will be equivalent to the robust Huber–White variance estimator.

To consider the asymptotic distribution of the subgroup difference-in-means estimator, we must account for the fact that as the sample size increases, the underlying subgroup allocation will also change. We leverage recent work in developing central limit theorem results for finite populations (e.g., Schochet, 2024; Schochet et al., 2022; Li and Ding, 2017) to show that under mild regularity conditions, the subgroup difference-in-means estimator will be asymptotically normal.

Theorem 3.3 (Asymptotic Normality of Subgroup Difference-in-Means Estimator)

Assume that as the sample size $n \rightarrow \infty$, the total number of subgroups G remain fixed. Furthermore, assume the proportion of units in each subgroup converges to a proportion $\pi_g^ \in (0, 1)$ (i.e., $n_g/n \rightarrow \pi_g^*$, where $0 < \pi_g^* < 1$ for all $g \in \{1, \dots, G\}$ and $\sum_{g=1}^G \pi_g^* = 1$), and the proportion of treated units converges to p_z , where $p_z \in (0, 1)$ (i.e., $\frac{1}{n} \sum_{i=1}^n Z_i \rightarrow p_z$). Then, for $z \in \{0, 1\}$ and $g \in \{1, \dots, G\}$, if the following condition holds:*

$$\lim_{n \rightarrow \infty} \frac{1}{\left(\sum_{i=1}^n \mathbb{1}\{Z_i = z\} \right)^2} \frac{\max_{1 \leq i \leq n} \hat{\mathcal{G}}_g(X_i) Y_i^2(z)}{\text{var}(\hat{\tau}^{(g)})} = 0, \tag{7}$$

then the subgroup difference-in-means estimator will converge in distribution to a normal distribution:

$$\frac{\sqrt{n} \left(\hat{\tau}^{(g)} - \mathbb{E}(\hat{\tau}^{(g)}) \right)}{\sqrt{\text{var}(\hat{\tau}^{(g)})}} \xrightarrow{d} N(0, 1).$$

The results of Theorem 3.3 can be viewed as a special case of Schochet (2024), Theorem 1. The

condition in (7) is a Lindeberg-type condition, which restricts the tail behavior of the underlying potential outcome distribution and is relatively weak. Importantly, both Theorem 3.2 and 3.3 highlight that the stability improvements we obtain from distillation affect not only our ability to better recover estimates of the subgroups, but also our ability to perform inference.

Following Theorem 3.3, we can apply standard nonparametric tests of treatment effect heterogeneity. See Appendix A for details. In settings when researchers are interested in evaluating whether the largest treatment effect across the subgroups is statistically significantly different than the other treatment effects, we caution that a different test is needed due to post-selection bias. See Wei et al. (2024) for more discussion on valid re-sampling procedures for inference in these settings.

4 A stability-driven approach for teacher model selection

In Section 3, we showed that the benefits of distillation arise from the teacher model’s ability to construct a meaningful basis representation of the individual-level treatment effect using the covariate data. In practice, there are different metalearners that researchers must choose from to estimate the individual-level treatment effect.

Although many model selection procedures exist for choosing the best prediction model (e.g., Stone, 1974; Akaike, 1974; Schwarz, 1978; Therneau et al., 1997; Breiman et al., 1984), they cannot be directly used to assess the goodness-of-fit of our teacher models, which predict individual-level treatment effects — quantities that are not observable in practice. Furthermore, even checking whether the predicted outcomes match the observed outcomes is insufficient to guarantee that we have modeled the *treatment effects* well (Künzel et al., 2019).

In the following section, we develop a novel model selection procedure, designed specifically for subgroup estimation, that selects a teacher model based on its ability to stably reconstruct subgroups. Stable reconstruction refers to being able to estimate similar subgroups, given various perturbations in the underlying data generating process (i.e., sampling error). Following previous studies (e.g., Yu, 2013; Yu and Kumbier, 2020), we argue that teacher models that are able to construct similar subgroups across these different perturbations are likely more appropriate models for the data.

4.1 Quantifying Subgroup Similarity

Before introducing the model selection procedure, we must first quantify what it means for two subgroups to be ‘similar’ and develop a novel measure, termed the Jaccard Subgroup Similarity Index (SSI). Informally, SSI considers two different sets of estimated subgroups $\{\hat{\mathcal{G}}^{(1)}, \hat{\mathcal{G}}^{(2)}\}$, and computes the proportion of units that belong to the same subgroup across both partitions. If the units are similarly grouped in the two different partitions, then $\hat{\mathcal{G}}^{(1)}$ and $\hat{\mathcal{G}}^{(2)}$ are similar, and SSI is high. If the units are grouped differently, then $\hat{\mathcal{G}}^{(1)}$ and $\hat{\mathcal{G}}^{(2)}$ are less similar, and SSI will be low.

To formalize this, let $\hat{\mathcal{G}}^{(1)} = \{\hat{\mathcal{G}}_1^{(1)}(X), \dots, \hat{\mathcal{G}}_G^{(1)}(X)\}$ and $\hat{\mathcal{G}}^{(2)} = \{\hat{\mathcal{G}}_1^{(2)}(X), \dots, \hat{\mathcal{G}}_G^{(2)}(X)\}$ denote two different sets of partitionings into subgroups. Then, for $k \in \{1, 2\}$, define the matrix $C^{(k)} \in \mathbb{R}^{n \times n}$ which denotes whether or not two distinct units belong in the same subgroup in $\hat{\mathcal{G}}^{(k)}$:

$$C_{ij}^{(k)} = \begin{cases} 1 & \text{if } X_i \text{ and } X_j \text{ belong to the same subgroup in } \hat{\mathcal{G}}^{(k)} \text{ and } i \neq j, \\ 0 & \text{otherwise,} \end{cases}$$

for $i, j = 1, \dots, n$. We define the *Jaccard Subgroup Similarity Index* (denoted as SSI) as

$$\text{SSI}(\hat{\mathcal{G}}^{(1)}, \hat{\mathcal{G}}^{(2)}) = \frac{1}{2G} \sum_{\mathcal{H} \in \hat{\mathcal{G}}^{(1)} \cup \hat{\mathcal{G}}^{(2)}} \frac{N_{11}(\mathcal{H})}{N_{01}(\mathcal{H}) + N_{10}(\mathcal{H}) + N_{11}(\mathcal{H})}, \quad (8)$$

where $N_{qr}(\mathcal{H}) = |\{(i, j) \in [n] \times [n] : C_{ij}^{(1)} = q, C_{ij}^{(2)} = r, X_i \in \mathcal{H}(X)\}|$ for each subgroup $\mathcal{H} \in \hat{\mathcal{G}}^{(1)} \cup \hat{\mathcal{G}}^{(2)}$ and $q, r = 0, 1$. Note that $N_{11}(\mathcal{H})$ is the number of sample pairs that belong to the same subgroup in both partitions ($\hat{\mathcal{G}}^{(1)}$ and $\hat{\mathcal{G}}^{(2)}$) but conditioned on the sample pair belonging to subgroup $\mathcal{H}(X)$, while $N_{01}(\mathcal{H}) + N_{10}(\mathcal{H})$ is the number of sample pairs that belong to subgroup $\mathcal{H}(X)$ in one partition but two different subgroups in the other partition. The subgroup similarity index will be bounded between 0 and 1, such that when SSI is close to 1 (that is, when $N_{11}(\mathcal{H})$ is much larger than $N_{01}(\mathcal{H}) + N_{10}(\mathcal{H})$), this implies the two sets of subgroups are similar. Figure A1 illustrates the computation of SSI for an example subgroup $\mathcal{H} \in \hat{\mathcal{G}}^{(1)} \cup \hat{\mathcal{G}}^{(2)}$.

SSI is similar to the Jaccard index (Jaccard, 1901) used in comparing similarities across clusters (Ben-Hur et al., 2001). However, unlike the standard Jaccard index, which weights individual units equally, SSI re-weights units to give equal weight to each subgroup. This is necessary to penalize

subgroups that comprise of very few units, which are typically highly unstable.³

4.2 Teacher Model Selection Procedure

Using SSI, researchers can then consider how similar the estimated subgroups are across repeated data samples. To mimic repeated sampling, we propose a bootstrapping procedure and detail the proposed teacher model selection procedure in Algorithm 1. At a high-level, for each candidate teacher model, researchers can use SSI to evaluate the stability of the estimated subgroups, obtained using the given candidate teacher model, across the different bootstrapped iterations. The teacher model that produces the highest SSI across the different bootstrapped iterations corresponds to the most stable teacher model and should be selected.

The teacher model selection procedure requires choosing a desired tree depth d , or equivalently, the number of rules in the estimated subgroups. As an example, a subgroup in a depth $d = 2$ tree could be $\mathcal{G}_g(X) = \mathbb{1}\{X_{\text{gender}} = \text{Female}\} \cdot \mathbb{1}\{X_{\text{age}} < 35\}$ while $\mathcal{G}_g(X) = \mathbb{1}\{X_{\text{gender}} = \text{Female}\} \cdot \mathbb{1}\{X_{\text{age}} < 35\} \cdot \mathbb{1}\{X_{\text{height}} > 66\}$ is a subgroup in a depth $d = 3$ tree. Domain expertise can sometimes dictate the choice of d . However, when researchers do not have a strong substantive prior for d , researchers can repeat the above procedure for multiple choices of d and select the teacher model that yields the highest subgroup Jaccard stability scores across a majority of these d 's. We demonstrate the effectiveness of this approach for teacher model selection in Section 5.3.

5 Simulations

In the following section, we demonstrate the effectiveness of CDT in accurately estimating subgroups through extensive simulations. We consider two different teacher models: causal forest (Wager and Athey, 2018) and R-learner with boosting (rboost) (Nie and Wager, 2021). We benchmark CDT's performance, relative to popular subgroup estimation approaches — namely, causal trees (Athey and Imbens, 2016), virtual twins (Foster et al., 2011), and interacted linear models, fitted without regularization (i.e., ordinary least squares) and with Lasso (L_1) regularization (e.g., Imai and Ratkovic, 2013). Details regarding the implementation of each CDT and comparison

³We can consider the extreme setting, in which a subgroup contains only a single individual. An estimated subgroup with only one unit would have very little impact on the standard Jaccard index, even though in practice, such a subgroup would not be substantively meaningful and would be undesirable.

Algorithm 1: Selecting the teacher model for CDT

Input: training data $\mathcal{D}^{train} = \{X^{train}, Z^{train}, Y^{train}\}$, set of candidate teacher (CATE) models $\{\mathcal{M}^1, \dots, \mathcal{M}^L\}$, student (decision tree) model m , number of bootstraps B , depth of tree d

- 1 **for** $l = 1, \dots, L$ **do**
- 2 Fit \mathcal{M}^l on \mathcal{D}^{train} to obtain estimates of the individual-level treatment effects $\hat{\tau}^l(X_i)$ for each unit in \mathcal{D}^{train} (via lines 2-16 in Algorithm 2)
- 3 **for** $b = 1, \dots, B$ **do**
- 4 **for** $t = 1, 2$ **do**
- 5 Get bootstrap sample of $\{(X_i, \hat{\tau}^l(X_i)) : i \in \text{training unit}\}$
- 6 Fit decision tree m on the bootstrapped X_i 's to predict the bootstrapped $\hat{\tau}^l(X_i)$'s \rightarrow estimated decision tree $\hat{m}^{(b_t)}$
- 7 Prune the decision tree $\hat{m}^{(b_t)}$ to have depth d and obtain estimated subgroups $\hat{\mathcal{G}}^{(b_t)}$
- 8 **end**
- 9 Compute $J_b^l := \mathcal{J}^{subgroup}(\hat{\mathcal{G}}^{(b_1)}, \hat{\mathcal{G}}^{(b_2)})$
- 10 **end**
- 11 **end**
- 12 Select the teacher model \mathcal{M}^{l^*} such that $l^* = \arg \max_{l=1, \dots, L} \frac{1}{B} \sum_{b=1}^B J_b^l$

method can be found in Appendix C. Across the different simulation scenarios, we find that CDT consistently estimates the true subgroup features, thresholds, and CATEs with greater accuracy than existing methods. Moreover, our model selection procedure using the Jaccard SSI provides an effective data-driven approach to choosing an appropriate teacher model for CDT.

5.1 Simulation Setup

We consider a random treatment assignment process, where $Z_i \stackrel{iid}{\sim} \text{Bernoulli}(1/2)$ for $i = 1, \dots, n$ samples. Furthermore, we generate n samples and p covariates from a standard multivariate normal distribution (i.e., $X_i \stackrel{iid}{\sim} \text{MVN}(0, I)$, where $X_i \in \mathbb{R}^p$ and $i = 1, \dots, n$).

To capture a broad range of subgroup data-generating processes (DGPs), we consider three different treatment effect heterogeneity models:

1. ‘AND’ Subgroup DGP: $\tau_i = 2\mathbf{1}\{X_i^{(1)} > 0\} \cdot \mathbf{1}\{X_i^{(2)} > 0.5\} + \epsilon_i$
2. ‘Additive’ Subgroup DGP: $\tau_i = 2\mathbf{1}\{X_i^{(1)} > 0\} - \mathbf{1}\{X_i^{(2)} < -0.5\} + \epsilon_i$
3. ‘OR’ Subgroup DGP: $\tau_i = 2\mathbf{1}\{X_i^{(1)} > 0\} - \mathbf{1}\{(X_i^{(2)} > 0.5) \text{ or } (X_i^{(2)} < -0.5)\} + \epsilon_i$

where $\epsilon_i \stackrel{iid}{\sim} N(0, \sigma_\tau^2)$. The goal of the simulation study is to evaluate whether the different subgroup estimation methods can accurately find the subgroups associated with $\tau(X_i)$. For example, for the ‘AND’ subgroup DGP, an accurate subgroup estimation method would correctly estimate $\mathbb{1}\{X_i^{(1)} > 0\} \cdot \mathbb{1}\{X_i^{(2)} > 0.5\}$ as a subgroup. For each setting, we also vary σ_τ such that the proportion of variance explained in $\tau(X)$ by the covariates X vary across the values $\{0.2, 0.4, 0.6, 0.8, 1\}$.⁴

The outcome process is a function of the underlying treatment effect heterogeneity model:

$$Y_i = Z_i \cdot \tau_i + X_i^{(3)} + X_i^{(4)} + \nu_i,$$

where $\nu_i \stackrel{iid}{\sim} N(0, 0.1^2)$ is an additive noise term.

To evaluate the effectiveness of each subgroup estimation method, we consider the accuracy of subgroup identification from three perspectives:

1. **Selected subgroup features:** Whether the features used to define the estimated subgroups match the features used to define the true subgroups (i.e., $X^{(1)}$ and $X^{(2)}$), as measured by the accuracy of the selected subgroup features, we calculate the number of true positives, false positives, and F_1 score.⁵
2. **Estimated subgroup thresholds:** Whether the estimated subgroup thresholds are close to the true subgroup thresholds, as measured via the root mean squared error (RMSE).
3. **Estimated Subgroup ATEs:** Whether the estimated subgroup average treatment effects $\hat{\tau}^{(g)}$ are close to the true subgroup average treatment effects (i.e., $\tau^{(g)} := \mathbb{E}[\tau_i | \mathcal{G}_g(X_i)]$), as measured via the RMSE.

For each simulation replicate, we generate $n = 500$ samples and $p = 10$ features. We consider additional data generating processes in Appendix C, but find that the results are largely consistent, even across more complex settings.

⁴The proportion of variance explained in $\tau(X)$ by X is defined as $\text{var}(\mathbb{E}[\tau_i | X]) / \text{var}(\tau_i) \in [0, 1]$.

⁵The F_1 score summarizes the number of true positives (TP), false positives (FP), and false negatives (FN) into a single quantity (i.e., $F_1 = \frac{2 \cdot TP}{2 \cdot TP + FP + FN}$)

5.2 Main Simulation Results

Across the different simulation settings, we find that the CDT methods are able to accurately estimate the true subgroups, both in terms of finding the correct features (as measured by F_1 score), as well as estimating the correct thresholds to construct the decision rules. In contrast, standard subgroup estimation methods (i.e., causal trees and virtual twins) result in many erroneously constructed subgroups, often overfitting to noise features, while linear approaches (i.e., linear regression and Lasso) often fail to pick up on existing subgroups. Figure 4 visualizes the key simulation results, with more detailed summaries in Appendix C.

There are several key takeaways from the simulation results. First, the simulations highlight the advantages of distillation for subgroup estimation. In particular, when comparing distillation with traditional tree-based subgroup estimation methods (i.e., causal tree and virtual twins), we find that the relative improvement in F_1 score from distillation arises from reducing the number of false positives. In particular, virtual twins and causal tree often split on noise features, particularly, $X^{(3)}$ and $X^{(4)}$, while the distilled methods avoid selecting such features (see Appendix C). In other words, without distilling, the tree-based approaches end up erroneously constructing subgroups. This reinforces our theoretical findings from Section 3 that distillation can improve the stability in recovering subgroups, and mitigate potential overfitting in the presence of noise. In comparing the estimated subgroup thresholds for $X^{(1)}$ and $X^{(2)}$, we find that the CDT methods also yield the most accurate and precise estimates of the subgroup thresholds for $X^{(1)}$ and $X^{(2)}$ across the various subgroup DGPs and treatment effect heterogeneity strengths.

We can similarly compare distillation with linear-based approaches (i.e., linear regression and Lasso). In higher noise settings, the linear approaches suffer from the opposite problem as standard tree-based methods. Instead of overfitting to create erroneous subgroups, the linear methods fail to detect any subgroups. This results in substantially lower true positive rates when compared to CDT. In contrast, CDT is still able to detect subgroups in high noise settings. When moving to lower noise settings (i.e., DGPs with moderate-to-high signal strengths), we see that CDT generally outperforms the linear approaches on every accuracy measure (i.e., lower false positives, higher true positives, and higher F_1 scores).

Second, the simulations highlight advantages from distillation in estimating the subgroup ATEs.

In particular, improvements in accurately recovering the subgroups result in lower RMSE in recovering the subgroup ATEs. Moreover, we find that the performance of the traditional tree-based approaches and the linear methods depend heavily on the structure of the underlying outcome model. For example, in the DGP considered in the main manuscript, the outcome model depends on linear functions of the other covariates (namely, $X^{(3)}$ and $X^{(4)}$). Here, the linear-based methods, unsurprisingly, perform well, while the traditional tree-based approaches frequently perform worse in noisy regimes. In contrast, in Appendix D, we additionally consider settings when the outcome model is solely a function of the conditional average treatment effect. In these settings, the existing tree-based methods yield relatively low subgroup ATE errors, while the linear methods result in substantially higher subgroup ATE RMSE. In comparison, the distillation methods appear to be relatively robust to the underlying outcome model’s specification, and perform well in both settings.

5.3 Teacher Model Selection Simulations

In addition to the subgroup estimation performance, we also examine our proposed model selection procedure using the Jaccard SSI under each of the aforementioned simulation scenarios. We compute the Jaccard SSI for both Distilled Causal Forests and Distilled Rboost using $B = 100$ bootstrap samples and four different choices of tree depths ($d = 1, 2, 3, 4$). As a baseline, we also compute the Jaccard SSI for the causal tree. Figure 5 provides a visual summary of the results.

We find that regardless of the noise level, Distilled Causal Forest almost uniformly yields the highest subgroup Jaccard stability score, even varying different tree depths. This implies that according to our proposed teacher model selection procedure, researchers should be using a Causal Forest instead of Rboost as the teacher model. We can directly check the performance of the two teacher models, and find that indeed, the Distilled Causal Forest resulted in higher F_1 scores for the selected subgroup features, and a lower CATE RMSE as compared to Distilled Rboost.

In general, we see that a higher Jaccard SSI generally corresponds to more accurate subgroup estimation. A similar pattern emerges when examining other simulation scenarios (see Appendix E for additional discussion), thereby demonstrating the efficacy of our stability-driven procedure to select the teacher model.

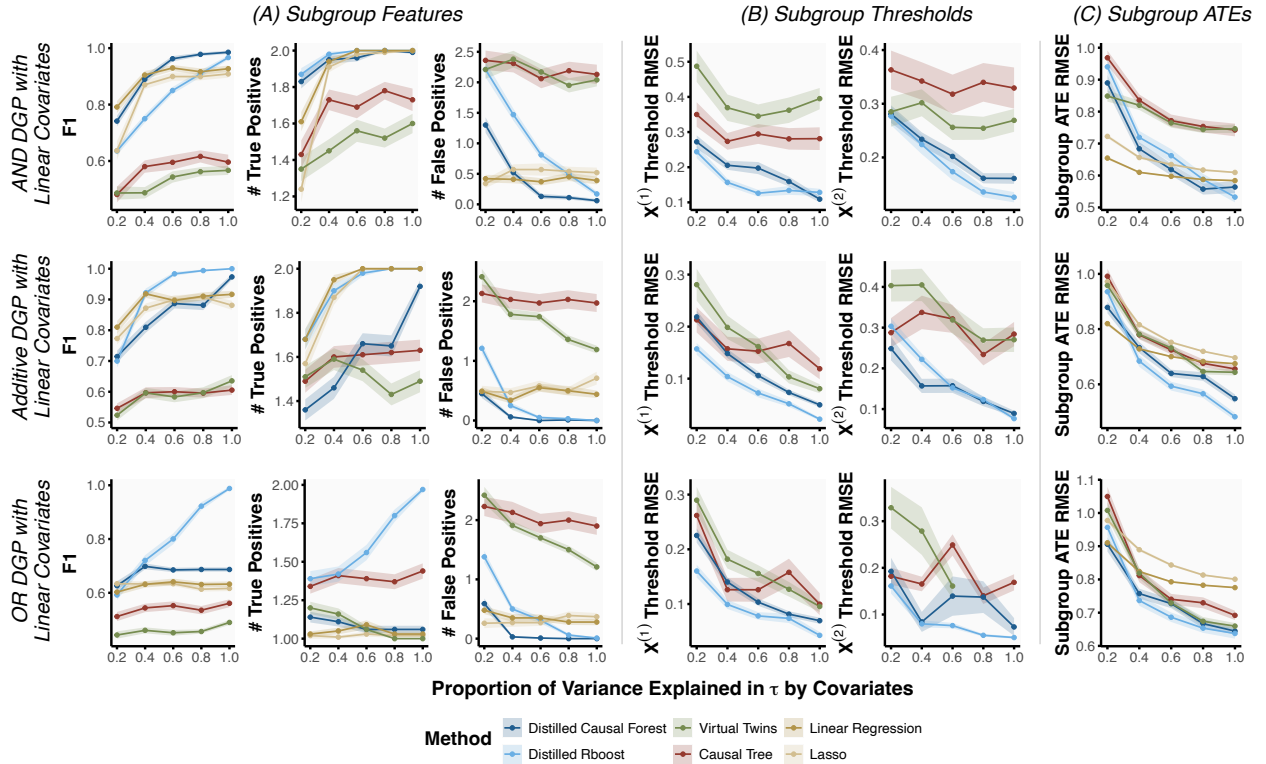


Figure 4: Performance of subgroup estimation methods for (A) identifying the true subgroup features, measured via F_1 score, number of true positives, and number of false positives, (B) estimating the true subgroup thresholds, measured via root mean squared error (RMSE) for each true subgroup feature, and (C) estimating the true subgroup ATE, measured via RMSE, across increasing treatment effect heterogeneity strengths (x-axis) and different subgroup data-generating processes with linear covariate effects (rows). CDT with various teacher models (i.e., Distilled Causal Forest and Distilled Rboost) frequently yields the highest F_1 and number of true positives alongside the lowest number of false positives, threshold RMSEs, and CATE RMSE, demonstrating its effectiveness for accurate subgroup estimation. Results are averaged across 100 simulation replicates with ribbons denoting $\pm 1SE$.

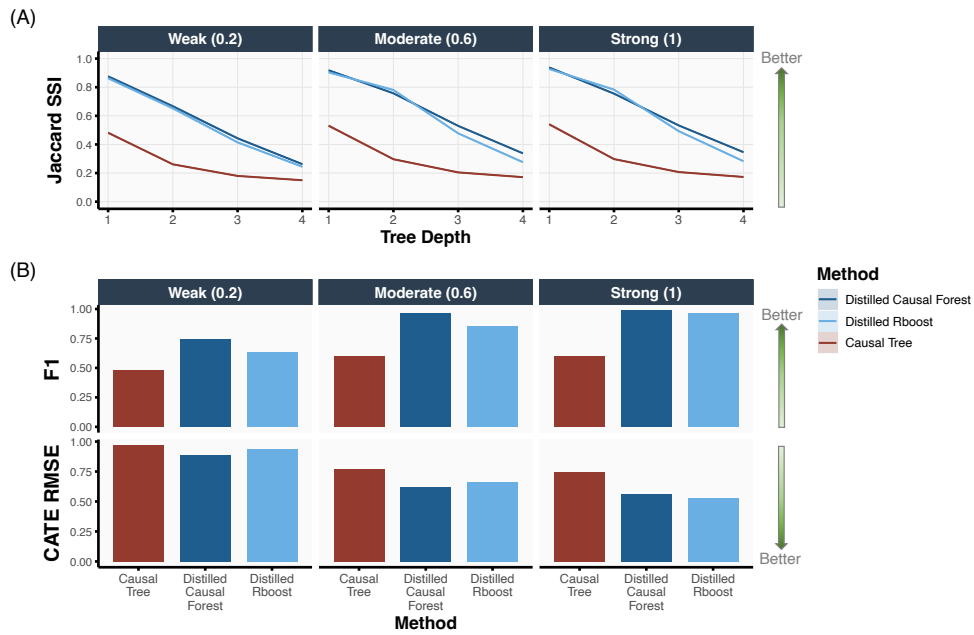


Figure 5: Under the ‘AND’ subgroup data-generating process with linear covariate effects, we examine (A) the Jaccard SSI across a range of tree depths and (B) the corresponding subgroup estimation accuracy for various subgroup estimation methods (colors) and treatment effect heterogeneity strengths, measured via the proportion of variance explained in τ by the covariates (columns). Choosing the teacher model in CDT which leads to the highest Jaccard SSI (in this case, the Distilled Causal Forest) generally corresponds to more accurate subgroup estimation.

6 Case Study: AIDS Clinical Trials Group Study 175

To illustrate the stability and interpretability of CDT on real data, we turn to the AIDS Clinical Trials Group Study 175 (also referred to as ACTG 175). ACTG 175 was a randomized controlled trial to determine the effectiveness of monotherapy compared to combination therapy on HIV-1 infected patients. To enter the study, participants' CD4 cell counts had to be between 200 to 500 cells per cubic millimeter upon screening. The main outcome of interest was whether a patient reached the primary end point ($Y_i = 0$), defined by at least a 50% decline in CD4 cell count, the development of acquired immunodeficiency syndrome (AIDS), or death.

	Estimated Treatment Effect
Overall	0.13 (0.027)
Subgroup Results	
1) Low to high CD8; none to some prior treatment; low to medium weight	0.03 (0.12)
2) Low to high CD8; none to some prior treatment; medium to high weight	0.18 (0.09)
3) Low to high CD8; some to substantial prior treatment; low to medium weight	0.16 (0.16)
4) Low to high CD8; some to substantial prior treatment; medium to high weight	0.12 (0.12)
5) Very high CD8; none to medium prior treatment; low to medium weight	0.03 (0.11)
6) Very high CD8; none to medium prior treatment; medium to high weight	0.25 (0.09)
7) Very high CD8; medium to substantial prior treatment; low to medium weight	0.148 (0.15)
8) Very high CD8; medium to substantial prior treatment; medium to high weight	0.151 (0.13)

Table 1: We provide the average treatment effect across subgroups estimated by CDT using Rboost as the teacher model. CDT is trained on 50% of the study and treatment effects are estimated on the remaining 50% for honest estimation. Bootstrapped standard errors are reported in parentheses.

Combination therapy was shown to slow the progression of HIV-1. However, our goal in this case study is to further characterize subgroups of the population that may experience varying effectiveness of combination therapy. Although we have no underlying ground truth to compare results with as in our simulation study, given substantial medical advances and follow-up research has been performed since this study was conducted in 1996, we can at least compare to current knowledge to vet our results. Here, we focus specifically on the impact of a combination of zidovudine and zalcitabine as our treatment compared to a monotherapy regime that only includes zidovudine. We used a combination of medical records and demographic information as covariates to estimate subgroups and their corresponding treatment effects.

6.1 Estimating subgroups

To illustrate a standard application of the proposed method, we apply CDT using Rboost as the teacher model to a 50% split of the study and estimate subgroup average treatment effects on the remaining 50%. Note we are focusing on results from Distilled Rboost because it yielded a higher subgroup Jaccard stability score across varying tree depths (see Appendix F). In Table 1, we provide the estimated treatment effects and descriptions of each subgroup, and in Figure 6, we visualize the resulting tree structure, where values in the leaf nodes denote the estimated subgroup effects. Across estimated groups, the average number of treatment and control samples is 32 and 34 respectively.

Interactions between CD8 cell counts, weight at the start of the study, and the amount of previous exposure to anti-retroviral therapy are the key characteristics forming our estimated subgroups. Interestingly, these variables are now well-known to influence the progression of HIV-1. For instance, the HIV-1 viral load and resulting decrease in CD4 cell counts traditionally was the major marker to measure response to treatment. However, absolute CD4 counts may not accurately reflect the risks facing patients given immune dysfunction persists despite normalization of counts (McBride and Striker, 2017). The CD4/CD8 ratio, where a value above 1 is considered healthy, is now known to more accurately characterize overall immune dysfunction and may be a stronger indicator of disease progression, response to treatment, morbidity, and mortality. For added context on our estimated subgroups, in this study 99% of individuals had CD4 cell counts below 700, following the rule of thumb that a healthy CD4/CD8 ratio is above 1, CD8 values above 700 would place the majority in an unhealthy range.

Similarly, zidovudine is associated with lipodystrophy (Finkelstein et al., 2015)—a condition that affects how the body stores fat resulting in weight gain in harmful parts of the body (e.g., organs) and loss in others. Thus, a higher or much lower starting weight can put individuals at higher risk of reaching the primary endpoint. Finally, those with previous anti-retroviral therapy improve their chances of longer life expectancy and balanced CD4/CD8 counts. Thus, those entering the study with less experience may benefit the most from a more aggressive treatment regime.

These three covariates clearly interact in specific ways across our eight subgroups. For instance, for those with high CD8 counts, combination therapy is more effective when individuals also have

a higher starting weight and less treatment exposure as in Group 6. The effectiveness decreases when combined with a lower starting weight (Group 5). Even if CD8 counts are lower (i.e., bringing the CD4/CD8 ratio closer to 1), a similar though slightly weaker effect is observed with a stronger impact on those with less treatment exposure and a higher starting weight (Group 2). In contrast, a lower starting weight and less treatment hinders the effectiveness (Group 1). Note while in Table 1, we are referring to “low to medium” CD8 counts, this is relative to our study population. As discussed above, this includes CD8 counts well above 700, placing most in the unhealthy range.

To summarize, CDT recovers clinically-relevant subgroups in the AIDS Clinical Trial data that we now know to be substantively important, thus providing a helpful validity check on the usefulness of the proposed method. However, this illustration also highlights that had researchers utilized CDT when the initial trial was conducted, they could have identified these potential drivers of treatment effect heterogeneity, without having to *a priori* specify what to search for.

6.2 Stability analysis

To consider the stability of the different methods, we perform a bootstrap analysis. Across 100 different bootstrap samples, we apply CDT, virtual twins, as well as tree-based methods and linear methods, to compare the different subgroups obtained under each technique. For each bootstrap instance, we compute the proportion of times features were used to construct subgroups. We summarize the results across these runs in Figure 6.

From the bootstrap analysis, we find that the distillation methods consistently split on the same set of features, regardless of the data perturbations. Furthermore, CDT resulted in fewer subgroups with lower variability, and the estimated subgroups were overwhelmingly characterized by features with direct clinical relevance. Consistent with the one-shot analysis, we see that the three main features chosen by the CDT methods were CD8 cell count at baseline, participants weight at the start of the study, and the number of days of pre-175 antiretroviral therapy.

Comparing the CDT results with the causal tree, we see that the causal tree also similarly constructs subgroups using CD8 cell count, participants’ starting weight, and the number of days of pre-175 antiretroviral therapy. However, it additionally splits on other covariates, depending on the bootstrap iteration, though with less consistency. Virtual twins consistently constructs subgroups on those same three features, but also constructs substantially more across several of

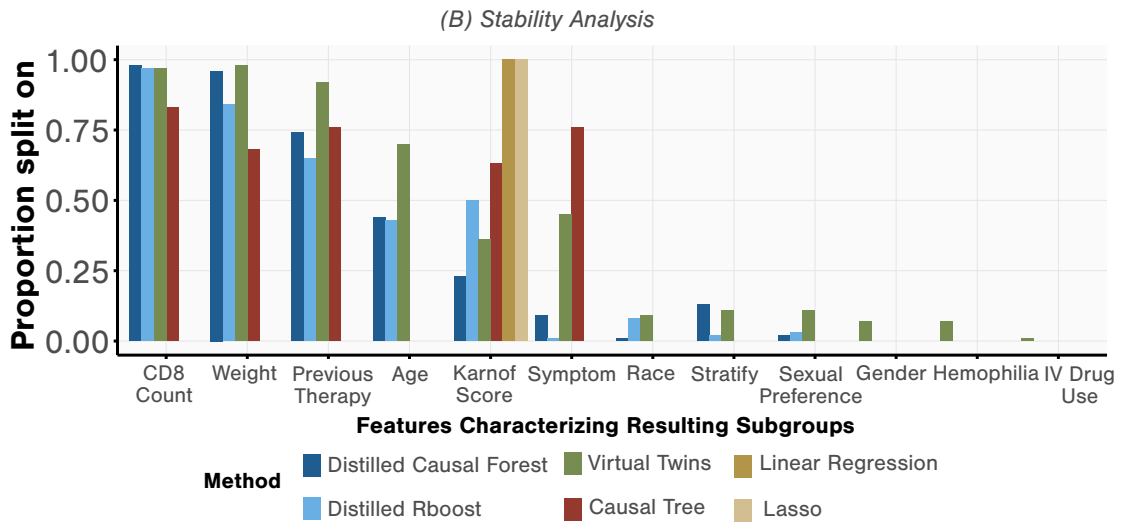
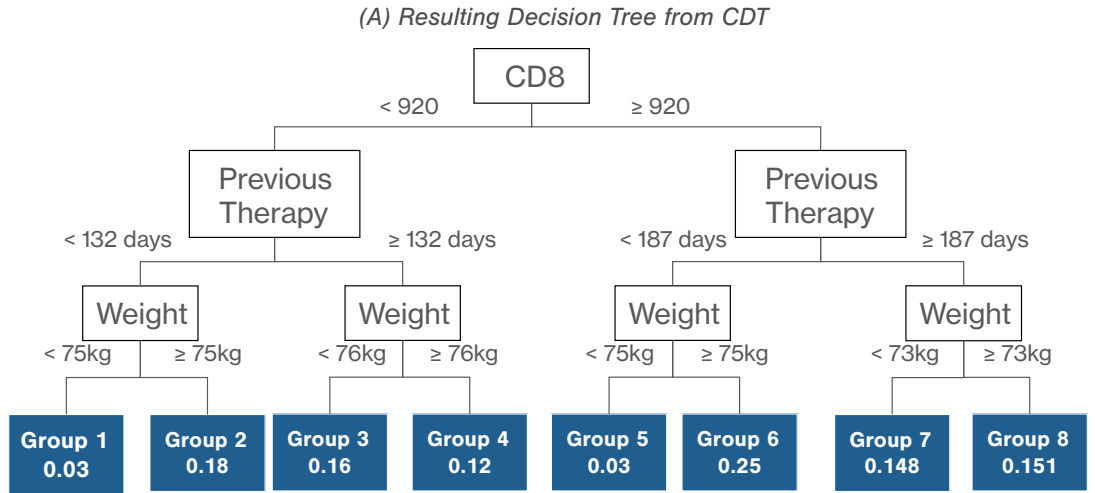


Figure 6: For our case study, we summarize (A) the resulting decision tree produced by CDT using a Causal Forest as the teacher model and (B) the proportion of times across the 100 bootstrap instances features are split upon to form rules and compose subgroups across methods (colors). Proportions closer to one indicate more stability and robustness to small data perturbations.

the other features producing more subgroups that are challenging to interpret.

Interestingly, the linear-based approaches (i.e., linear regression and Lasso) generally fail to pick up on *any* of the features, except for the Karnofsky score. The Karnofsky score is an assessment tool intended to assist clinicians and caregivers in gauging a patient’s functional status and ability to carry out activities of daily living (Schag et al., 1984). While it would normally be assumed to be an informative and clinically relevant feature, the study eligibility criteria required that all participants have a performance score of at least 70; in fact, the median score in the study was 100, translating to a normal status with no evidence of disease. As a result, there is little heterogeneity across the Karnofsky score of the patients in the study and it would not likely moderate the treatment in a meaningful way.

7 Discussion

In the following paper, we introduced a novel method, *causal distillation trees*, for interpretable subgroup estimation in causal inference. CDT allows researchers to leverage the flexibility and power of black-box metalearner approaches, while preserving the interpretability of simple decision trees. We prove that CDT allows researchers to consistently estimate the optimal set of subgroups, and we introduce a novel model selection procedure to help researchers use CDT in practice. To help researchers implement CDT in practice, we have developed an R package `causalDT` available at <https://github.com/tiffanymtang/causalDT>, which not only fits CDT but also automatically conducts the subgroup stability and diagnostic checks, thus enabling researchers to interpret their estimated subgroups from CDT alongside important and informative diagnostics in a holistic manner.

There are several promising avenues for future research. First, recent literature in external validity has emphasized the importance of recruiting a sufficiently heterogeneous experimental sample that adequately captures the total treatment effect variation across the target population (e.g., Huang and Parikh, 2024; Egami and Lee, 2024; Hoellerbauer and Laterzo-Tingley, 2024; Tipton and Mamakos, 2023; Zhang et al., 2024). Failing to do so can result in systematically omitting key segments of the target population, making it infeasible to generalize the causal effect from an experimental sample to the target population of interest (e.g., Huang, 2024). CDT offers an

opportunity for researchers to characterize the underlying treatment effect heterogeneity in a given study and to consider how to optimally recruit these subgroups of participants for an externally valid study. Integrating CDT into external validity concerns would be an interesting avenue of future research.

Second, CDT provides a very general and flexible two-stage framework. Throughout the paper, we focused on CART as the second-stage learner. However, there are numerous alternative tree-based models (Loh, 2002; Quinlan, 2014; Hu et al., 2019) and many that have been developed specifically for subgroup estimation (e.g., Loh et al., 2015; Su et al., 2009; Lipkovich et al., 2011; Seibold et al., 2016; Wang et al., 2024), which can be used as second-stage learners in CDT and may further improve performance. Theoretical properties of these learners remain understudied. Similarly, efforts to further enhance the stability of distillation-based methods (Zhou et al., 2024) can be easily incorporated into the broader CDT framework.

Finally, while the paper considers the causal inference setting, where researchers are interested in estimating relevant subgroups across which they expect there to be treatment effect heterogeneity, an extension of CDT could consider prediction models, where there may be variation in the underlying predictive performance of a specific model. Thoroughly vetting models based on predictive stability has improved the interpretability and predictive performance across several substantive areas including cancer screening and genetic drivers of heart disease (Irajizad et al., 2023; Wang et al., 2023), and a more in-depth approach at the subgroup level could help diagnose potential disparities in the performance of predictive models. Furthermore, while splits from our second stage learner were directly used to characterize subgroups, substantial work has been done to improve feature importances on black-box methods (Lundberg, 2017), especially tree-based approaches (Agarwal et al., 2023; Li et al., 2019), to determine how heavily different features influence predictive performance. These approaches can be combined with CDT to inform which characteristics will most heavily impact the subgroup estimation.

References

- Agarwal, A., A. Kenney, Y. Tan, T. Tang, and B. Yu (2023). Mdi+: A flexible random forest-based feature importance framework. *arXiv preprint arXiv:2307.01932*.
- Akaike, H. (1974). A new look at the statistical model identification. *IEEE transactions on automatic control* 19(6), 716–723.
- Athey, S. and G. Imbens (2016). Recursive partitioning for heterogeneous causal effects. *Proceedings of the National Academy of Sciences* 113(27), 7353–7360.
- Athey, S., G. Imbens, and Y. Kong (2016). *causalTree: Recursive Partitioning Causal Trees*. R package version 0.0, commit 48604762b7db547f49e0e50460eb31a344933bba.
- Banerjee, M. and I. W. McKeague (2007). Confidence sets for split points in decision trees.
- Bargagli-Stoffi, F. J., R. Cadei, K. Lee, and F. Dominici (2020). Causal rule ensemble: Interpretable discovery and inference of heterogeneous treatment effects. *arXiv preprint arXiv:2009.09036*.
- Bargagli Stoffi, F. J. and G. Gnecco (2020). Causal tree with instrumental variable: an extension of the causal tree framework to irregular assignment mechanisms. *International Journal of Data Science and Analytics* 9(3), 315–337.
- Ben-Hur, A., A. Elisseeff, and I. Guyon (2001). A stability based method for discovering structure in clustered data. In *Biocomputing 2002*, pp. 6–17. World Scientific.
- Breiman, L., J. Friedman, C. J. Stone, and R. A. Olshen (1984). *Classification and Regression Trees*. CRC press.
- Buhlmann, P. and B. Yu (2002). Analyzing bagging. *Annals of statistics* 30(4), 927–961.
- Cattaneo, M. D., J. M. Klusowski, and P. M. Tian (2022). On the pointwise behavior of recursive partitioning and its implications for heterogeneous causal effect estimation. *arXiv preprint arXiv:2211.10805*.
- Chan, K.-S. (1993). Consistency and limiting distribution of the least squares estimator of a threshold autoregressive model. *The annals of statistics*, 520–533.

- Chernozhukov, V., D. Chetverikov, M. Demirer, E. Duflo, C. Hansen, W. Newey, and J. Robins (2018). Double/debiased machine learning for treatment and structural parameters.
- Chernozhukov, V., M. Demirer, E. Duflo, and I. Fernandez-Val (2018). Generic machine learning inference on heterogeneous treatment effects in randomized experiments, with an application to immunization in india. Technical report, National Bureau of Economic Research.
- Duncan, J., T. Tang, C. F. Elliott, P. Boileau, and B. Yu (2024). simchef: High-quality data science simulations in r. *Journal of Open Source Software* 9(95), 6156.
- Dwivedi, R., Y. S. Tan, B. Park, M. Wei, K. Horgan, D. Madigan, and B. Yu (2020). Stable discovery of interpretable subgroups via calibration in causal studies. *International Statistical Review* 88, S135–S178.
- Egami, N. and D. D. I. Lee (2024). Designing multi-site studies for external validity: Site selection via synthetic purposive sampling. *Available at SSRN 4717330*.
- Escanciano, J. C. (2020). Estimation of split points in misspecified decision trees.
- Finkelstein, J. L., P. Gala, R. Rochford, M. J. Glesby, and S. Mehta (2015). Hiv/aids and lipodystrophy: implications for clinical management in resource-limited settings. *African Journal of Reproduction and Gynaecological Endoscopy* 18(1).
- Fokkema, M. (2020). Fitting prediction rule ensembles with R package pre. *Journal of Statistical Software* 92(12), 1–30.
- Foster, J. C., J. M. Taylor, and S. J. Ruberg (2011). Subgroup identification from randomized clinical trial data. *Statistics in medicine* 30(24), 2867–2880.
- Friedman, J., R. Tibshirani, and T. Hastie (2010). Regularization paths for generalized linear models via coordinate descent. *Journal of Statistical Software* 33(1), 1–22.
- Friedman, J. H. and B. E. Popescu (2008). Predictive learning via rule ensembles. *The Annals of Applied Statistics* 2(3), 916 – 954.
- Furlanello, T., Z. Lipton, M. Tschannen, L. Itti, and A. Anandkumar (2018). Born again neural networks. In *International conference on machine learning*, pp. 1607–1616. PMLR.

- Groeneboom, P. (1989). Brownian motion with a parabolic drift and airy functions. *Probability theory and related fields* 81(1), 79–109.
- Hill, J. L. (2011). Bayesian nonparametric modeling for causal inference. *Journal of Computational and Graphical Statistics* 20(1), 217–240.
- Hinton, G. (2015). Distilling the knowledge in a neural network. *arXiv preprint arXiv:1503.02531*.
- Hoellerbauer, S. and I. Laterzo-Tingley (2024). Post hoc synthetic purposive sampling for post hoc external validity assessment.
- Hu, X., C. Rudin, and M. Seltzer (2019). Optimal sparse decision trees. *Advances in Neural Information Processing Systems* 32.
- Huang, M. (2024+). Overlap violations in external validity. *Annals of Applied Statistics (Forthcoming)*.
- Huang, M. Y. and H. Parikh (2024). Towards generalizing inferences from trials to target populations. *Harvard Data Science Review*.
- Imai, K. and M. L. Li (2024). Statistical inference for heterogeneous treatment effects discovered by generic machine learning in randomized experiments. *Journal of Business & Economic Statistics* (just-accepted), 1–29.
- Imai, K. and M. Ratkovic (2013). Estimating treatment effect heterogeneity in randomized program evaluation.
- Irajizad, E., A. Kenney, T. Tang, J. Vykoukal, R. Wu, E. Murage, J. B. Dennison, M. Sans, J. P. Long, M. Loftus, et al. (2023). A blood-based metabolomic signature predictive of risk for pancreatic cancer. *Cell Reports Medicine* 4(9).
- Jaccard, P. (1901). Étude comparative de la distribution florale dans une portion des alpes et des jura. *Bull Soc Vaudoise Sci Nat* 37, 547–579.
- Janson, S. (2013). Moments of the location of the maximum of brownian motion with parabolic drift. *Electronic Communications in Probability* 18(15).

- Javanmard, A. and A. Montanari (2013). Model selection for high-dimensional regression under the generalized irrepresentability condition. *Advances in neural information processing systems* 26.
- Kang, J. D. and J. L. Schafer (2007). Demystifying double robustness: A comparison of alternative strategies for estimating a population mean from incomplete data. *Statistical Sciences*.
- Kennedy, E. H. (2023). Towards optimal doubly robust estimation of heterogeneous causal effects. *Electronic Journal of Statistics* 17(2), 3008–3049.
- Kennedy, E. H., S. Balakrishnan, J. M. Robins, and L. Wasserman (2022). Minimax rates for heterogeneous causal effect estimation. *arXiv preprint arXiv:2203.00837*.
- Kosorok, M. R. (2008). *Introduction to empirical processes and semiparametric inference*, Volume 61. Springer.
- Künzel, S. R., J. S. Sekhon, P. J. Bickel, and B. Yu (2019). Metalearners for estimating heterogeneous treatment effects using machine learning. *Proceedings of the national academy of sciences* 116(10), 4156–4165.
- Li, X. and P. Ding (2017). General forms of finite population central limit theorems with applications to causal inference. *Journal of the American Statistical Association* 112(520), 1759–1769.
- Li, X., Y. Wang, S. Basu, K. Kumbier, and B. Yu (2019). A debiased mdi feature importance measure for random forests. *Advances in Neural Information Processing Systems* 32.
- Lin, J., C. Zhong, D. Hu, C. Rudin, and M. Seltzer (2020). Generalized and scalable optimal sparse decision trees. In *International Conference on Machine Learning*, pp. 6150–6160. PMLR.
- Lipkovich, I., A. Dmitrienko, and R. B D’Agostino Sr (2017). Tutorial in biostatistics: data-driven subgroup identification and analysis in clinical trials. *Statistics in medicine* 36(1), 136–196.
- Lipkovich, I., A. Dmitrienko, J. Denne, and G. Enas (2011). Subgroup identification based on differential effect search—a recursive partitioning method for establishing response to treatment in patient subpopulations. *Statistics in medicine* 30(21), 2601–2621.
- Loh, W.-Y. (2002). Regression tress with unbiased variable selection and interaction detection. *Statistica sinica*, 361–386.

- Loh, W.-Y., X. He, and M. Man (2015). A regression tree approach to identifying subgroups with differential treatment effects. *Statistics in medicine* 34(11), 1818–1833.
- Lundberg, S. (2017). A unified approach to interpreting model predictions. *arXiv preprint arXiv:1705.07874*.
- McBride, J. A. and R. Striker (2017). Imbalance in the game of t cells: What can the cd4/cd8 t-cell ratio tell us about hiv and health? *PLoS pathogens* 13(11), e1006624.
- Meinshausen, N. and P. Bühlmann (2006). High-dimensional graphs and variable selection with the lasso.
- Menon, A. K., A. S. Rawat, S. Reddi, S. Kim, and S. Kumar (2021). A statistical perspective on distillation. In *International Conference on Machine Learning*, pp. 7632–7642. PMLR.
- Miratrix, L. W., J. S. Sekhon, and B. Yu (2013). Adjusting treatment effect estimates by post-stratification in randomized experiments. *Journal of the Royal Statistical Society Series B: Statistical Methodology* 75(2), 369–396.
- Nie, X., A. Schuler, and S. Wager (2021). *rlearner: R-learner for Heterogeneous Treatment Effect Estimation*. R package version 1.1.0, commit 6806396960e672214e2ef36e16c76bbb58ef9114.
- Nie, X. and S. Wager (2021). Quasi-oracle estimation of heterogeneous treatment effects. *Biometrika* 108(2), 299–319.
- Oprescu, M., J. Dorn, M. Ghoummaid, A. Jesson, N. Kallus, and U. Shalit (2023). B-learner: Quasi-oracle bounds on heterogeneous causal effects under hidden confounding. In *International Conference on Machine Learning*, pp. 26599–26618. PMLR.
- Quinlan, J. R. (2014). *C4. 5: programs for machine learning*. Elsevier.
- R Core Team (2024). *R: A Language and Environment for Statistical Computing*. Vienna, Austria: R Foundation for Statistical Computing.
- Rehill, P. (2024). Distilling interpretable causal trees from causal forests. *arXiv preprint arXiv:2408.01023*.

- Schag, C. C., R. L. Heinrich, and P. A. Ganz (1984). Karnofsky performance status revisited: reliability, validity, and guidelines. *Journal of Clinical Oncology* 2(3), 187–193.
- Schochet, P. Z. (2024). Design-based rct estimators and central limit theorems for baseline subgroup and related analyses. *Journal of Causal Inference* 12(1), 20230056.
- Schochet, P. Z., N. E. Pashley, L. W. Miratrix, and T. Kautz (2022). Design-based ratio estimators and central limit theorems for clustered, blocked rcts. *Journal of the American Statistical Association* 117(540), 2135–2146.
- Schwarz, G. (1978). Estimating the dimension of a model. *The annals of statistics*, 461–464.
- Seibold, H., A. Zeileis, and T. Hothorn (2016). Model-based recursive partitioning for subgroup analyses. *The international journal of biostatistics* 12(1), 45–63.
- Stone, M. (1974). Cross-validatory choice and assessment of statistical predictions. *Journal of the royal statistical society: Series B (Methodological)* 36(2), 111–133.
- Su, X., C.-L. Tsai, H. Wang, D. M. Nickerson, and B. Li (2009). Subgroup analysis via recursive partitioning. *Journal of Machine Learning Research* 10(2).
- Tan, Y. S., J. M. Klusowski, and K. Balasubramanian (2024). Statistical-computational trade-offs for greedy recursive partitioning estimators. *arXiv preprint arXiv:2411.04394*.
- Therneau, T. and B. Atkinson (2023). *rpart: Recursive Partitioning and Regression Trees*. R package version 4.1.23.
- Therneau, T. M., E. J. Atkinson, et al. (1997). An introduction to recursive partitioning using the rpart routines. Technical report, Technical report Mayo Foundation.
- Tibshirani, J., S. Athey, E. Sverdrup, and S. Wager (2024). *grf: Generalized Random Forests*. R package version 2.3.2.
- Tipton, E. and M. Mamakos (2023). Designing randomized experiments to predict unit-specific treatment effects. *arXiv preprint arXiv:2310.18500*.

- van der Linden, J. G., D. Vos, M. M. de Weerd, S. Verwer, and E. Demirović (2024). Optimal or greedy decision trees? revisiting their objectives, tuning, and performance. *arXiv preprint arXiv:2409.12788*.
- Van der Vaart, A. W. (2000). *Asymptotic statistics*, Volume 3. Cambridge university press.
- Wager, S. and S. Athey (2018). Estimation and inference of heterogeneous treatment effects using random forests. *Journal of the American Statistical Association* 113(523), 1228–1242.
- Wan, K., K. Tanioka, and T. Shimokawa (2023). Rule ensemble method with adaptive group lasso for heterogeneous treatment effect estimation. *Statistics in Medicine* 42(19), 3413–3442.
- Wang, Q., T. M. Tang, N. Youlton, C. S. Weldy, A. M. Kenney, O. Ronen, J. W. Hughes, E. T. Chin, S. C. Sutton, A. Agarwal, et al. (2023). Epistasis regulates genetic control of cardiac hypertrophy. *Research Square*.
- Wang, T., A. P. Keil, S. Kim, R. Wyss, P. T. Htoo, M. J. Funk, J. B. Buse, M. R. Kosorok, and T. Stürmer (2024). Iterative causal forest: A novel algorithm for subgroup identification. *American journal of epidemiology* 193(5), 764–776.
- Wang, T. and C. Rudin (2022). Causal rule sets for identifying subgroups with enhanced treatment effects. *INFORMS Journal on Computing* 34(3), 1626–1643.
- Wei, W., Y. Zhou, Z. Zheng, and J. Wang (2024). Inference on the best policies with many covariates. *Journal of Econometrics* 239(2), 105460.
- Wright, M. N. and A. Ziegler (2017). ranger: A fast implementation of random forests for high dimensional data in C++ and R. *Journal of Statistical Software* 77(1), 1–17.
- Xie, Y., J. E. Brand, and B. Jann (2012). Estimating heterogeneous treatment effects with observational data. *Sociological methodology* 42(1), 314–347.
- Yu, B. (2013). Stability.
- Yu, B. and K. Kumbier (2020). Veridical data science. *Proceedings of the National Academy of Sciences* 117(8), 3920–3929.

- Zhang, Y., M. Huang, and K. Imai (2024). Minimax regret estimation for generalizing heterogeneous treatment effects with multisite data. *arXiv preprint arXiv:2412.11136*.
- Zhang, Y., P. Schnell, C. Song, B. Huang, and B. Lu (2021). Subgroup causal effect identification and estimation via matching tree. *Computational Statistics & Data Analysis* 159, 107188.
- Zhao, P. and B. Yu (2006). On model selection consistency of lasso. *The Journal of Machine Learning Research* 7, 2541–2563.
- Zhou, S. and L. Mentch (2023). Trees, forests, chickens, and eggs: when and why to prune trees in a random forest. *Statistical Analysis and Data Mining: The ASA Data Science Journal* 16(1), 45–64.
- Zhou, Y., Z. Zhou, and G. Hooker (2024). Approximation trees: statistical reproducibility in model distillation. *Data Mining and Knowledge Discovery* 38(5), 3308–3346.
- Zou, H. (2006). The adaptive lasso and its oracle properties. *Journal of the American statistical association* 101(476), 1418–1429.

Appendix: “Distilling heterogeneous treatment effects: Stable subgroup estimation in causal inference”

A Extended Discussion

A.1 Pruning

As in the supervised learning setting, decision trees for causal effect estimation (including in the second stage of CDT) are often pruned to avoid overfitting. There are generally two types of pruning: pre-pruning and post-pruning. Pre-pruning refers to techniques or early stopping criteria that are used to stop growing the decision tree during the tree construction process. Common pre-pruning approaches include setting constraints on the maximum depth of the tree, the minimum number of samples per node, or the minimum information gain from making each split. Post-pruning refers to techniques used to remove uninformative nodes from the decision tree after it has already been constructed. For example, in the `rpart` R package (Therneau et al., 1997), cross-validation is performed to choose the best complexity parameter α , where α measures the cost of adding another split to the tree, and all nodes with a cost greater than α are subsequently removed or pruned from the tree.

Through simulations (see Section 5), we demonstrate that standard pre-pruning and post-pruning approaches used in ordinary decision trees (e.g., CART (Breiman et al., 1984)) also work well for the student decision tree model in CDT and are hence recommended. In particular, standard here means using the default pre-pruning criteria in the `rpart` R package and post-pruning based upon the cross-validated complexity parameter α , as described previously. We provide additional simulation results for pruning in Appendix D.

A.2 Extended discussion on valid teacher models

Throughout the manuscript, we rely on assuming a valid teacher model—i.e., a teacher model that results in distilled treatment effects with the same optimal partitioning as the original individual-level treatment effects. A sufficient, but not necessary, condition for the teacher model to be valid is exogeneity, i.e., $(\tau_i - \hat{\tau}_i^d) \perp\!\!\!\perp X_i$. In what follows, we will show that under exogeneity, distillation

does not affect the optimal splits found. In other words, the optimal splits s found using the distilled individual-level treatment effects $\hat{\tau}_i^d$ will be the same as the optimal splits s^d found using the original individual-level treatment effects τ_i .

Let s and s^d respectively be the optimal splits using the original individual-level treatment effects τ_i and distilled individual-level treatment effects $\hat{\tau}_i^d$, as defined in Assumption (2). Also, define $v_i := \tau_i - \hat{\tau}_i^d$ for each $i = 1, \dots, n$. We can then write

$$\begin{aligned}\tau^v(X_i; s) &:= \tau(X_i; s) - \tau^d(X_i; s) \\ &= \mathbb{1}\{X_i \leq s\}\mathbb{E}(v_i \mid X_i \leq s) + \mathbb{1}\{X_i > s\}\mathbb{E}(v_i \mid X_i > s) \\ &= \mathbb{E}(v_i),\end{aligned}$$

where the last equality follows by exogeneity.

Thus, we have that

$$\begin{aligned}\mathbb{E} \left[\ell(\hat{\tau}_i^d; X_i, s) \right] &= \mathbb{E} \left[\left\{ \hat{\tau}_i^d - \tau^d(X_i; s) \right\}^2 \right] \\ &= \mathbb{E} \left[\left\{ \tau_i - \tau(X_i; s) + \tau(X_i; s) - \tau^d(X_i; s) - v_i \right\}^2 \right] \\ &= \mathbb{E} \left[\left\{ \tau_i - \tau(X_i; s) - (v_i - \tau^v(X_i; s)) \right\}^2 \right] \\ &= \mathbb{E} \left[\left\{ \tau_i - \tau(X_i; s) \right\}^2 \right] + \mathbb{E} \left[\left\{ v_i - \tau^v(X_i; s) \right\}^2 \right] - 2\mathbb{E} \left[\left\{ \tau_i - \tau(X_i; s) \right\} \cdot \left\{ v_i - \tau^v(X_i; s) \right\} \right] \\ &= \mathbb{E} \left[\left\{ \tau_i - \tau(X_i; s) \right\}^2 \right] + \text{var}(v_i) - 2 \underbrace{\mathbb{E} \left[\left\{ \tau_i - \tau(X_i; s) \right\} \cdot \left\{ v_i - \mathbb{E}(v_i) \right\} \right]}_{(*)}.\end{aligned}$$

Continuing with (*),

$$\mathbb{E} \left[\left\{ \tau_i - \tau(X_i; s) \right\} \cdot \left\{ v_i - \mathbb{E}(v_i) \right\} \right] = \mathbb{E} \left((\hat{\tau}_i^d + v_i)(v_i - \mathbb{E}(v_i)) - \tau(X_i; s) \cdot (v_i - \mathbb{E}(v_i)) \right)$$

Applying Law of Iterated Expectations:

$$= \mathbb{E} \left(\mathbb{E} \left((\hat{\tau}_i^d + v_i)(v_i - \mathbb{E}(v_i)) - \tau(X_i; s) \cdot (v_i - \mathbb{E}(v_i)) \mid X_i \right) \mid X_i \right)$$

Since $\hat{\tau}_i^d$ and $\tau(X_i; s)$ are functions of X_i :

$$\begin{aligned} &= \mathbb{E}(\hat{\tau}_i^d \mathbb{E}(v_i - \mathbb{E}(v_i) \mid X_i) + \mathbb{E}(v_i(v_i - \mathbb{E}(v_i)) \mid X_i) - \\ &\quad \tau(X_i; s) \mathbb{E}(v_i - \mathbb{E}(v_i) \mid X_i)) \\ &= \text{var}(v_i), \end{aligned}$$

where the last inequality follows from exogeneity.

Thus,

$$\mathbb{E} [\ell(\hat{\tau}_i^d; X_i, s)] = \mathbb{E} [\ell(\tau_i; X_i, s)] - \text{var}(v_i),$$

which implies $s^d := \arg \min_{s' \in \mathcal{X}} \mathbb{E} [\ell(\hat{\tau}_i^d; X_i, s')] = \arg \min_{s' \in \mathcal{X}} \mathbb{E} [\ell(\tau_i; X, s')] =: s$, since $\text{var}(v_i)$ is not a function of the decision rule split. We have thus shown that exogeneity implies $s = s^d$ as desired.

In settings when we do not have a valid teacher model (such that $s^d \neq s$), the resulting subgroups will be systematically biased, where

$$\mathbb{E} \left[\left| \hat{\mathcal{G}}_1(X_i) - \mathcal{G}_1(X_i) \right| \right] \leq 2 \left| \hat{s}_n - s^d \right| + \varepsilon,$$

where $\varepsilon = 2|s^d - s|$.

A.3 Non-parametric test of treatment effect heterogeneity

We propose a nonparametric test of treatment effect heterogeneity. Following [Imai and Li \(2024\)](#), we consider the following null hypothesis of no treatment effect heterogeneity:

$$H_0 : \tau^{(1)} = \dots = \tau^{(G)} = \tau, \tag{9}$$

for all subgroups $g \in \{1, \dots, G\}$, with the following estimator:

$$\hat{\boldsymbol{\tau}} = (\hat{\tau}^{(1)} - \hat{\tau}, \dots, \hat{\tau}^{(g)} - \hat{\tau})^\top,$$

where $\hat{\tau} := \frac{1}{\sum_{i=1}^n Z_i} Y_i Z_i - \frac{1}{\sum_{i=1}^n (1-Z_i)} Y_i (1 - Z_i)$ is the usual difference-in-means estimator across the entire sample. Then, following Theorem 3.3, we can show that under the null hypothesis, the test statistic can be asymptotically approximated using a χ^2 distribution. The following corollary formalizes.

Corollary A.1 (Non-Parametric Test of Treatment Effect Heterogeneity) *Under the null hypothesis in (9), with the alternative $H_A : \exists \hat{\tau}^{(g)} \neq \tau$, then:*

$$\hat{\tau}^\top \Sigma \hat{\tau} \xrightarrow{d} \chi^2.$$

A.4 Improving Finite-Sample Performance

While the main manuscript focused on experimental settings, we can similarly estimate the subgroup average treatment effect in observational settings. However, we must account for potential confounding within a given subgroup.

To begin, we must assume conditional ignorability of treatment and outcome.

Assumption A.1 (Conditional ignorability of treatment and outcome)

$$Y(1), Y(0) \perp\!\!\!\perp Z \mid X$$

This assumption states that given a set of pre-treatment covariates X , the treatment assignment process is effectively ‘as-if’ random. While the subgroups themselves are functions of the pre-treatment covariates, they represent a coarsened subset of units in the study. As such, we do not generally expect that all units within a given subgroup have identical covariate values X , especially in settings when X is high dimensional. As such, we can no longer rely on just a subgroup difference-in-means estimator, and must adjust for potential confounding of treatment within a subgroup.

Instead of estimating the subgroup difference-in-means, researchers can estimate $\hat{\tau}_{\text{W-ADJ}}^{(g)}$:

$$\left\{ \hat{\tau}_{\text{W-ADJ}}^{(g)}, \hat{\alpha}, \hat{\beta} \right\} = \arg \min_{\tau, \alpha, \beta} \frac{1}{n_g} \sum_{i: \hat{G}_g(X_i)=1} \hat{w}_i \left\{ Y_i - \left(\tau Z_i + \alpha + \beta^\top X_i \right) \right\}^2,$$

where \hat{w}_i is defined as the inverse propensity score weights:

$$\hat{w}_i = \begin{cases} 1/\hat{e}(X_i) & \text{if } Z_i = 1 \\ 1/\{1 - \hat{e}(X_i)\} & \text{if } Z_i = 0 \end{cases},$$

and $\hat{e}(X_i)$ is the estimated probability of being assigned to treatment, given the covariates X . $\hat{\tau}_{\text{W-ADJ}}^{(g)}$ provides a doubly robust approach to estimating the subgroup average treatment effect (e.g., [Kang and Schafer, 2007](#)), with potential efficiency gains in finite samples. Theorem 3.3 can be extended for $\hat{\tau}_{\text{W-ADJ}}^{(g)}$, allowing for valid inference and analogous hypothesis tests.

There are two components to $\hat{\tau}_{\text{W-ADJ}}^{(g)}$: (1) the covariate adjustment taking place within the regression, and (2) a re-weighting adjustment to balance the treatment and control groups. The covariate adjustment within the weighted regression allows researchers to leverage variation across covariates within a specific subgroup. In particular, because the subgroups are defined using covariates that are explanatory of the treatment effect variation, we generally expect a sparser set of covariates that explain the treatment effect variation in contrast to covariates that can explain variation in the outcome. As such, within each subgroup, while we expect relatively small amounts of treatment effect variation, there could still be residual variation in the outcomes that can be explained by the other covariates. The re-weighting component of $\hat{\tau}_{\text{W-ADJ}}^{(g)}$ ensures that within each subgroup, researchers can also account for finite-sample imbalances that are present ([Xie et al., 2012](#)).

Notably, $\hat{\tau}_{\text{W-ADJ}}^{(g)}$ can similarly be used in experimental contexts to improve finite-sample performance. In practice, a drawback to subgroup analyses is the relatively small number of observations within each subgroup. In particular, even if the overall study contains a large number of observations, the number of observations available within a subgroup can be relatively limited. As a result, using the standard difference-in-means estimator can result in poor finite-sample performance.

A.5 Detailed CDT Algorithm

Algorithm 2: Causal Distillation Trees

Input: data $\mathcal{D} = \{X, Z, Y\}$, teacher (CATE) model \mathcal{M} , student (decision tree) model m , training proportion π_{train} , number of cross-fitting replicates R (if necessary)

- 1 Randomly split data \mathcal{D} into $\mathcal{D}^{train} = \{X^{train}, Z^{train}, Y^{train}\}$ and $\mathcal{D}^{est} = \{X^{est}, Z^{est}, Y^{est}\}$ with probability π_{train} and $1 - \pi_{train}$, respectively
- 2 // Stage 1: estimate individual-level treatment effects via teacher model
- 3 **if** *using model-specific out-of-sample estimation* **then**
- 4 // e.g., if teacher model has out-of-bag estimation procedure
- 5 Fit CATE model \mathcal{M} using $\mathcal{D}^{train} \rightarrow \widehat{\mathcal{M}}$
- 6 Use $\widehat{\mathcal{M}}$ to estimate $\hat{\tau}(X_i)$ for each unit i in \mathcal{D}^{train}
- 7 **else**
- 8 // do repeated cross-fitting
- 9 **for** $r = 1, \dots, R$ **do**
- 10 Randomly split \mathcal{D}^{train} into two equally-sized partitions \mathcal{D}_{in}^{train} and $\mathcal{D}_{out}^{train}$
- 11 Fit CATE model \mathcal{M} using $\mathcal{D}_{in}^{train} \rightarrow \widehat{\mathcal{M}}$
- 12 Use $\widehat{\mathcal{M}}$ to estimate $\hat{\tau}^{(r)}(X_i)$ for each unit i in $\mathcal{D}_{out}^{train}$
- 13 Reverse roles of \mathcal{D}_{in}^{train} and $\mathcal{D}_{out}^{train}$ and repeat lines 11-12
- 14 **end**
- 15 Average across cross-fits: $\hat{\tau}(X_i) = \sum_{r=1}^R \hat{\tau}_i^{(r)}(X_i)$ for each unit i in \mathcal{D}^{train}
- 16 **end**
- 17 // Stage 2: estimate subgroups via student model
- 18 Fit decision tree m on X^{train} to predict $\hat{\tau}(X_i)$'s \rightarrow estimated subgroups $\{\hat{\mathcal{G}}_1(X), \dots, \hat{\mathcal{G}}_G(X)\}$
- 19 // Honestly estimate subgroup average treatment effects
- 20 Estimate $\hat{\tau}^{(g)}$ via (6) for each $g = 1, \dots, G$ using \mathcal{D}^{est}

A.6 Additional Discussion of Teacher Model Selection Algorithm

The proposed teacher model selection procedure in Algorithm 1 requires choosing the desired tree depth d , or equivalently, the number of binary decision rules characterizing each subgroup. This ensures that there are the same number of subgroups (i.e., 2^d) per tree (or partition). Having the same number of subgroups per tree is necessary to ensure that the subgroup Jaccard indices are comparable across both bootstraps and teacher models. Otherwise, a teacher model, such as a constant predictor, that results in fewer decision tree splits (or a smaller depth d) is inherently going to be more stable than a teacher model that results in more decision tree splits.

A.7 Diagnostic Tools for CDT

To help researchers evaluate the quality of the estimated subgroups from CDT, we recommend several important diagnostics.

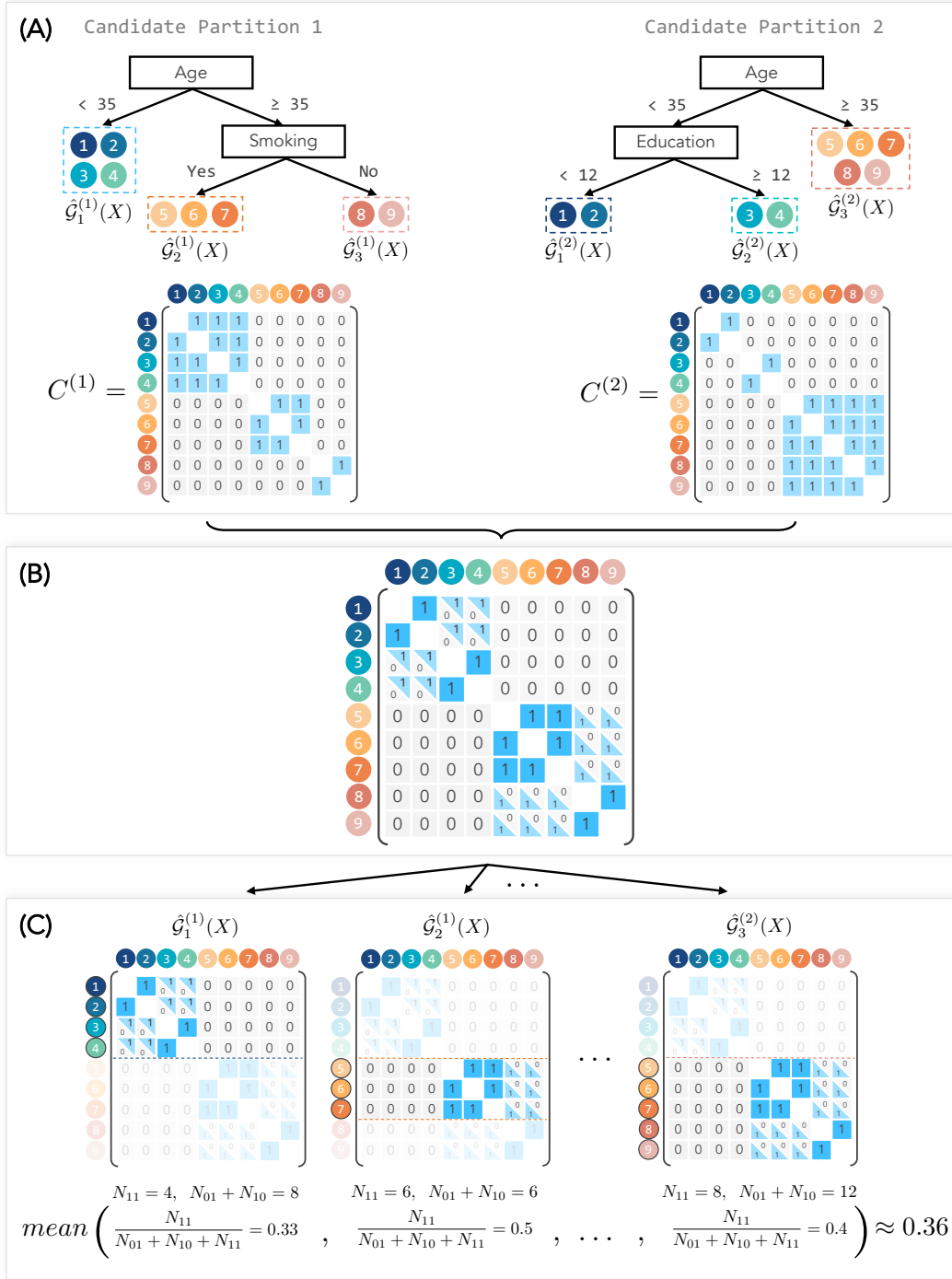


Figure A1: Jaccard subgroup similarity index (SSI). (A) Given two candidate partitionings into subgroups, two binary matrices, denoted $C^{(1)}$ and $C^{(2)}$, are constructed, indicating whether or not two distinct units belong in the same subgroup in $\hat{\mathcal{G}}^{(1)}$ and $\hat{\mathcal{G}}^{(2)}$, respectively. (B) $C^{(1)}$ and $C^{(2)}$ are compared to identify the sample pairs which (i) belong to the same subgroup in both partitions (i.e., N_{11} shown as full blue cells), (ii) belong to the same subgroup in one partition and a different subgroup in the other partition (i.e., $N_{01} + N_{10}$ shown as divided blue and gray cells), and (iii) belong to different subgroups in both partitions (i.e., N_{00} shown as full gray cells). (C) Finally, $N_{11}(\mathcal{H})/(N_{01}(\mathcal{H}) + N_{10}(\mathcal{H}) + N_{11}(\mathcal{H}))$ is computed per subgroup (\mathcal{H}) and averaged across all subgroups to obtain the Jaccard SSI.

Prediction accuracy of student model. First, researchers can assess how well the student model fits the teacher model’s estimated CATEs. We quantify this via the prediction accuracy (e.g., root mean squared error (RMSE)) between the student model predictions and the CATEs, estimated by the teacher model. High concordance between the student model predictions and the teacher model CATEs is a positive sign while low concordance suggests that the student model is not compatible or a good proxy for the teacher model and should lower our degree of trust in the student model’s estimated subgroups.

Distribution of teacher-estimated CATEs. Secondly, researchers can quantify and visualize the variance or distribution of CATEs, estimated by the teacher model, in each decision tree split in the student model. This is important for understanding both how much heterogeneity occurs within each subgroup (or node) and how much the subgroup CATEs (i.e., the mean CATE per node) change after making each split. A good split (or decision rule) will result in a large change in the mean subgroup CATE and low heterogeneity within the resulting subgroups. In contrast, splits that do not substantively change the mean subgroup CATE nor reduce the amount of heterogeneity within the subgroups can be deemed as uninformative and unnecessary splits.

Number of treated and control units per subgroup. Thirdly, we recommend reporting the number of treated and control units from the training data that fall in each subgroup. Since the student model only uses X to predict the teacher-estimated CATEs, it is possible that only control or only treated units fall into a student-estimated subgroup. If the training and estimation data splits (i.e., D^{train} and D^{est} from Algorithm 2) are from similar populations, then the estimation data split may similarly yield only control or only treated units (or some highly imbalanced ratio of treated-to-control units) in that subgroup. In these cases, estimation of the subgroup ATE would be highly variable or not possible using (6). It may also suggest that the tree has been grown too deep and that there is currently not sufficient sample size to estimate such a subgroup.

Stability of selected features. Finally, in addition to evaluating the subgroup Jaccard stability across the different bootstrap samples in Algorithm 1, we can also track the selected features across these bootstraps for each chosen tree depth and plot their distribution (e.g., Figures A9-A14). Similar to the subgroup Jaccard stability, a more stable (or homogeneous) distribution of

selected features should elucidate greater trust in that model or tree depth. On the flip side, a very heterogeneous distribution of selected features indicates that the estimated decision tree structure is highly volatile, depending heavily on the training data subset.

B Proofs and Derivations

B.1 Proof of Proposition 3.1

Proof: We can re-write the difference in $\hat{\mathcal{G}}_1(X_i)$ and $\mathcal{G}_1(X_i)$ as:

$$\begin{aligned} \mathbb{E} \left[\left| \hat{\mathcal{G}}_1(X_i) - \mathcal{G}_1(X_i) \right| \right] &= \mathbb{E} \left[\left| \mathbb{1}\{X_i \leq \hat{s}_n\} - \mathbb{1}\{X_i \leq s\} \right| \right] \\ &= \mathbb{E} \left[\mathbb{1}\{X_i \leq \hat{s}_n\} - \mathbb{1}\{X_i \leq s\} \mid \hat{s}_n > s \right] \Pr(\hat{s}_n > s) \\ &\quad + \mathbb{E} \left[\mathbb{1}\{X_i \leq s\} - \mathbb{1}\{X_i \leq \hat{s}_n\} \mid \hat{s}_n \leq s \right] \Pr(\hat{s}_n \leq s) \\ &= 2 \left| \mathbb{E} \left[\mathbb{1}\{X_i \leq \hat{s}_n\} - \mathbb{1}\{X_i \leq s\} \right] \right| \\ &= 2 \left| F_X(\hat{s}_n) - F_X(s) \right| \end{aligned}$$

Because F_X is continuously differentiable by Assumption (1), there must exist a positive, real-valued constant M such that $f_X(x) \leq M < \infty$:

$$\leq 2M |\hat{s}_n - s|.$$

Then, applying the results from Escanciano (2020) and Banerjee and McKeague (2007):

$$\mathbb{E} \left[\left| \hat{\mathcal{G}}_1(X_i) - \mathcal{G}_1(X_i) \right| \right] = O_p(n^{-1/2(\alpha-\eta)}).$$

□

B.2 Proof of Theorem 3.1

To prove Theorem 3.1, we will use two useful lemmas. Lemma B.1 states that the sample loss function will converge in probability to the population-level loss.

Lemma B.1 (Bounded Loss) *Without loss of generality, assume $s_n^{(k)} < s$. Then for $k \in \{1, \dots, p\}$:*

$$\left| \mathbb{E}_n \left[\ell(\hat{\tau}_i^d; X^{(k)}; \hat{s}_n^{(k)}) \right] - \mathbb{E} \left[\ell(\hat{\tau}_i^d; X^{(k)}, s^{(k)}) \right] \right| \leq C_\tau^{(k)} \times \left| \hat{s}_n^{(k)} - s^{(k)} \right| + \left| \mathbb{E}_n \left[\ell(\hat{\tau}_i^d; X, s) \right] - \mathbb{E} \left[\ell(\hat{\tau}_i^d; X, s) \right] \right|$$

where $C_\tau^{(k)} = 2 \max_{c \in [\hat{s}_n^{(k)}, s^{(k)}]} \mathbb{E}(\hat{\tau}_i^d \mid X_i^{(k)} < c) \times \mathbb{E}_n \left| \tau^d(X_i^{(k)}; \hat{s}_n^{(k)}) - \hat{\tau}_i^d \right|$.

An immediate implication of Lemma B.1 is that the within-sample loss at the sample-optimal split \hat{s}_n will converge in probability to the population-level loss at the population-optimal split point s .

Lemma B.2 *Let $X^{(a)}$ be a relevant covariate that has been omitted, whereas $X^{(b)}$ is an irrelevant covariate, erroneously chosen. We can upper bound the probability of the within-sample loss for an irrelevant covariate $X^{(b)}$ being less than a relevant covariate $X^{(a)}$:*

$$\begin{aligned} \Pr \left[\mathbb{E}_n \left\{ \ell(\hat{\tau}_i^d; X^{(b)}, \hat{s}_n^{(b)}) \right\} < \mathbb{E}_n \left\{ \ell(\hat{\tau}_i^d; X^{(a)}, \hat{s}_n^{(a)}) \right\} \right] \\ \leq \frac{2}{\delta_{ba}} \mathbb{E} \left[\left| \mathbb{E}_n \left\{ \ell(\hat{\tau}_i^d; X^{(a)}, \hat{s}_n^{(a)}) \right\} - \mathbb{E} \left\{ \ell(\hat{\tau}_i^d; X^{(a)}, s^{(a)}) \right\} \right| \right], \end{aligned}$$

where $\delta_{ba} := \mathbb{E} \left\{ \ell(\hat{\tau}_i^d; X^{(b)}, s^{(b)}) \right\} - \mathbb{E} \left\{ \ell(\hat{\tau}_i^d; X^{(a)}, s^{(a)}) \right\}$.

Intuitively, if the *population-level* losses between an irrelevant and relevant covariate is relatively small (i.e., δ_{ba} is small), then it will take longer for the upper bound to approach zero.

We can now prove Theorem 3.1. Let $s^{(k)}$ be the population-level optimal split for covariate k and $\hat{s}_n^{(k)}$ be the estimated optimal split for covariate k using a sample size of n .

Simple Case: Single rule. We consider the simple setting in which there is a single rule. Assume $X^{(a)}$ is the covariate that the estimated subgroup chooses to construct a rule with, while $X^{(b)}$ is the covariate that the true subgroup uses to construct a rule. We can bound the difference between the estimated and optimal subgroup:

$$\begin{aligned} \mathbb{E} \left[\left| \hat{\mathcal{G}}_1(X) - \mathcal{G}_1(X) \right| \right] \\ = \mathbb{E} \left[\left| \mathbb{1}\{X^{(a)} < \hat{s}_n^{(a)}\} - \mathbb{1}\{X^{(b)} < s^{(b)}\} \right| \right] \end{aligned}$$

$$\leq \underbrace{\mathbb{E} \left[\left| \mathbb{1}\{X^{(a)} < \hat{s}_n^{(a)}\} - \mathbb{1}\{X^{(b)} < \hat{s}_n^{(b)}\} \right| \right]}_{(1)} + \underbrace{\mathbb{E} \left[\left| \mathbb{1}\{X^{(b)} < \hat{s}_n^{(b)}\} - \mathbb{1}\{X^{(b)} < s^{(b)}\} \right| \right]}_{(2)} \quad (10)$$

First, consider Equation (10)-(1):

$$\begin{aligned} & \mathbb{E} \left[\left| \mathbb{1}\{X^{(a)} < \hat{s}_n^{(a)}\} - \mathbb{1}\{X^{(b)} < \hat{s}_n^{(b)}\} \right| \right] \\ &= \mathbb{E} \left[\left| \mathbb{1}\{X^{(a)} < \hat{s}_n^{(a)}\} - \mathbb{1}\{X^{(b)} < \hat{s}_n^{(b)}\} \mid X^{(a)} \neq X^{(b)} \right| \right] \Pr(X^{(a)} \neq X^{(b)}) \\ &= \mathbb{E} \left[\left| \mathbb{1}\{X^{(a)} < \hat{s}_n^{(a)}\} - \mathbb{1}\{X^{(b)} < \hat{s}_n^{(b)}\} \mid X^{(a)} \neq X^{(b)} \right| \right] \\ &\quad \times \Pr \left[\mathbb{E}_n \left\{ \ell(\hat{\tau}_i^d; X^{(a)}, \hat{s}_n^{(a)}) \right\} < \mathbb{E}_n \left\{ \ell(\hat{\tau}_i^d; X^{(b)}, \hat{s}_n^{(b)}) \right\} \right] \\ &\leq \Pr \left[\mathbb{E}_n \left\{ \ell(\hat{\tau}_i^d; X^{(a)}, \hat{s}_n^{(a)}) \right\} < \mathbb{E}_n \left\{ \ell(\hat{\tau}_i^d; X^{(b)}, \hat{s}_n^{(b)}) \right\} \right], \end{aligned}$$

where the first equality follows from Law of Total Expectation, and the second equality follows from noting that the covariate chosen for the first split will differ from the population-level split covariate if the within-sample loss for covariate $X^{(a)}$ is lower than the within-sample loss for covariate $X^{(b)}$. The final inequality follows from the fact that $\mathbb{E} \left[\left| \mathbb{1}\{X^{(a)} < \hat{s}_n^{(a)}\} - \mathbb{1}\{X^{(b)} < \hat{s}_n^{(b)}\} \mid X^{(a)} \neq X^{(b)} \right| \right]$ must be bounded between 0 and 1. In settings when $X^{(a)}$ and $X^{(b)}$ are very correlated, then it could be the case that in fact, $\mathbb{E} \left[\left| \mathbb{1}\{X^{(a)} < \hat{s}_n^{(a)}\} - \mathbb{1}\{X^{(b)} < \hat{s}_n^{(b)}\} \mid X^{(a)} \neq X^{(b)} \right| \right]$ is quite close to zero as the set of units for whom $\mathbb{1}\{X^{(a)} < \hat{s}_n^{(a)}\}$ and $\mathbb{1}\{X^{(b)} < \hat{s}_n^{(b)}\}$ may be quite similar.

Equation (10)-(2) can be bounded by applying the results from Proposition 3.1:

$$\mathbb{E} \left[\left| \mathbb{1}\{X^{(b)} < \hat{s}_n^{(b)}\} - \mathbb{1}\{X^{(b)} < s^{(b)}\} \right| \right] \leq 2M \left| \hat{s}_n^{(b)} - s^{(b)} \right|,$$

for some constant $M > 0$.

Extending to r total rules: For $k = 1, \dots, r$, assume $X^{(a_k)}$ is the covariate that the estimated subgroup chooses to construct a rule with at the k^{th} step, while $X^{(b_k)}$ is the covariate that the true subgroup uses to construct a rule at the k^{th} step.

$$\begin{aligned} & \mathbb{E} \left[\left| \prod_{k=1}^r \mathbb{1}\{X^{(a_k)} < \hat{s}_n^{(a_k)}\} - \prod_{k=1}^r \mathbb{1}\{X^{(b_k)} < \hat{s}_n^{(b_k)}\} \right| \right] \\ &\leq \Pr(X^{(a_1)} \neq X^{(b_1)}) + \Pr(X^{(a_1)} = X^{(b_1)}) \cdot \Pr(X^{(a_2)} \neq X^{(b_2)} \mid X^{(a_1)} = X^{(b_1)}) + \dots \end{aligned}$$

$$\begin{aligned}
& + \Pr(X^{(a_1)} = X^{(b_1)}, \dots, \Pr(X^{(a_{r-1})} = X^{(b_{r-1})})) \Pr(X^{(a_r)} \neq X^{(b_r)} \mid X^{(a_1)} = X^{(b_1)}, \dots, X^{(a_{r-1})} = X^{(b_{r-1})}) \\
& \leq \sum_{k=1}^r \Pr \left[\mathbb{E}_n \left\{ \ell(\hat{\tau}_i^d; X^{(a_k)}, \hat{s}_n^{(a_k)}) \right\} < \mathbb{E}_n \left\{ \ell(\hat{\tau}_i^d; X^{(b_k)}, \hat{s}_n^{(b_k)}) \right\} \right] + 2M \left| \hat{s}_n^{(b_k)} - s^{(b_k)} \right|
\end{aligned}$$

Let $k^* := \arg \max_{k'} \left| \hat{s}_n^{(k')} - s^{(k')} \right| + \mathbb{E}_n \left[\ell(\hat{\tau}_i^d; X^{(k')}, s^{(k')}) \right] - \mathbb{E} \left[\ell(\hat{\tau}_i^d; X^{(k')}, s^{(k')}) \right]$, and $\delta = \min \delta_{ba}$.

Applying Lemma B.1 and B.2:

$$\begin{aligned}
& \leq \frac{2r}{\delta} \mathbb{E} \left\{ \left| \mathbb{E}_n \left[\ell(\hat{\tau}_i^d; X^{(k^*)}, \hat{s}_n^{(k^*)}) \right] - \mathbb{E} \left[\ell(\hat{\tau}_i^d; X^{(k^*)}, s^{(k^*)}) \right] \right| \right\} + 2Mr \left| \hat{s}_n^{(k^*)} - s^{(k^*)} \right| \\
& \leq \frac{2rC_\tau}{\delta} \left| \hat{s}_n^{(k^*)} - s^{(k^*)} \right| + \frac{2r}{\delta} \left(\mathbb{E}_n \left[\ell(\hat{\tau}_i^d; X^{(k^*)}, s^{(k^*)}) \right] - \mathbb{E} \left[\ell(\hat{\tau}_i^d; X^{(k^*)}, s^{(k^*)}) \right] \right) + 2Mr \left| \hat{s}_n^{(k^*)} - s^{(k^*)} \right| \\
& = \underbrace{\frac{2r(C_\tau + M\delta)}{\delta} \left| \hat{s}_n^{(k^*)} - s^{(k^*)} \right|}_{(1)} + \underbrace{\frac{2r}{\delta} \left\{ \mathbb{E}_n \left[\ell(\hat{\tau}_i^d; X^{(k^*)}, s^{(k^*)}) \right] - \mathbb{E} \left[\ell(\hat{\tau}_i^d; X^{(k^*)}, s^{(k^*)}) \right] \right\}}_{(2)}.
\end{aligned}$$

Term (1) represents the gap between an estimated split and true optimal split. Term (2) is the gap between the empirical loss and the population-level loss. From Proposition 3.1, term (1) converges to zero at rate $O_p(n^{-1/2(\alpha-\eta)})$. All that remains is to show that the second term also converges to zero.

To begin, we re-write term (2) as:

$$\begin{aligned}
& \mathbb{E}_n \left[\ell(\hat{\tau}_i^d; X, s) \right] - \mathbb{E} \left[\ell(\hat{\tau}_i^d; X, s) \right] \\
& = \mathbb{E}_n \left\{ \left(\hat{\tau}_i^d \right)^2 \right\} - 2\mathbb{E}_n \left\{ \hat{\tau}_i^d \cdot \hat{\tau}^d(X_i, s) \right\} + \mathbb{E}_n \left\{ \hat{\tau}^d(X_i, s)^2 \right\} - \left[\mathbb{E} \left\{ \left(\hat{\tau}_i^d \right)^2 \right\} - 2\mathbb{E} \left\{ \hat{\tau}_i^d \cdot \tau^d(X_i, s) \right\} + \mathbb{E} \left\{ \tau^d(X_i, s)^2 \right\} \right]
\end{aligned}$$

where $\hat{\tau}^d(X_i, s) := \mathbb{1}\{X_i \leq s\} \mathbb{E}_n(\hat{\tau}_i^d \mid X_i \leq s) + \mathbb{1}\{X_i > s\} \mathbb{E}_n(\hat{\tau}_i^d \mid X_i > s)$ is the sample analog to $\tau^d(X, s)$. Then:

$$= \underbrace{\mathbb{E}_n \left\{ \left(\hat{\tau}_i^d \right)^2 \right\} - \mathbb{E} \left\{ \left(\hat{\tau}_i^d \right)^2 \right\}}_{(a)} - \underbrace{\left[\mathbb{E}_n \left\{ \hat{\tau}^d(X_i, s)^2 \right\} - \mathbb{E} \left\{ \tau^d(X_i, s)^2 \right\} \right]}_{(b)}.$$

We will now tackle each term. For term (a), we can directly apply Chebyshev's Inequality, where for $c > 0$:

$$\Pr \left(\left| \mathbb{E}_n \left\{ \left(\hat{\tau}_i^d \right)^2 \right\} - \mathbb{E} \left\{ \left(\hat{\tau}_i^d \right)^2 \right\} \right| \geq \frac{c}{2r} \right) \leq \frac{4M_4r^2}{nc^2},$$

where the inequality follows from the assumption of bounded 4th moment. Then, taking $c = 2\sqrt{3M_4rt}/\sqrt{n}$:

$$\Pr \left(\left| \mathbb{E}_n \left\{ (\hat{\tau}_i^d)^2 \right\} - \mathbb{E} \left\{ (\hat{\tau}_i^d)^2 \right\} \right| \geq \frac{\sqrt{3M_4t}}{\sqrt{n}} \right) \leq \frac{1}{3t^2}.$$

For term (b):

$$\begin{aligned} & \mathbb{E}_n \left\{ \hat{\tau}^d(X_i; s)^2 \right\} - \mathbb{E} \left\{ \tau^d(X_i; s)^2 \right\} \\ &= \mathbb{E}_n [\mathbb{1} \{X_i \leq s\}] \cdot \mathbb{E}_n(\hat{\tau}_i^d | X_i \leq s)^2 + \mathbb{E}_n [\mathbb{1} \{X_i > s\}] \cdot \mathbb{E}_n(\hat{\tau}_i^d | X_i > s)^2 \\ & \quad - \left(\mathbb{E} [\mathbb{1} \{X_i \leq s\}] \cdot \mathbb{E}(\hat{\tau}_i^d | X_i \leq s)^2 + \mathbb{E} [\mathbb{1} \{X_i > s\}] \cdot \mathbb{E}(\hat{\tau}_i^d | X_i > s)^2 \right) \\ &= (\mathbb{E}_n [\mathbb{1} \{X_i \leq s\}] - \mathbb{E} [\mathbb{1} \{X_i \leq s\}]) \cdot \mathbb{E}_n(\hat{\tau}_i^d | X_i \leq s)^2 + (\mathbb{E}_n [\mathbb{1} \{X_i > s\}] - \mathbb{E} [\mathbb{1} \{X_i > s\}]) \cdot \mathbb{E}_n(\hat{\tau}_i^d | X_i > s)^2 \\ & \quad - \left(\mathbb{E} [\mathbb{1} \{X_i \leq s\}] \cdot \left\{ \mathbb{E}(\hat{\tau}_i^d | X_i \leq s)^2 - \mathbb{E}_n(\hat{\tau}_i^d | X_i \leq s)^2 \right\} + \right. \\ & \quad \left. \mathbb{E} [\mathbb{1} \{X_i > s\}] \cdot \left\{ \mathbb{E}(\hat{\tau}_i^d | X_i > s)^2 - \mathbb{E}_n(\hat{\tau}_i^d | X_i > s)^2 \right\} \right) \end{aligned}$$

Let $p_n(s) = \mathbb{E}_n [\mathbb{1} \{X_i \leq s\}]$, and define $M_1 = \max_i \hat{\tau}_i^d$. Then:

$$\begin{aligned} & \leq 2 |p_n(s) - p(s)| \cdot M_1^2 + p(s) \cdot \left| \mathbb{E}(\hat{\tau}_i^d | X_i \leq s)^2 - \mathbb{E}_n(\hat{\tau}_i^d | X_i \leq s)^2 \right| \\ & \quad + (1 - p(s)) \cdot \left| \mathbb{E}(\hat{\tau}_i^d | X_i > s)^2 - \mathbb{E}_n(\hat{\tau}_i^d | X_i > s)^2 \right|. \end{aligned}$$

Then, applying Chebyshev's inequality again, for all $c > 0$:

$$\Pr \left(\left| \mathbb{E}_n [\mathbb{1} \{X_i \leq s\}] - \mathbb{E} [\mathbb{1} \{X_i \leq s\}] \right| \geq \frac{c}{4M_1^2r} \right) \leq \frac{16p_n(s) \cdot (1 - p_n(s)) \cdot M_1^2r}{nc^2} \leq \frac{4M_1^2r}{nc^2},$$

where $M_1 < \infty$ is a constant, by the bounded first moment assumption.

Setting $c = \sqrt{12rt}M_1/\sqrt{n}$:

$$\Pr \left(\left| \mathbb{E}_n [\mathbb{1} \{X_i \leq s\}] - \mathbb{E} [\mathbb{1} \{X_i \leq s\}] \right| \geq \frac{\sqrt{12t}}{4M_1\sqrt{rn}} \right) \leq \frac{1}{3t^2}.$$

For the second piece, note the following:

$$\left| \mathbb{E}(\hat{\tau}_i^d | X_i \leq s)^2 - \mathbb{E}_n(\hat{\tau}_i^d | X_i \leq s)^2 \right| \leq 2 \left| \mathbb{E}(\hat{\tau}_i^d | X_i \leq s) \cdot \left\{ \mathbb{E}_n(\hat{\tau}_i^d | X_i \leq s) - \mathbb{E}(\hat{\tau}_i^d | X_i \leq s) \right\} \right| +$$

$$\begin{aligned}
& \left| \left\{ \mathbb{E}_n(\hat{\tau}_i^d \mid X_i \leq s) - \mathbb{E}(\hat{\tau}_i^d \mid X_i \leq s) \right\}^2 \right| \\
& \leq 2M_1 \left| \left\{ \mathbb{E}_n(\hat{\tau}_i^d \mid X_i \leq s) - \mathbb{E}(\hat{\tau}_i^d \mid X_i \leq s) \right\} \right| + \\
& \quad \left| \left\{ \mathbb{E}_n(\hat{\tau}_i^d \mid X_i \leq s) - \mathbb{E}(\hat{\tau}_i^d \mid X_i \leq s) \right\}^2 \right|.
\end{aligned}$$

Then for $c_1 > 0$ and $c_2 > 0$

$$\begin{aligned}
& \Pr \left(\left| \mathbb{E}_n(\hat{\tau}_i^d \mid X_i \leq s) - \mathbb{E}(\hat{\tau}_i^d \mid X_i \leq s) \right| \geq \frac{c_1}{2M_1 r} \right) \leq \frac{4M_1^2 r^2 \cdot M_2}{c_1^2 n}, \\
& \text{and } \Pr \left(\left| \left\{ \mathbb{E}_n(\hat{\tau}_i^d \mid X_i \leq s) - \mathbb{E}(\hat{\tau}_i^d \mid X_i \leq s) \right\}^2 \right| \geq c_2 \right) \leq \frac{M_2}{c_2 n}.
\end{aligned}$$

Once again, taking $c_1 = \frac{2\sqrt{3}M_1 r t \sqrt{M_2}}{\sqrt{n}}$ and $c_2 = \frac{M_2 t}{n}$:

$$\begin{aligned}
& \Pr \left(\left| \mathbb{E}_n(\hat{\tau}_i^d \mid X_i \leq s) - \mathbb{E}(\hat{\tau}_i^d \mid X_i \leq s) \right| \geq \frac{t\sqrt{3M_2}}{\sqrt{n}} \right) \leq \frac{1}{3t^2}, \\
& \text{and } \Pr \left(\left| \left\{ \mathbb{E}_n(\hat{\tau}_i^d \mid X_i \leq s) - \mathbb{E}(\hat{\tau}_i^d \mid X_i \leq s) \right\}^2 \right| \geq \frac{M_2 t}{n} \right) \leq \frac{1}{t}.
\end{aligned}$$

Combining together, with probability $1 - 1/t - 1/t^2$:

$$\left| \mathbb{E}_n \left[\ell(\hat{\tau}_i^d; X^{(k^*)}, s^{(k^*)}) \right] - \mathbb{E} \left[\ell(\hat{\tau}_i^d; X^{(k^*)}, s^{(k^*)}) \right] \right| \leq \frac{K_1}{\sqrt{n}} + \frac{K_2}{n},$$

where K_1 and K_2 are functions of t and the constants M_1 , M_2 , and M_4 .

B.3 Proof of Theorem 3.2

To prove Theorem 3.2, we will introduce a lemma that will be helpful in the following derivation. We define n_g as the total number of units in a subgroup g , and $n_g(1) = \sum_{i=1}^n \hat{G}_g(X_i) Z_i$ - i.e., $n_g(1)$ is equal to the number of units in subgroup g who are treated. We similarly define $n_g(0)$ as the number of units in subgroup g who are not treated.

Assumption B.1 (Assignment Symmetry (Miratrix et al., 2013))

1. *Equiprobable treatment assignment patterns. For each subgroup $g \in \{1, \dots, G\}$, all $\binom{n_g}{n_g(1)}$ combination of ways to treat $n_g(1)$ units are equiprobable, given the subgroup size n_g .*

2. *Independent treatment assignment patterns: for all subgroups g, g' , the treatment assignment process in group g is independent of the treatment assignment process in group g' , given $n_g(1)$ and $n_{g'}(1)$.*

We are considering designs that satisfy assignment symmetry. For example, experimental designs such as complete randomization, Bernoulli randomization, or blocking with independent treatment assignment across blocks, would satisfy assignment symmetry. However, cluster randomization would not satisfy assignment symmetry. Furthermore, we do not account for settings in which some units within a subgroup are more likely to receive treatment.

Lemma B.3 (Implications of Assignment Symmetry) *Under Assumption (B.1), we have assumed that conditional on the number of units within a subgroup $g \in \{1, \dots, G\}$, the probability of receiving treatment for units in a subgroup is equiprobable and independent:*

$$\mathbb{E}\{Z_i \mid n_g(1)\} = \frac{n_g(1)}{n_g} \equiv \frac{1}{n_g} \sum_{i=1}^n \hat{\mathcal{G}}_g(X_i) Z_i, \text{ and } \mathbb{E}\{Z_i Z_j \mid n_g(1) = a\} = \frac{a(a-1)}{n_g(n_g-1)} \quad (11)$$

We can then derive the distribution of $Z_i/n_g(1)$:

- $\mathbb{E}\left[\frac{Z_i}{n_g(1)}\right] = \frac{1}{n_g}$
- $\mathbb{E}\left[\frac{Z_i^2}{n_g(1)^2}\right] = \frac{1}{n_g} \mathbb{E}\left[\frac{1}{n_g(1)}\right]$
- $\mathbb{E}\left[\frac{Z_i Z_j}{n_g(1)^2}\right] = \frac{1}{n_g(n_g-1)} \mathbb{E}\left[\frac{n_g(1)-1}{n_g(1)}\right] = \frac{1}{n_g(n_g-1)} \left(1 - \mathbb{E}\left[\frac{1}{n_g(1)}\right]\right)$
- $\mathbb{E}\left[\frac{Z_i(1-Z_j)}{n_g(1)n_g(0)}\right] = \frac{1}{n_g \cdot (n_g-1)} \cdot \mathbb{E}\left[\frac{n_g - n_g(1)}{n_g(0)}\right] = \frac{1}{n_g \cdot (n_g-1)}$

The results of Lemma B.3 follow directly from first noting that conditional on the number of units in each subgroup g , randomization within a subgroup can be viewed as complete randomization, and then applying law of iterated expectations.

To begin, we can take the expectation of $\hat{\tau}^{(g)}$ to show that it is a function of $\mathbb{E}(\tau_i \mid \hat{\mathcal{G}}_g(X_i) = 1)$.

$$\begin{aligned} \mathbb{E}\left(\hat{\tau}^{(g)}\right) &= \mathbb{E}\left\{\frac{1}{\sum_{i=1}^n Z_i \hat{\mathcal{G}}_g(X_i)} \sum_{i=1}^n Z_i Y_i \hat{\mathcal{G}}_g(X_i) - \frac{1}{\sum_{i=1}^n (1-Z_i) \hat{\mathcal{G}}_g(X_i)} \sum_{i=1}^n (1-Z_i) Y_i \hat{\mathcal{G}}_g(X_i)\right\} \\ &= \sum_{i=1}^n \mathbb{E}\left\{\frac{Z_i}{\sum_{i=1}^n Z_i \hat{\mathcal{G}}_g(X_i)}\right\} Y_i(1) \hat{\mathcal{G}}_g(X_i) - \mathbb{E}\left\{\frac{1-Z_i}{\sum_{i=1}^n (1-Z_i) \hat{\mathcal{G}}_g(X_i)}\right\} Y_i(0) \hat{\mathcal{G}}_g(X_i) \end{aligned}$$

Under Assumption (B.1) (Assignment Symmetry), we can apply the results from Lemma B.3:

$$= \frac{1}{n_g} \sum_{i=1}^n \hat{\mathcal{G}}_g(X_i) \{Y_i(1) - Y_i(0)\} \quad (12)$$

As such:

$$\begin{aligned} \left| \mathbb{E}(\hat{\tau}^{(g)}) - \tau^{(g)} \right| &= \left| \frac{1}{n_g} \sum_{i=1}^n \hat{\mathcal{G}}_g(X_i) \{Y_i(1) - Y_i(0)\} - \frac{1}{n_g} \sum_{i=1}^n \mathcal{G}_g(X_i) \{Y_i(1) - Y_i(0)\} \right| \\ &= \left| \frac{1}{n_g} \sum_{i=1}^n \{ \hat{\mathcal{G}}_g(X_i) - \mathcal{G}_g(X_i) \} \{Y_i(1) - Y_i(0)\} \right| \\ &\leq \frac{1}{n_g} \sum_{i=1}^n \left| \hat{\mathcal{G}}_g(X_i) - \mathcal{G}_g(X_i) \right| \left| Y_i(1) - Y_i(0) \right|, \end{aligned}$$

From Theorem 3.1, we know that $\left| \hat{\mathcal{G}}_g(X_i) - \mathcal{G}_g(X_i) \right| \xrightarrow{p} 0$.

Part 2. Variance derivation. To derive the variance of the subgroup difference-in-means estimator, we apply results from Miratrix et al. (2013), who derives the variance of a post-stratification estimator. We can extend the results by treating each subgroup as a strata, where the subgroup difference-in-means estimator is analogous to the difference-in-means estimator across a specific strata. We provide the full derivation for completeness.

Proof:

$$\begin{aligned} \text{var}(\hat{\tau}^{(g)}) &= \text{var} \left\{ \frac{1}{\sum_{i=1}^n \hat{\mathcal{G}}_g(X_i) Z_i} \sum_{i=1}^n \hat{\mathcal{G}}_g(X_i) Z_i Y_i - \frac{1}{\sum_{i=1}^n \hat{\mathcal{G}}_g(X_i) (1 - Z_i)} \sum_{i=1}^n \hat{\mathcal{G}}_g(X_i) (1 - Z_i) Y_i \right\} \\ &= \text{var} \left\{ \frac{1}{n_g(1)} \sum_{i: \hat{\mathcal{G}}_g(X_i)=1} Z_i Y_i(1) - \frac{1}{n_g(0)} \sum_{i: \hat{\mathcal{G}}_g(X_i)=1} (1 - Z_i) Y_i(0) \right\} \\ &= \underbrace{\text{var} \left\{ \frac{1}{n_g(1)} \sum_{i: \hat{\mathcal{G}}_g(X_i)=1} Z_i Y_i(1) \right\}}_{(1)} + \underbrace{\text{var} \left\{ \frac{1}{n_g(0)} \sum_{i: \hat{\mathcal{G}}_g(X_i)=1} (1 - Z_i) Y_i(0) \right\}}_{(2)} \\ &\quad - 2 \underbrace{\text{cov} \left\{ \frac{1}{n_g(1)} \sum_{i: \hat{\mathcal{G}}_g(X_i)=1} Z_i Y_i(1), \frac{1}{n_g(0)} \sum_{i: \hat{\mathcal{G}}_g(X_i)=1} (1 - Z_i) Y_i(0) \right\}}_{(3)} \end{aligned} \quad (13)$$

Beginning with term (1):

$$\begin{aligned}
& \text{var} \left\{ \frac{1}{n_g(1)} \sum_{i:\hat{\mathcal{G}}_g(X_i)=1} Z_i Y_i(1) \right\} \tag{14} \\
&= \sum_{i,j:\hat{\mathcal{G}}_g(X)=1} \text{cov} \left(\frac{Z_i}{n_g(1)} Y_i(1), \frac{Z_j}{n_g(1)} Y_j(1) \right) \\
&= \sum_{i:\hat{\mathcal{G}}_g(X_i)=1} \left[\text{var} \left\{ \frac{Z_i}{n_g(1)} Y_i(1) \right\} + \sum_{i \neq j} \text{cov} \left\{ \frac{Z_i}{n_g(1)} Y_i(1), \frac{Z_j}{n_g(1)} Y_j(1) \right\} \right] \\
&= \sum_{i:\hat{\mathcal{G}}_g(X_i)=1} \left[\frac{1}{n_g} \mathbb{E} \left\{ \frac{1}{n_g(1)} \right\} Y_i(1)^2 - \frac{1}{n_g^2} Y_i(1)^2 \right] + \\
& \sum_{i \neq j} \frac{1}{n_g} \cdot \frac{1}{n_g - 1} \cdot \left(1 - \mathbb{E} \left\{ \frac{1}{n_g(1)} \right\} \right) Y_i(1) Y_j(1) - \frac{1}{n_g^2} Y_i(1) Y_j(1) \\
&= \frac{1}{n_g} \sum_{i:\hat{\mathcal{G}}_g(X_i)=1} \left(\mathbb{E} \left\{ \frac{1}{n_g(1)} \right\} - \frac{1}{n_g} \right) Y_i(1)^2 + \frac{1}{n_g} \sum_{i \neq j:\hat{\mathcal{G}}_g(X)=1} \left(\frac{1}{n_g - 1} \left(1 - \mathbb{E} \left\{ \frac{1}{n_g(1)} \right\} \right) - \frac{1}{n_g} \right) Y_i(1) Y_j(1)
\end{aligned}$$

Let $\tilde{\beta}_g(z) := \mathbb{E}\{1/n_g(1)\}$:

$$\begin{aligned}
&= \frac{1}{n_g} \sum_{i:\hat{\mathcal{G}}_g(X_i)=1} \left[\left\{ \tilde{\beta}_g(1) - \frac{1}{n_g} \right\} Y_i(1)^2 - \frac{1}{n_g - 1} \sum_{i \neq j} \left\{ \beta_g(1) - \frac{1}{n_g} \right\} Y_i(1) Y_j(1) \right] \\
&= \left\{ \tilde{\beta}_g(1) - \frac{1}{n_g} \right\} \cdot \frac{1}{n_g} \sum_{i:\hat{\mathcal{G}}_g(X_i)=1} \left[Y_i(1)^2 - \sum_{i \neq j} Y_i(1) Y_j(1) \right] \\
&= \left\{ \tilde{\beta}_g(1) - \frac{1}{n_g} \right\} \text{var}_g \{ Y_i(1) \} \tag{15}
\end{aligned}$$

We can similarly show term (2) can be rewritten as:

$$\text{var} \left\{ \frac{1}{n_g(0)} \sum_{i:\hat{\mathcal{G}}_g(X_i)=1} (1 - Z_i) Y_i(0) \right\} = \left\{ \beta_g(0) - \frac{1}{n_g} \right\} \text{var}_g \{ Y_i(0) \}. \tag{16}$$

Finally, to derive an expression for term (3), we begin by noting the following:

$$\mathbb{E} \left[\left\{ \frac{1}{n_g(1)} \sum_{i:\hat{\mathcal{G}}_g(X_i)=1} Z_i Y_i(1) \right\} \left\{ \frac{1}{n_g(0)} \sum_{i:\hat{\mathcal{G}}_g(X_i)=1} (1 - Z_i) Y_i(0) \right\} \right]$$

$$= \mathbb{E} \left\{ \frac{1}{n_g(1) \cdot n_g(0)} \sum_{i:\hat{\mathcal{G}}_g(X_i)=1} Z_i(1 - Z_i)Y_i(1)Y_i(0) + \sum_{i \neq j} Z_i(1 - Z_j)Y_i(1)Y_j(0) \right\}$$

Because $Z_i \cdot (1 - Z_i) = 0$:

$$\begin{aligned} &= \mathbb{E} \left\{ \frac{1}{n_g(1) \cdot n_g(0)} \sum_{i:\hat{\mathcal{G}}_g(X_i)=1} \sum_{i \neq j} Z_i(1 - Z_j)Y_i(1)Y_j(0) \right\} \\ &= \frac{1}{n_g \cdot (n_g - 1)} \sum_{i:\hat{\mathcal{G}}_g(X_i)=1} \sum_{i \neq j} Y_i(1)Y_j(0) \end{aligned}$$

Then, we can re-write term (3) as:

$$\begin{aligned} &\text{cov} \left\{ \frac{1}{n_g(1)} \sum_{i:\hat{\mathcal{G}}_g(X_i)=1} Z_i Y_i(1), \frac{1}{n_g(0)} \sum_{i:\hat{\mathcal{G}}_g(X_i)=1} (1 - Z_i) Y_i(0), \right\} \\ &= \frac{1}{n_g} \frac{1}{n_g - 1} \sum_{i:\hat{\mathcal{G}}_g(X_i)=1} \sum_{i \neq j} Y_i(1)Y_j(0) - \left\{ \frac{1}{n_g} \sum_{i:\hat{\mathcal{G}}_g(X_i)=1} Y_i(1) \right\} \cdot \left\{ \frac{1}{n_g} \sum_{i:\hat{\mathcal{G}}_g(X_i)=1} Y_i(0) \right\} \\ &= \frac{1}{n_g} \frac{1}{n_g - 1} \sum_{i:\hat{\mathcal{G}}_g(X_i)=1} \sum_{i \neq j} Y_i(1)Y_j(0) - \left[\frac{1}{n_g^2} \sum_{i:\hat{\mathcal{G}}_g(X_i)=1} \left\{ Y_i(1)Y_i(0) + \sum_{i \neq j} Y_i(1)Y_j(0) \right\} \right] \\ &= \frac{1}{n_g} \left(\sum_{i:\hat{\mathcal{G}}_g(X_i)} \frac{1}{n_g} Y_i(1)Y_i(0) + \left(\frac{1}{n_g - 1} - \frac{1}{n_g} \right) \sum_{i \neq j} Y_i(1)Y_j(0) \right) \\ &= \frac{1}{n_g} \left(\sum_{i:\hat{\mathcal{G}}_g(X_i)} \frac{1}{n_g} Y_i(1)Y_i(0) - \frac{1}{n_g(n_g - 1)} \sum_{i \neq j} Y_i(1)Y_j(0) \right) \\ &= -\frac{1}{n_g} \text{cov}_g(Y_i(1), Y_i(0)) \end{aligned} \tag{17}$$

Substituting the expressions in Equation (15)-(17) into Equation (13):

$$\text{var}(\hat{\tau}^{(g)}) = \left\{ \tilde{\beta}_g(1) - \frac{1}{n_g} \right\} \text{var}_g \{Y_i(1)\} + \left\{ \tilde{\beta}_g(0) - \frac{1}{n_g} \right\} \text{var}_g \{Y_i(0)\} + \frac{2}{n_g} \text{cov}_g \{Y_i(1), Y_i(0)\}$$

Defining $\beta_g(z) := n_g \tilde{\beta}_g(z)$ (i.e., the reciprocal of the proportion of units in group g who are assigned $Z_i = z$):

$$\begin{aligned} &= \frac{\beta_g(1)}{n_g} \text{var}_g \{Y_i(1)\} + \frac{\beta_g(0)}{n_g} \text{var}_g \{Y_i(0)\} - \frac{1}{n_g} [\text{var}_g \{Y_i(1)\} + \text{var}_g \{Y_i(0)\} - 2\text{cov}_g \{Y_i(1), Y_i(0)\}] \\ &= \frac{\beta_g(1)}{n_g} \text{var}_g \{Y_i(1)\} + \frac{\beta_g(0)}{n_g} \text{var}_g \{Y_i(0)\} - \frac{1}{n_g} \text{var}_g(\tau_i) \end{aligned}$$

□

B.4 Proof of Theorem 3.3

We formally impose the following regularity assumptions.

Assumption B.2 (Regularity Conditions)

1. As the sample size $n \rightarrow \infty$, the total number of subgroups G remain fixed.
2. The proportion of units in each subgroup converges to a proportion $\pi_g^* \in (0, 1)$ (i.e., $n_g/n \rightarrow \pi_g^*$, where $0 < \pi_g^* < 1$ for all $g \in \{1, \dots, G\}$ and $\sum_{g=1}^G \pi_g^* = 1$).
3. The proportion of treated units converges to π_z^* , where $\pi_z^* \in (0, 1)$ (i.e., $\lim_{n \rightarrow \infty} \frac{1}{n} \sum_{i=1}^n Z_i = \pi_z^*$).

4. Lindeberg Condition:

$$\lim_{n \rightarrow \infty} \frac{1}{n_z^2} \frac{\max_{1 \leq i \leq n} \hat{\mathcal{G}}_g(X_i) Y_i^2(z)}{\text{var}(\hat{\tau}(g))} = 0.$$

5. $\lim_{n \rightarrow \infty} \text{var}_g(Y_i(z)) \leq c_1$, and $\text{cov}_g(Y_i(1), Y_i(0)) \leq c_2$ where $c_1, c_2 < \infty$.

We would like to show that as $n \rightarrow \infty$, $(1 - \frac{n_z}{n}) \cdot \frac{1}{n_z} \text{var}(\hat{\mathcal{G}}_g(X_i)) \rightarrow 0$.

Claim: $\text{var}(\hat{\mathcal{G}}_g(X_i)) = \frac{n}{n-1} \frac{1-\pi_g}{\pi_g}$.

Then,

$$\left(1 - \frac{n_z}{n}\right) \cdot \frac{1}{n_z} \text{var}(\hat{\mathcal{G}}_g(X_i)) = \frac{1}{n} \frac{1 - n_z/n}{n_z/n} \cdot \frac{n}{n-1} \frac{1 - \pi_g}{\pi_g}.$$

As $n \rightarrow \infty$, $n_z/n \rightarrow \pi_z^*$ and $\pi_g \rightarrow \pi_g^*$, both of which will be bounded away from 0 and 1 (by Assumption (B.2)(b)-(c)):

$$\lim_{n \rightarrow \infty} \left(1 - \frac{n_z}{n}\right) \cdot \frac{1}{n_z} \text{var}(\hat{\mathcal{G}}_g(X_i)) = \lim_{n \rightarrow \infty} \frac{1}{n} \frac{1 - p_z^*}{p_z^*} \cdot \frac{1 - \pi_g^*}{\pi_g^*} = 0$$

Then, we can apply Schochet (2024), Theorem 1 to show:

$$\frac{\hat{\tau}^{(g)} - \mathbb{E}(\hat{\tau}^{(g)})}{\sqrt{\text{var}(\hat{\tau}^{(g)})}} \xrightarrow{d} N(0, 1)$$

B.5 Proof of Corollary

Because each subgroup is a distinct partition, $\hat{\tau}^{(g)}$ and $\hat{\tau}_{g'}$ will be asymptotically independent from one another. As a result, we can straightforwardly apply the Cramer-Wold device and

$$\hat{\boldsymbol{\tau}} - \boldsymbol{\tau} \xrightarrow{d} N(0, \boldsymbol{\Sigma}_G)$$

Thus:

$$\hat{\boldsymbol{\tau}}^\top \boldsymbol{\Sigma}_G^{-1} \hat{\boldsymbol{\tau}} \xrightarrow{d} \chi_G^2$$

B.6 Proof of Example 3.1

Assumption B.3 (Regularity Conditions)

- (a) *Smoothness of $\tau(X)$: $\tau(X)$ is continuous, and $\tau'(X)$, $\tau''(X)$ exist and are uniformly bounded in a neighborhood around s , and $\tau'(s) \neq 0$.*
- (b) *Smoothness condition on density of X and v : dF'_X exists and is uniformly bounded in a neighborhood around s . Furthermore, $dF_X(s) \neq 0$.*
- (c) *Moment condition: $\mathbb{E}(v_i) = 0$, $\mathbb{E}(v_i^2) = \sigma^2$.*
- (d) *Tail condition: $dF_\tau = o(|\tau|^{-4+\delta})$ as $|\tau| \rightarrow \infty$ for some $\delta > 0$.*
- (e) *Signal condition: $\text{var}(\tau(X_i)) > 0$.*

These are common assumptions (see e.g., [Buhlmann and Yu, 2002](#)). The first three conditions are straightforward. The tail condition (i.e., Assumption (B.3)-(d)) rules out settings in which the density of τ_i concentrates at an infinitely large value. Informally, this implies that the treatment effect cannot explode to be infinitely large, which is reasonable in many substantive contexts of interest. The final condition (i.e., Assumption (B.3)-(e)) which we refer to as a signal condition, rules out settings in which there is no amount of variation in τ_i that can be explained by the covariates X_i (i.e., the underlying data generating process is pure noise). In other words, the covariates we have collected must have *some* degree of explanatory power. This rules out the setting considered in [Cattaneo et al. \(2022\)](#).

Lemma B.4 (Asymptotic Variance of Splits) *Under Assumption (B.3) and squared loss, the asymptotic variance of the estimated splits is:*

$$\text{asyvar}(\hat{s}_n) = (dF_X(s)\sigma^2)^2 \cdot \frac{2^{-2/3}}{6\pi i} \left(\frac{1}{2} \frac{V}{dF_X(s)\sigma^2} \right)^{-4/3} \int_{-\infty}^{\infty} \frac{t}{Ai(it)^2} dt,$$

where $V = -dF_X(s)f'(s) \neq 0$.

Proof: Under Assumption (B.3) and squared loss, we apply [Buhlmann and Yu \(2002\)](#), Theorem 3.1 to show that as $n \rightarrow \infty$,

$$n^{1/3}(\hat{s}_n - s) \xrightarrow{d} W_{\sigma^2, s} := \arg \max_t [Q(t) \cdot \text{sign}(\mathbb{E}(\tau_i | X_i < s) - \mathbb{E}(\tau_i | X_i \geq s))],$$

and $Q(t)$ is a scaled, two-sided Brownian motion, originating from zero, with a quadratic drift:

$$Q(t) = dF_X(s)\sigma^2 B(t) - \frac{1}{2} V t^2,$$

where $B(t)$ is a two-sided Brownian motion, originating from zero, and $V = -dF_X(s)f'(s) \neq 0$. To derive the variance of $W_{\sigma^2, s}$, we can exploit the fact that $W_{\sigma^2, s}$ follows Chernoff's distribution ([Groeneboom, 1989](#)).

To begin, define the random variable Z as:

$$Z_\gamma := \arg \max_t B(t) - \gamma t^2,$$

where $B(t)$ is a standard Brownian motion, and $c > 0$. Then, from [Groeneboom \(1989\)](#) (Corollary 3.3), the density of Z is given as $dF_Z(t) = g_\gamma(t)g_\gamma(-t)$, and $g_\gamma(t)$ is defined as:

$$g_\gamma(t) = \left(\frac{2}{\gamma}\right)^{1/3} \frac{1}{2\pi i} \int_{c_1-i\infty}^{c_1+i\infty} \frac{\exp(-tu)}{\text{Ai}((2\gamma^2)^{-1/3}u)} du, \quad (18)$$

where $c_1 > a_1$, and a_1 is the largest zero of the Airy function Ai . We can apply [Janson \(2013\)](#) (Theorem 1.1) to obtain a closed form solution for the variance of Z_γ :

$$\text{var}(Z_\gamma) = \frac{2^{-2/3}\gamma^{-4/3}}{6\pi i} \int_{-\infty}^{\infty} \frac{t}{\text{Ai}(it)^2} dt.$$

Furthermore, in settings when the Brownian motion is scaled (i.e., $B(at)$), we can exploit the fact that for all $a > 0$, $B(at) = a^{1/2}B(t)$, and:

$$Z_\gamma =^d a \arg \max(a^{1/2}B(t) - a^2\gamma t^2) = aZ_{a^{3/2}\gamma}.$$

We then solve for the variance of $W_{\sigma^2,s}$ by substituting $a^{1/2} = dF_X(s)\sigma^2$, and $\gamma = \frac{1}{2}V/(dF_X(s)^2\sigma^4)^2$.

Thus, the asymptotic variance of a split \hat{s}_n can be written as follows:

$$\text{asyvar}(\hat{s}_n) = (dF_X(s)\sigma^2)^2 \cdot \frac{2^{-2/3}}{6\pi i} \left(\frac{1}{2} \frac{V}{dF_X(s)\sigma^2}\right)^{-4/3} \int_{-\infty}^{\infty} \frac{t}{\text{Ai}(it)^2} dt.$$

□

B.7 Proof of Lemmas

B.7.1 Proof of Lemma [B.1](#)

Proof: We can re-write the difference in the within-sample loss and the population loss as:

$$\begin{aligned} & \left| \mathbb{E}_n \left[\ell(\hat{\tau}_i^d, X; \hat{s}_n) \right] - \mathbb{E} \left[\ell(\hat{\tau}_i^d, X, s) \right] \right| \\ &= \left| \mathbb{E}_n \left[\ell(\hat{\tau}_i^d, X; \hat{s}_n) \right] - \mathbb{E}_n \left[\ell(\hat{\tau}_i^d, X, s) \right] + \mathbb{E}_n \left[\ell(\hat{\tau}_i^d, X, s) \right] - \mathbb{E} \left[\ell(\hat{\tau}_i^d, X, s) \right] \right| \\ &\leq \underbrace{\left| \mathbb{E}_n \left[\ell(\hat{\tau}_i^d, X; \hat{s}_n) \right] - \mathbb{E}_n \left[\ell(\hat{\tau}_i^d, X, s) \right] \right|}_{(*)} + \left| \mathbb{E}_n \left[\ell(\hat{\tau}_i^d, X, s) \right] - \mathbb{E} \left[\ell(\hat{\tau}_i^d, X, s) \right] \right| \end{aligned}$$

We will construct an upper bound on the first term (*):

$$\begin{aligned}
& \left| \mathbb{E}_n \left[\ell(\hat{\tau}_i^d; X, \hat{s}_n) \right] - \mathbb{E}_n \left[\ell(\hat{\tau}_i^d; X, s) \right] \right| \\
&= \left| \mathbb{E}_n \left[(\hat{\tau}_i^d - \tau^d(X_i; \hat{s}_n))^2 - (\hat{\tau}_i^d - \tau^d(X_i; s))^2 \right] \right| \\
&= \left| \mathbb{E}_n \left[\tau^d(X_i; \hat{s}_n)^2 - \tau^d(X_i; s)^2 - 2\hat{\tau}_i^d \left(\tau^d(X_i; \hat{s}_n) - \tau^d(X_i; s) \right) \right] \right| \\
&= \left| \mathbb{E}_n \left[\left(\tau^d(X_i; \hat{s}_n) - \tau^d(X_i; s) \right) \left(\tau^d(X_i; \hat{s}_n) + \tau^d(X_i; s) - 2\hat{\tau}_i^d \right) \right] \right| \\
&\leq \mathbb{E}_n \left[\left| \left(\tau^d(X_i; \hat{s}_n) - \tau^d(X_i; s) \right) \right| \left| \left(\tau^d(X_i; \hat{s}_n) + \tau^d(X_i; s) - 2\hat{\tau}_i^d \right) \right| \right] \\
&= \mathbb{E}_n \left[\left| \left(\mathbb{E}(\hat{\tau}_i^d | X_i < \hat{s}_n) - \mathbb{E}(\hat{\tau}_i^d | X_i < s) \right) \right| \left| \left(\tau^d(X_i; \hat{s}_n) + \tau^d(X_i; s) - 2\hat{\tau}_i^d \right) \right| \right] \\
&= \mathbb{E}_n \left[|\hat{s}_n - s| \times \max_{c \in [\hat{s}_n, s]} \mathbb{E}(\hat{\tau}_i^d | X_i < c) \left| \tau^d(X_i; \hat{s}_n) + \tau^d(X_i; s) - 2\hat{\tau}_i^d \right| \right] \\
&= |\hat{s}_n - s| \mathbb{E}_n \left[\max_{c \in [\hat{s}_n, s]} \mathbb{E}(\hat{\tau}_i^d | X_i < c) \left| \left(\tau^d(X_i; \hat{s}_n) - \hat{\tau}_i^d \right) + \left(\tau^d(X_i; s) - \hat{\tau}_i^d \right) \right| \right] \\
&\leq |\hat{s}_n - s| \times \max_{c \in [\hat{s}_n, s]} \mathbb{E}(\hat{\tau}_i^d | X_i < c) \times \left(\mathbb{E}_n \left| \tau^d(X_i; \hat{s}_n) - \hat{\tau}_i^d \right| + \mathbb{E}_n \left| \tau^d(X_i; s) - \hat{\tau}_i^d \right| \right) \\
&\leq 2 |\hat{s}_n - s| \times \max_{c \in [\hat{s}_n, s]} \mathbb{E}(\hat{\tau}_i^d | X_i < c) \times \mathbb{E}_n \left| \tau^d(X_i; \hat{s}_n) - \hat{\tau}_i^d \right| \\
&= C_\tau \times |\hat{s}_n - s|
\end{aligned}$$

Then:

$$\left| \mathbb{E}_n \left[\ell(\hat{\tau}_i^d; X; \hat{s}_n) \right] - \mathbb{E} \left[\ell(\hat{\tau}_i^d; X, s) \right] \right| \leq C_\tau \times |\hat{s}_n - s| + \left| \mathbb{E}_n \left[\ell(\hat{\tau}_i^d; X, s) \right] - \mathbb{E} \left[\ell(\hat{\tau}_i^d; X, s) \right] \right|,$$

which concludes the proof. \square

B.8 Proof of Lemma B.2

Proof: We have that

$$\begin{aligned}
& \Pr \left[\mathbb{E}_n \left\{ \ell(\hat{\tau}_i^d; X^{(b)}, \hat{s}_n^{(b)}) \right\} < \mathbb{E}_n \left\{ \ell(\hat{\tau}_i^d; X^{(a)}, \hat{s}_n^{(a)}) \right\} \right] \\
&= \Pr \left[\mathbb{E}_n \left\{ \ell(\hat{\tau}_i^d; X^{(b)}, \hat{s}_n^{(b)}) \right\} - \mathbb{E}_n \left\{ \ell(\hat{\tau}_i^d; X^{(a)}, \hat{s}_n^{(a)}) \right\} < 0 \right] \\
&= \Pr \left[\mathbb{E}_n \left\{ \ell(\hat{\tau}_i^d; X^{(b)}, \hat{s}_n^{(b)}) \right\} - \mathbb{E} \left\{ \ell(\hat{\tau}_i^d; X^{(b)}, s^{(b)}) \right\} + \right. \\
&\quad \left. \mathbb{E} \left\{ \ell(\hat{\tau}_i^d; X^{(b)}, s^{(b)}) \right\} - \mathbb{E}_n \left\{ \ell(\hat{\tau}_i^d; X^{(a)}, s^{(a)}) \right\} + \mathbb{E} \left\{ \ell(\hat{\tau}_i^d; X^{(a)}, s^{(a)}) \right\} - \mathbb{E} \left\{ \ell(\hat{\tau}_i^d; X^{(a)}, \hat{s}_n^{(a)}) \right\} < 0 \right]
\end{aligned}$$

By construction, $\mathbb{E} \left\{ \ell(\hat{\tau}_i^d; X^{(b)}, s^{(b)}) \right\} > \mathbb{E} \left\{ \ell(\hat{\tau}_i^d; X^{(a)}, s^{(a)}) \right\}$, as $X^{(a)}$ is a relevant covariate. Therefore, $\mathbb{E} \left\{ \ell(\hat{\tau}_i^d; X^{(b)}, s^{(b)}) \right\} - \mathbb{E} \left\{ \ell(\hat{\tau}_i^d; X^{(a)}, s^{(a)}) \right\} = \delta_{ba} > 0$:

$$\begin{aligned} &= \Pr \left(\mathbb{E}_n \left\{ \ell(\hat{\tau}_i^d; X^{(b)}, \hat{s}_n^{(b)}) \right\} - \mathbb{E} \left\{ \ell(\hat{\tau}_i^d; X^{(b)}, s^{(b)}) \right\} - \left[\mathbb{E}_n \left\{ \ell(\hat{\tau}_i^d; X^{(a)}, \hat{s}_n^{(a)}) \right\} - \mathbb{E} \left\{ \ell(\hat{\tau}_i^d; X^{(a)}, s^{(a)}) \right\} \right] + \delta_{ba} < 0 \right) \\ &= \Pr \left(\left[\mathbb{E}_n \left\{ \ell(\hat{\tau}_i^d; X^{(a)}, \hat{s}_n^{(a)}) \right\} - \mathbb{E} \left\{ \ell(\hat{\tau}_i^d; X^{(a)}, s^{(a)}) \right\} \right] - \left[\mathbb{E}_n \left\{ \ell(\hat{\tau}_i^d; X^{(b)}, \hat{s}_n^{(b)}) \right\} - \mathbb{E} \left\{ \ell(\hat{\tau}_i^d; X^{(b)}, s^{(b)}) \right\} \right] > \delta_{ba} \right) \\ &\leq \Pr \left(\left| \left[\mathbb{E}_n \left\{ \ell(\hat{\tau}_i^d; X^{(a)}, \hat{s}_n^{(a)}) \right\} - \mathbb{E} \left\{ \ell(\hat{\tau}_i^d; X^{(a)}, s^{(a)}) \right\} \right] - \left[\mathbb{E}_n \left\{ \ell(\hat{\tau}_i^d; X^{(b)}, \hat{s}_n^{(b)}) \right\} - \mathbb{E} \left\{ \ell(\hat{\tau}_i^d; X^{(b)}, s^{(b)}) \right\} \right] \right| > \delta_{ba} \right) \end{aligned}$$

Then, applying Markov's Inequality:

$$\begin{aligned} &\leq \frac{1}{\delta_{ba}} \mathbb{E} \left(\left| \left[\mathbb{E}_n \left\{ \ell(\hat{\tau}_i^d; X^{(a)}, \hat{s}_n^{(a)}) \right\} - \mathbb{E} \left\{ \ell(\hat{\tau}_i^d; X^{(a)}, s^{(a)}) \right\} \right] - \left[\mathbb{E}_n \left\{ \ell(\hat{\tau}_i^d; X^{(b)}, \hat{s}_n^{(b)}) \right\} - \mathbb{E} \left\{ \ell(\hat{\tau}_i^d; X^{(b)}, s^{(b)}) \right\} \right] \right| \right) \\ &\leq \frac{1}{\delta_{ba}} \left\{ \mathbb{E} \left[\left| \mathbb{E}_n \left\{ \ell(\hat{\tau}_i^d; X^{(a)}, \hat{s}_n^{(a)}) \right\} - \mathbb{E} \left\{ \ell(\hat{\tau}_i^d; X^{(a)}, s^{(a)}) \right\} \right| \right] + \mathbb{E} \left[\left| \mathbb{E}_n \left\{ \ell(\hat{\tau}_i^d; X^{(b)}, \hat{s}_n^{(b)}) \right\} - \mathbb{E} \left\{ \ell(\hat{\tau}_i^d; X^{(b)}, s^{(b)}) \right\} \right| \right] \right\} \end{aligned}$$

Without loss of generality, assume $\mathbb{E} \left[\left| \mathbb{E}_n \left\{ \ell(\hat{\tau}_i^d; X^{(a)}, \hat{s}_n^{(a)}) \right\} - \mathbb{E} \left\{ \ell(\hat{\tau}_i^d; X^{(a)}, s^{(a)}) \right\} \right| \right]$ is greater than or equal to $\mathbb{E} \left[\left| \mathbb{E}_n \left\{ \ell(\hat{\tau}_i^d; X^{(b)}, \hat{s}_n^{(b)}) \right\} - \mathbb{E} \left\{ \ell(\hat{\tau}_i^d; X^{(b)}, s^{(b)}) \right\} \right| \right]$. Then:

$$\leq \frac{2}{\delta_{ba}} \mathbb{E} \left[\left| \mathbb{E}_n \left\{ \ell(\hat{\tau}_i^d; X^{(a)}, \hat{s}_n^{(a)}) \right\} - \mathbb{E} \left\{ \ell(\hat{\tau}_i^d; X^{(a)}, s^{(a)}) \right\} \right| \right]$$

□

C Method Implementation Details

In this section, we describe the hyperparameters and implementation details for all methods used in the simulations and case study. All methods and code were implemented using **R** ([R Core Team, 2024](#)). For ease of reproducibility and communication of the simulation results, the simulation study was conducted using the `simChef` R package ([Duncan et al., 2024](#)).

Causal Distillation Trees (CDT). We considered causal distillation trees with two different teacher models: causal forest ([Wager and Athey, 2018](#)) and R-learner with boosting (`rboost`) ([Nie and Wager, 2021](#)). These teacher models were implemented using `grf::causal_forest()` ([Tibshirani et al., 2024](#)) and `rlearner::rboost()` ([Nie et al., 2021](#)), respectively, using their default

hyperparameter settings.

For the student model, we fit a CART decision tree (Breiman et al., 1984) using `rpart::rpart()` (Therneau and Atkinson, 2023), with the default settings. The CART was then pruned using the standard post-pruning procedure (i.e., choosing the complexity parameter α which minimizes the cross-validation error), as described in Section 3.1. Note that this post-pruning step does not drastically affect the subgroup estimation results, as shown in Figure A4.

To perform honest estimation of the subgroup ATEs, we set $\pi_{train} = 0.70$ for splitting the data into a training and hold-out estimation set. To estimate the individual-level treatment effects $\hat{\tau}(X_i)$, we used the out-of-bag sample estimates (without repeated cross-fitting) in the Distilled Causal Forest and the repeated cross-fitting procedure with $R = 50$ repeats in the Distilled Rboost. We also examined other choices of R in Figure A7. From these simulations, we found that $R = 50$ provided a good balance between the subgroup estimation accuracy and computational burden. However, more generally, the subgroup estimation results from Distilled Rboost were robust as long as R was sufficiently large enough.

Virtual Twins. We implemented the virtual twins algorithm (Foster et al., 2011) using the `ranger::ranger()` (Wright and Ziegler, 2017) implementation of random forests. Like in CDT, we set aside a hold-out estimation set to perform honest estimation of the subgroup average treatment effects and used $\pi_{train} = 0.70$.

Causal Trees. We implemented causal trees using the `causalTree` R package (Athey et al., 2016) and used the default parameters as shown in the example usage on GitHub — that is, `split.Rule = "CT"`, `cv.option = "CT"`, `split.Honest = TRUE`, `cv.Honest = "TRUE"`, `split.Bucket = FALSE`, `xval = 5`, `cp = 0`, `minsize = 20`, and `propensity = 0.5`. As in CDT, we pruned the causal tree using the standard post-pruning procedure, choosing the complexity parameter α which minimizes the cross-validation error.

Linear and Lasso Regression. In the linear and Lasso regressions, we included all main effects X and their interactions with the treatment variable Z as covariates to predict the response Y . In the linear regression, we defined a selected subgroup feature to be any covariate whose interaction with the treatment variable yielded a significant p-value ($p < 0.05$). In the Lasso regression,

we defined a selected subgroup feature to be any covariate whose interaction with the treatment variable received a non-zero coefficient. To estimate the CATE for each unit, we computed the difference between the predicted response when $Z_i = 1$ and the predicted response when $Z_i = 0$. The linear regression was implemented using `lm()`, and the Lasso regression was implemented using `glmnet::cv.glmnet()` (Friedman et al., 2010) with 5-fold cross-validation and the default hyperparameter grid.

D Additional Simulation Results

We next present additional simulation results to complement the main results, shown in Section 5. These results include additional subgroup data-generating processes, evaluation metrics, and alternative modeling choices in the CDT framework (e.g., different number of repeated cross-fits R , student model choices, and pruning choices).

CATE-only Outcome Model. In particular, to complement Figure 4 which examined the subgroup estimation performance under an outcome model including linear covariate effects (i.e., $Y_i = Z_i \cdot \tau_i + X_i^{(3)} + X_i^{(4)} + \nu_i$), we also examined the subgroup estimation performance under the following outcome model, which depends only on the conditional average treatment effect:

$$Y_i = Z_i \cdot \tau_i + \nu_i.$$

Besides this modification in the outcome model, all other simulation settings were kept the same. The results are shown in Figure A2. As seen under the previous outcome model, the distilled methods (Distilled Causal Forest and Distilled Rboost) generally outperformed existing methods in estimating the subgroup structure and the subgroup average treatment effects.

Threshold Distributions. When examining the distribution of the estimated subgroup thresholds from the tree-based methods in Figure A3, we uncover another benefit of distillation — the distribution of the CDT-estimated subgroup thresholds is much tighter (i.e., has smaller variance) than for other tree-based subgroup detection methods without distillation (i.e., causal trees and virtual twins). This again reinforces our theoretical understanding of CDT, where we have seen in

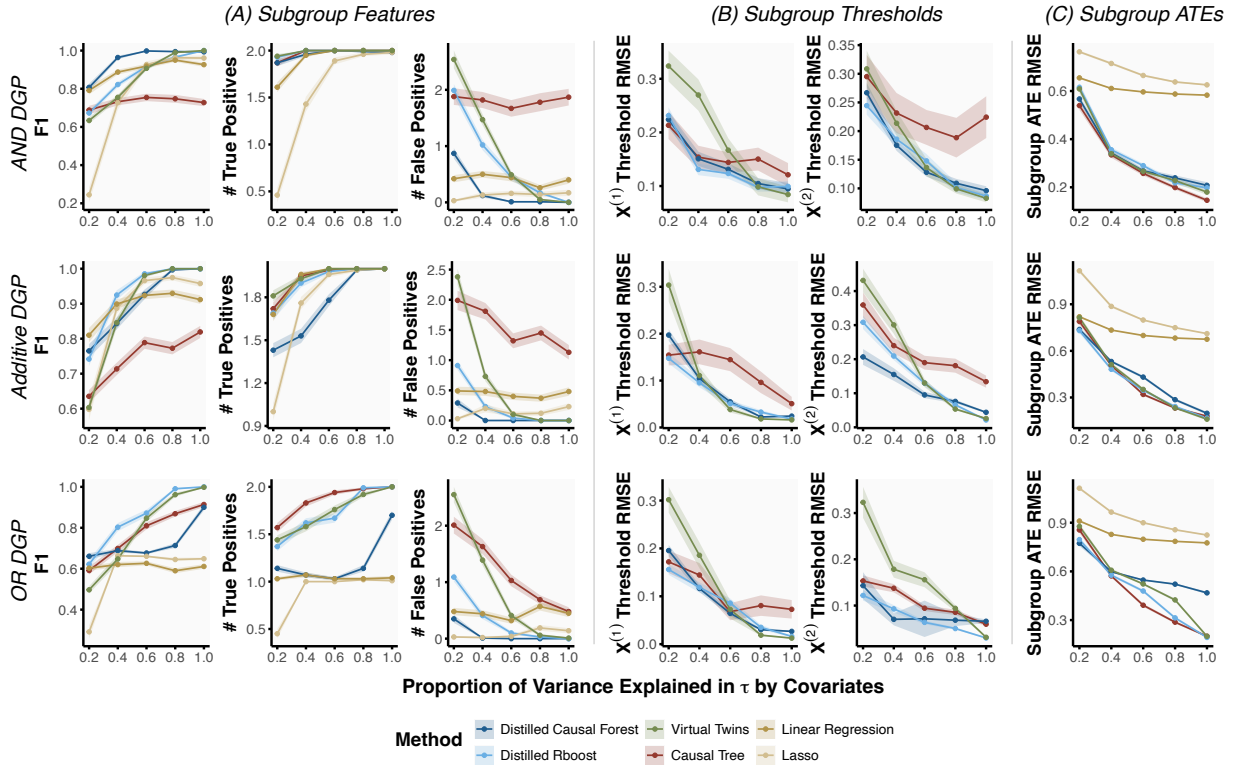


Figure A2: Performance of subgroup estimation methods for (A) identifying the true subgroup features, measured via F_1 score, number of true positives, and number of false positives, (B) estimating the true subgroup thresholds, measured via root mean squared error (RMSE) for each true subgroup feature, and (C) estimating the true subgroup ATE, measured via RMSE, across increasing treatment effect heterogeneity strengths (x-axis) and different subgroup data-generating processes in the **CATE-only outcome model** scenario (rows). CDT with various teacher models (i.e., Distilled Causal Forest and Distilled Rboost) frequently yields the highest F_1 and number of true positives alongside the lowest number of false positives, threshold RMSEs, and CATE RMSE, demonstrating its effectiveness for accurate subgroup estimation. Results are averaged across 100 simulation replicates with ribbons denoting $\pm 1SE$.

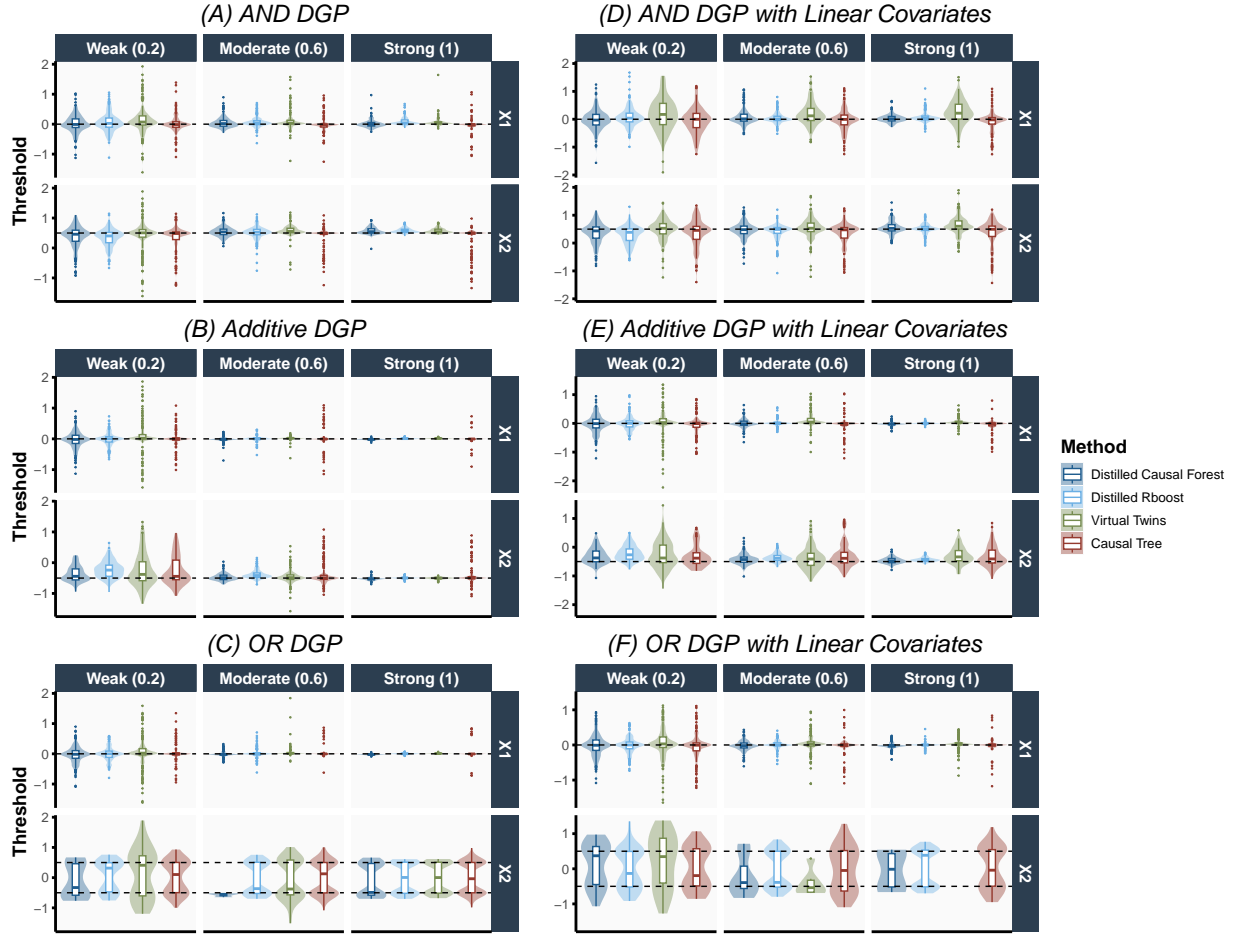


Figure A3: Distribution of estimated thresholds for each true subgroup feature (i.e., $X^{(1)}$ and $X^{(2)}$) using different subgroup estimation methods (color) under various treatment effect heterogeneity strengths (columns) and subgroup data-generating processes (subplots). The range of the threshold distributions from CDT (i.e., Distilled Causal Forest and Distilled Rboost) is often smaller than that from causal tree, especially as the treatment effect heterogeneity strength increases. Results are shown for 100 simulation replicates.

Example 3.1 that the first-stage learner in CDT acts as a de-noising step, leading to more stable splits (i.e., thresholds) in CDT compared to non-distilled tree-based methods.

Pruned versus Unpruned. Recall thus far that we have been implementing CDT and causal trees with the standard post-pruning procedure using cross-validation to tune the complexity parameter α . To investigate the impact of this post-pruning step, we compare the subgroup estimation performance of CDT and causal trees with and without post-pruning in Figure A4. While the performance of causal trees declines drastically without pruning, the performance of CDT with and without pruning is similarly strong, demonstrating CDT’s robustness with respect to this pruning

choice.

Evaluating using Oracle Tree Depth. In general, optimally pruning decision trees is a challenging problem and an active area of research (Zhou and Mentch, 2023). To investigate whether the observed difference in subgroup estimation performance between tree-based methods is due to suboptimal pruning or not, we show in Figure A5 the subgroup estimation performance of the tree-based methods, pruned to have a fixed depth of 2 (which is the oracle tree depth given our subgroup DGPs, described in Section 5.1). Even with this oracle pruning, we still observe improvements due to distillation. In particular, compared to causal tree and virtual twins, CDT yields fewer false positives and more accurate estimation of the subgroup ATEs.

Selection Frequency of Subgroup Features. In Figure A6, we show the number of simulation replicates (out of 100) that each variable was selected as a subgroup feature. Notably, when the outcome model includes linear covariate effects involving the features $X^{(3)}$ and $X^{(4)}$, causal tree and virtual twins frequently split on these irrelevant features, $X^{(3)}$ and $X^{(4)}$, whereas the distilled methods avoid this pitfall.

Choice of Repeated Cross-Fits R . In the CDT algorithm, we have been using $R = 50$ repeated cross-fits to estimate the individual-level treatment effects. To investigate the sensitivity of this choice, we show in Figure A7 the subgroup estimation performance of Distilled Rboost for varying choices of R , ranging between 1 and 100. In general, the subgroup estimation performance improves as R increases and tends to be relatively stable for $R > 10$.

Rulefit Student Model. Another choice in the CDT framework is the student model, for which we recommend and have been using a CART decision tree. In previous work (Bargagli-Stoffi et al., 2020; Wan et al., 2023), Rulefit (Friedman and Popescu, 2008) has been proposed to either generate subgroup rules or estimate subgroups with heterogeneous treatment effects. In Figure A8, we compare the performance of Distilled Causal Forest using CART as the student model to Distilled Causal Forest using various instantiations of rulefit as the student model. Namely, we include four different versions of rulefit, implemented using `pre::pre()` (Fokkema, 2020), with the following hyperparameter settings:

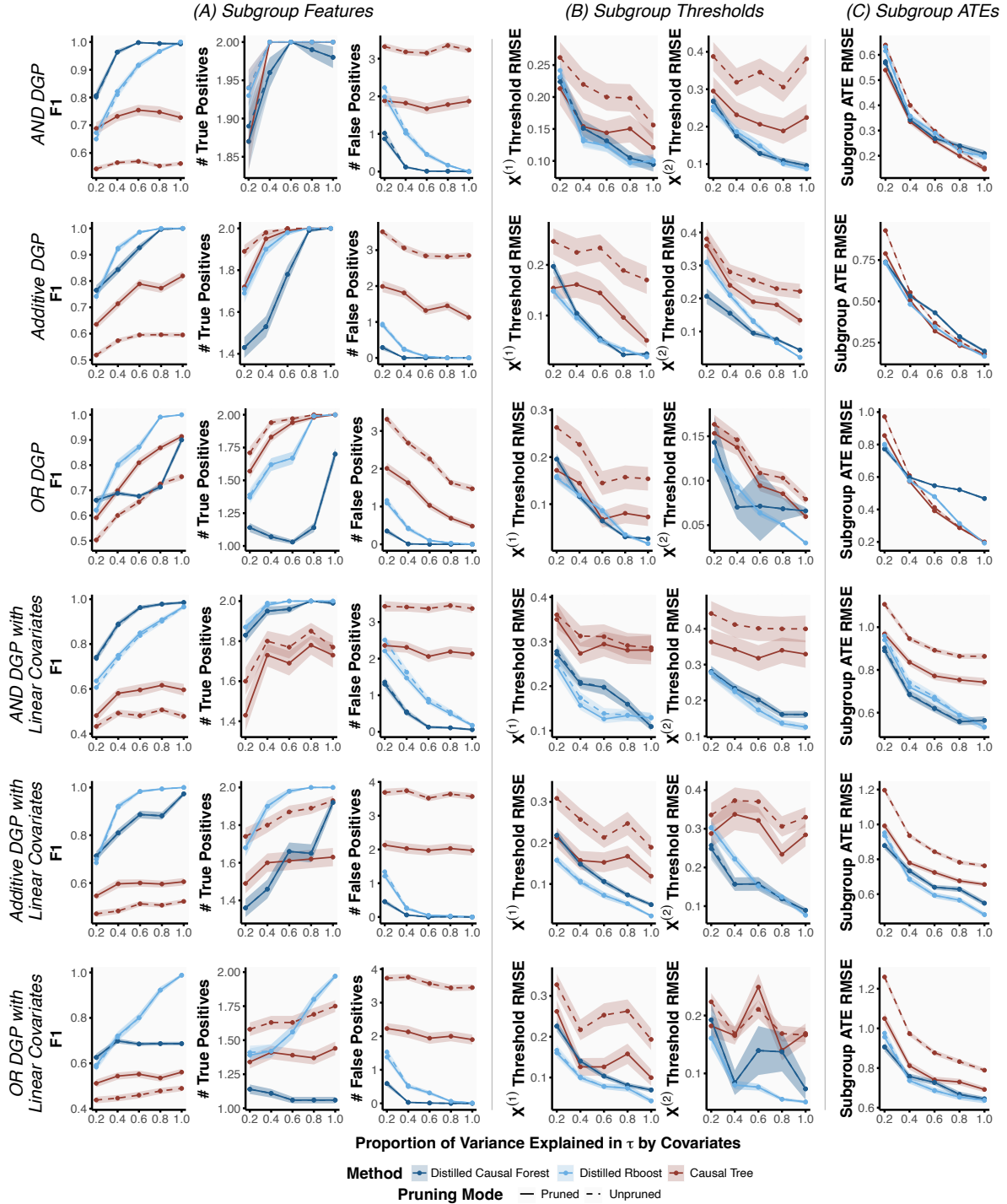


Figure A4: Performance of **pruned** and **unpruned** versions of CDT and causal trees for (A) identifying the true subgroup features, measured via F_1 score, number of true positives, and number of false positives, (B) estimating the true subgroup thresholds, measured via root mean squared error (RMSE) for each true subgroup feature, and (C) estimating the true subgroup ATE, measured via RMSE, across increasing treatment effect heterogeneity strengths (x-axis) and different subgroup data-generating processes (rows). While causal tree without pruning performs substantially worse than pruned causal tree, CDT with various teacher models (i.e., Distilled Causal Forest and Distilled Rboost) performs similarly well with or without pruning. Results are averaged across 100 simulation replicates with ribbons denoting $\pm 1SE$.

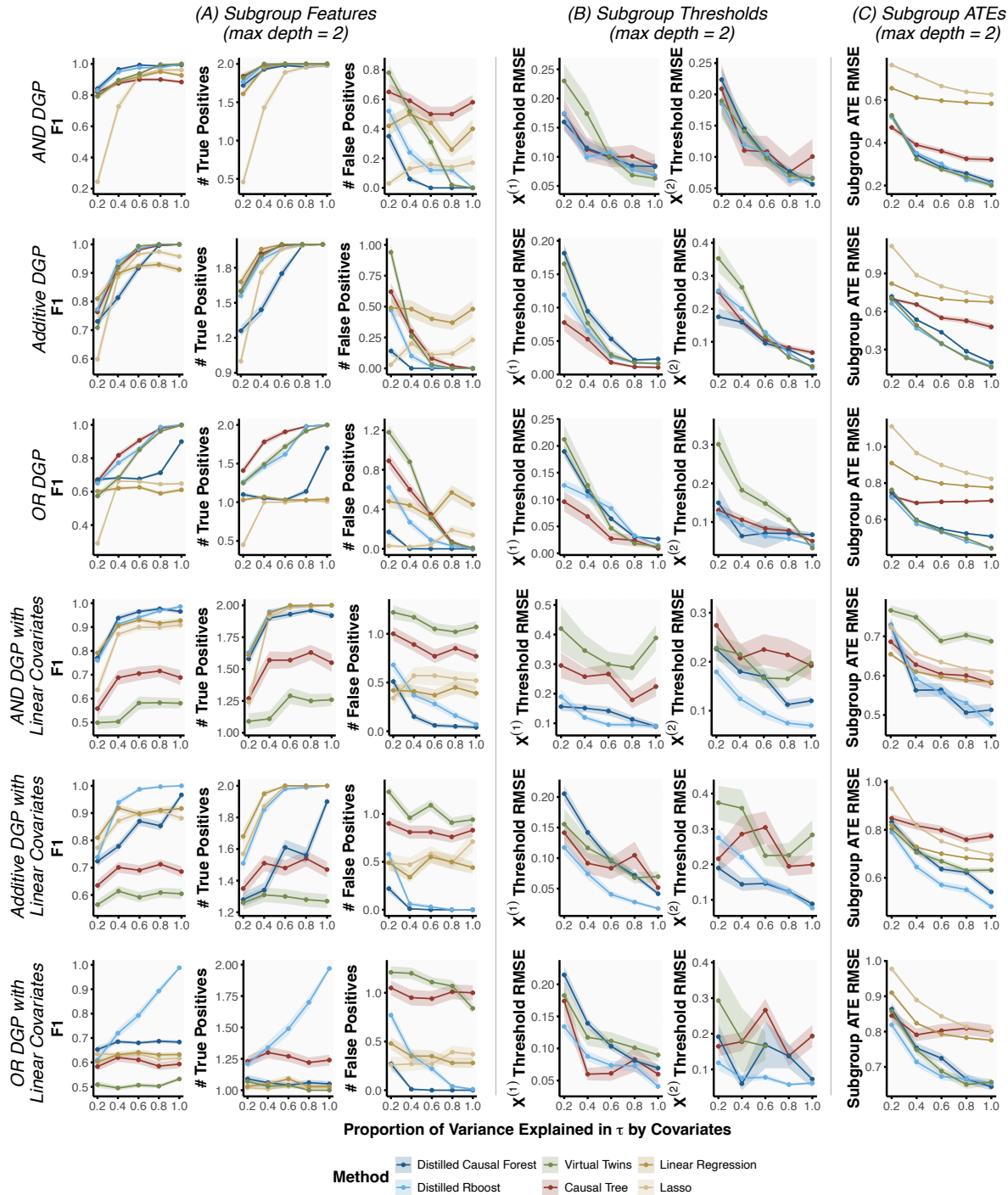


Figure A5: Performance of subgroup estimation methods **with oracle pruning** for (A) identifying the true subgroup features, measured via F_1 score, number of true positives, and number of false positives, (B) estimating the true subgroup thresholds, measured via root mean squared error (RMSE) for each true subgroup feature, and (C) estimating the true subgroup ATE, measured via RMSE, across increasing treatment effect heterogeneity strengths (x-axis) and different subgroup data-generating processes (rows). CDT with various teacher models (i.e., Distilled Causal Forest and Distilled Rboost) remains the most robust and accurate subgroup estimation method, as seen by its high F_1 and number of true positives alongside low number of false positives, threshold RMSEs, and CATE RMSE. Results are averaged across 100 simulation replicates with ribbons denoting $\pm 1SE$.

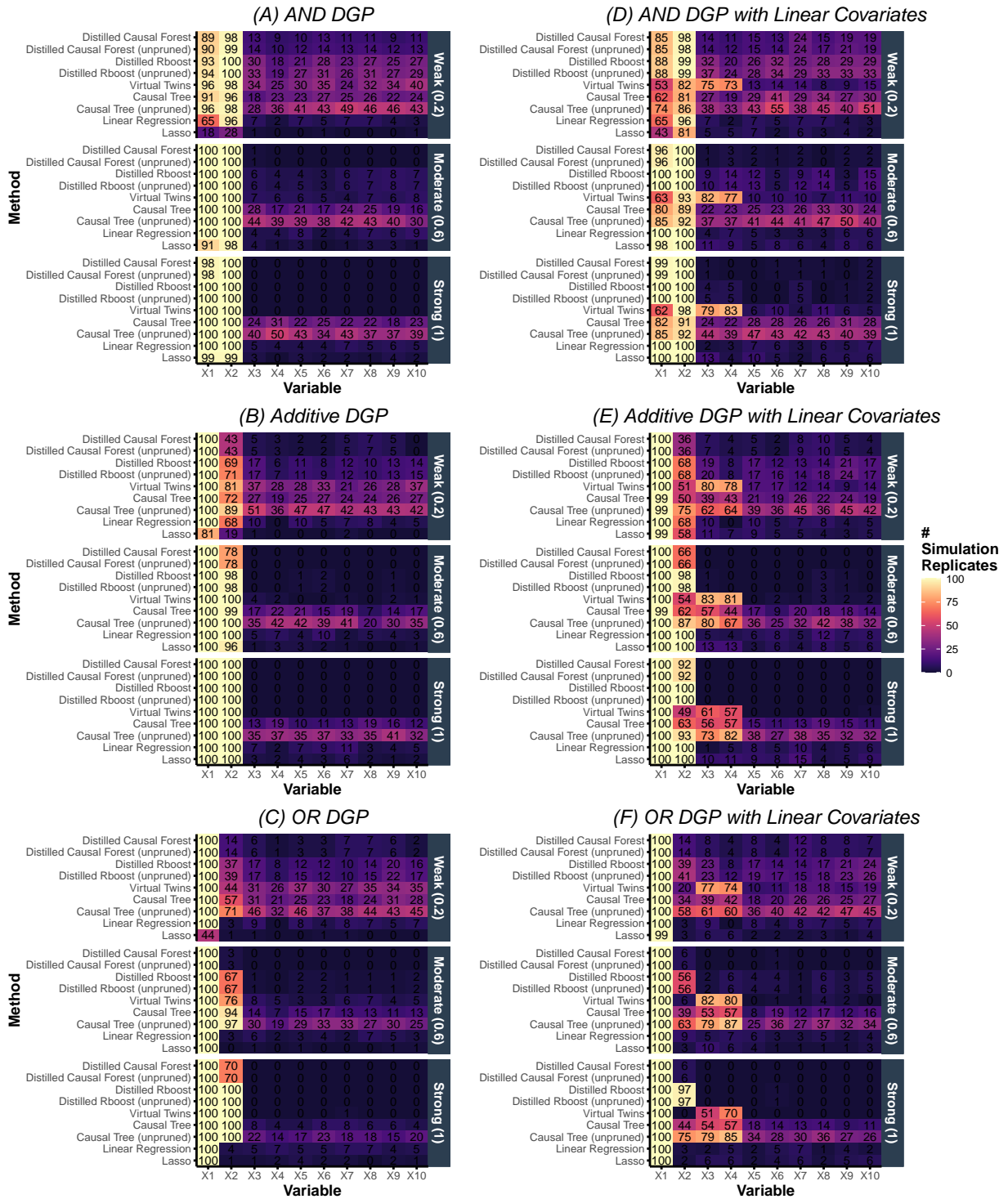


Figure A6: Number of simulation replicates out of 100, for which each variable was selected (at least once) in the estimated subgroups. Results are shown for different causal variables (x-axis), subgroup estimation methods (y-axis), treatment effect heterogeneity strengths (rows), and subgroup data-generating processes (subplots). Large values for variables $X^{(1)}$ and $X^{(2)}$ and small values for all other variables indicate a better-performing method.

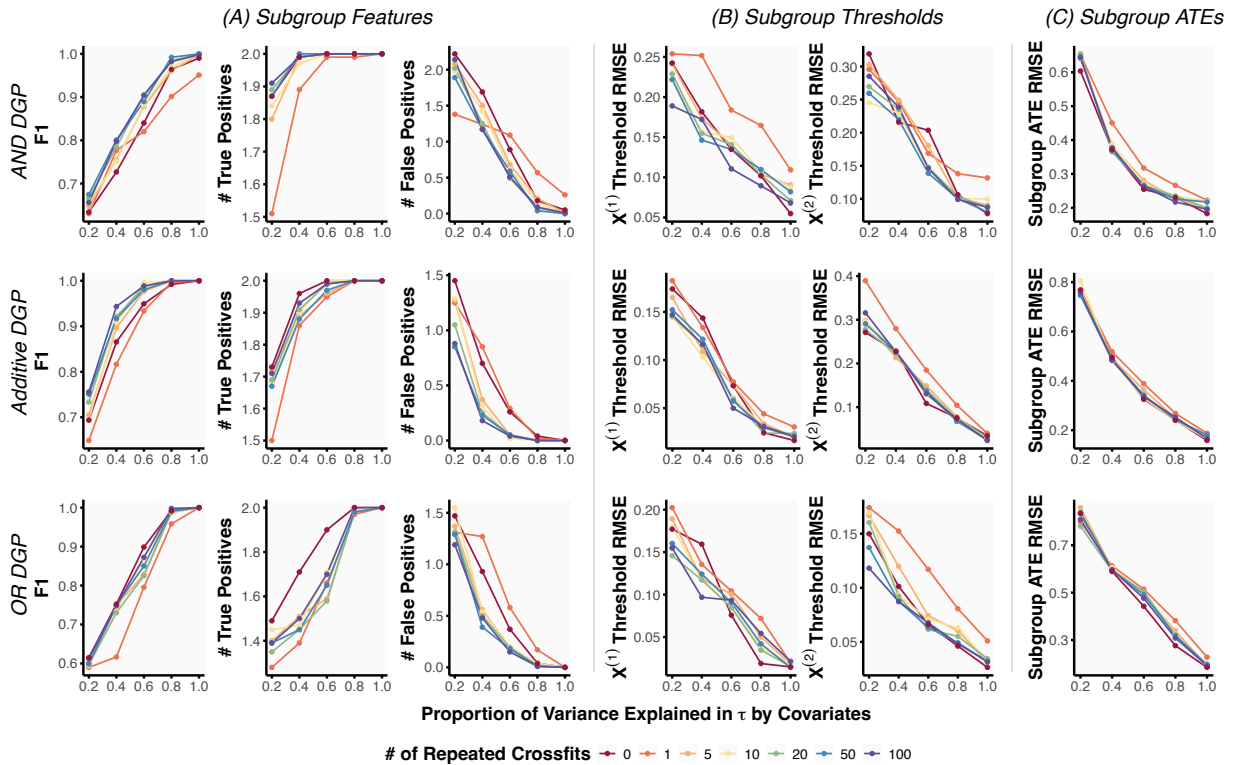


Figure A7: Performance of Distilled Rboost with varying number of repeated crossfits R (color) for (A) identifying the true subgroup features, measured via F_1 score, number of true positives, and number of false positives, (B) estimating the true subgroup thresholds, measured via root mean squared error (RMSE) for each true subgroup feature, and (C) estimating the true subgroup ATE, measured via RMSE, across increasing treatment effect heterogeneity strengths (x-axis) and different subgroup data-generating processes (rows). The subgroup estimation performance improves slightly as R increases and tends to be relatively stable for $R > 10$. Results are averaged across 100 simulation replicates.

1. Rulefit (rules only, max depth = 2): `type = "rules"` and `maxdepth = 2`
2. Rulefit (rules only, max depth = 3): `type = "rules"` and `maxdepth = 3`
3. Rulefit (linear + rules, max depth = 2): `type = "both"` and `maxdepth = 2`
4. Rulefit (linear + rules, max depth = 3): `type = "both"` and `maxdepth = 3` (i.e., the default settings in `pre::pre()`)

Although the rulefit student model sometimes results in more accurate estimation of the subgroup ATE, this is at the cost of a more complex model, illustrated by the substantially higher number of false positive features in rulefit compared to CART. CART thus appears to be a simpler and more interpretable student model choice for CDT.

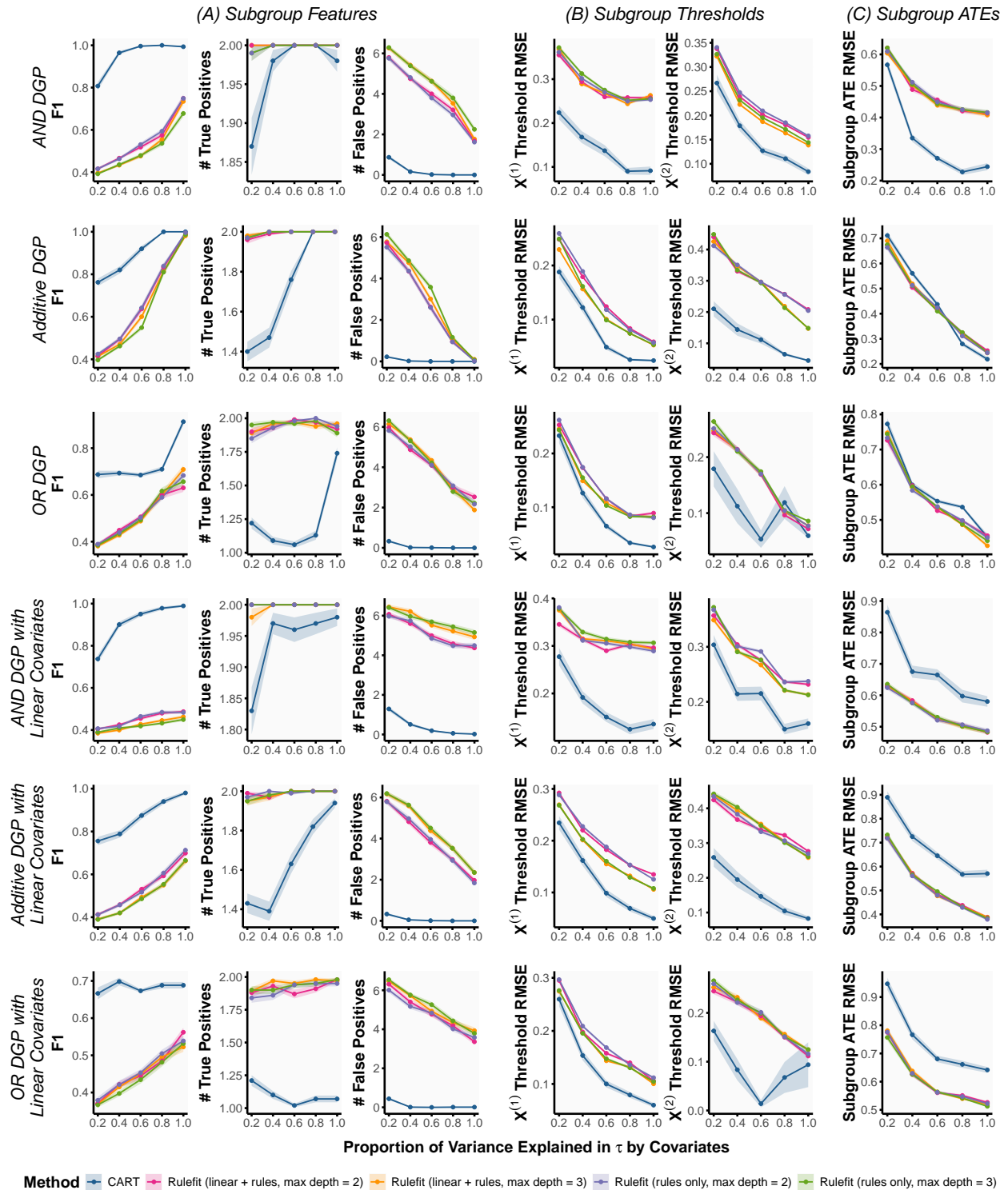


Figure A8: Performance of CDT with **CART** versus **Rulefit** student models for (A) identifying the true subgroup features, measured via F_1 score, number of true positives, and number of false positives, (B) estimating the true subgroup thresholds, measured via root mean squared error (RMSE) for each true subgroup feature, and (C) estimating the true subgroup ATE, measured via RMSE, across increasing treatment effect heterogeneity strengths (x-axis) and different subgroup data-generating processes (rows). The Rulefit student model tends to estimate unnecessarily complex subgroups, compared to CART. Results are averaged across 100 simulation replicates with ribbons denoting $\pm 1SE$.

E Additional Teacher Model Selection Simulation Results

In this section, we provide the Jaccard SSI simulation results (Figures A9-A14), used to select the teacher model, for each of the subgroup DGPs studied in Section 5 and Appendix D. As discussed in Section 5.3, higher Jaccard SSI generally corresponds to more accurate subgroup estimation regardless of the choice of subgroup DGP.

In practice, we reiterate that substantive researchers should leverage their domain knowledge when choosing the tree depth(s) d to consider in the teacher model selection procedure. In cases where such prior knowledge is limited, we recommend that researchers view the Jaccard SSI results alongside the feature stability distributions and other diagnostic tools (see Appendix A.7) to gain a more holistic perspective. This holistic view of the distilled method and its stability can often shed light on an appropriate choice of tree depth. For example, the feature stability distributions in Figures A9-A14 clearly illuminate that the trees grown to depths 3 and 4 are substantially more unstable than the depth-2 trees. That is, the distribution of features selected at depths 3 and 4 are far more heterogeneous than that at depth 2. As with the Jaccard SSI, a more stable or homogeneous feature distribution is generally a positive sign and may serve as heuristic to help choose the tree depth.

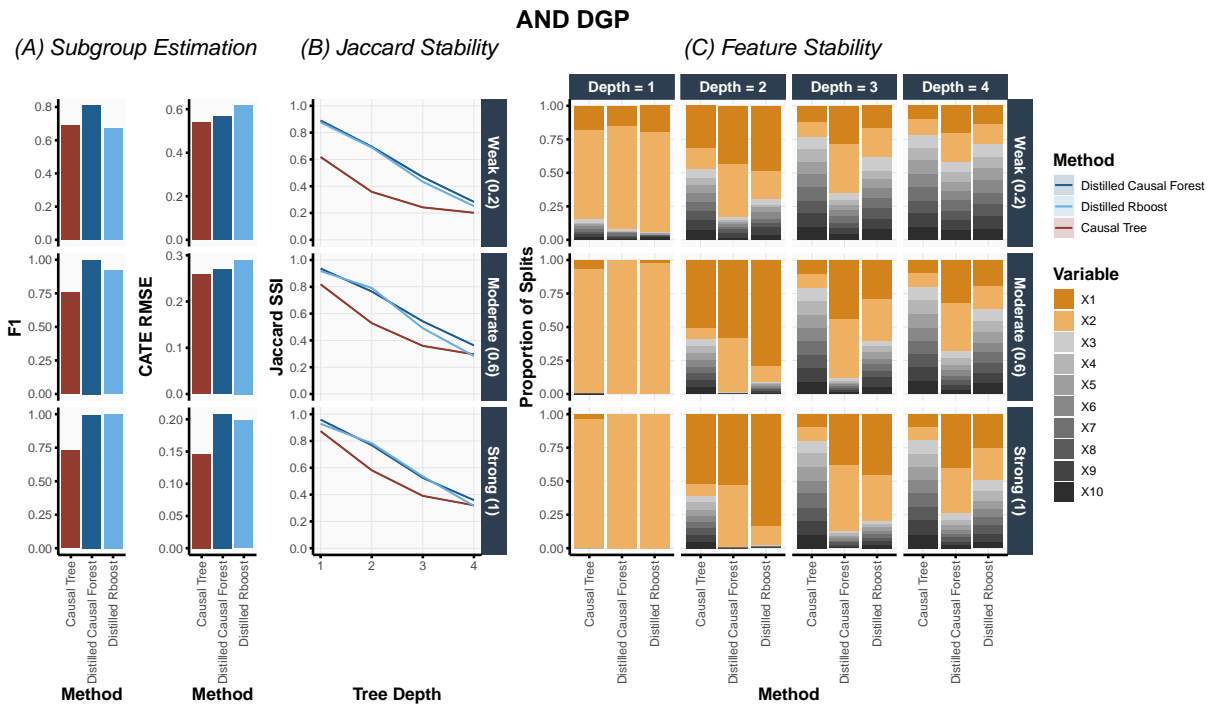


Figure A9: Under the ‘AND’ subgroup data-generating process (CATE-only), we examine (A) the subgroup estimation accuracy alongside (B) the Jaccard SSI for a range of tree depths and (C) the distribution of features selected at each tree depth across the 100 bootstraps. Results are shown for different subgroup estimation methods (colors) and treatment effect heterogeneity strengths (rows). Choosing the teacher model in CDT which leads to the highest Jaccard SSI generally corresponds to more accurate subgroup estimation. Moreover, the amount of heterogeneity in the distribution of selected subgroup features can help inform our degree of trust and guide selection for choosing the relevant tree depth(s).

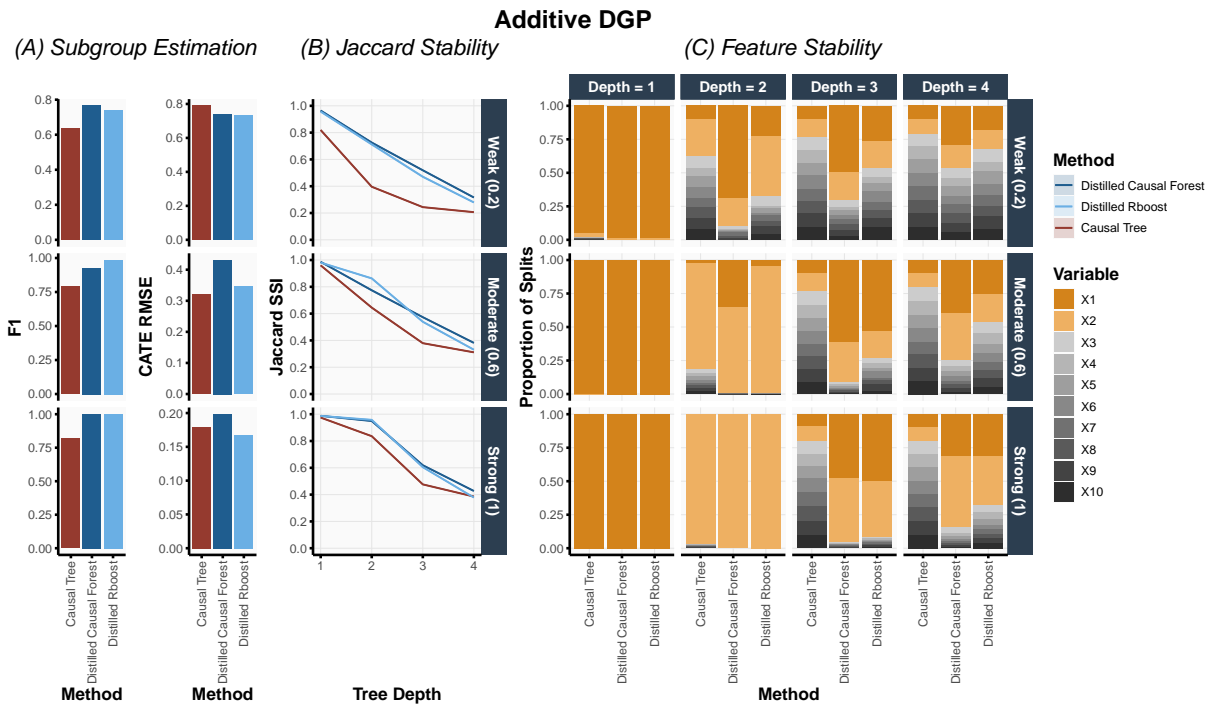


Figure A10: Under the ‘Additive’ subgroup data-generating process (CATE-only), we examine (A) the subgroup estimation accuracy alongside (B) the Jaccard SSI for a range of tree depths and (C) the distribution of features selected at each tree depth across the 100 bootstraps. Results are shown for different subgroup estimation methods (colors) and treatment effect heterogeneity strengths (rows). Choosing the teacher model in CDT which leads to the highest Jaccard SSI generally corresponds to more accurate subgroup estimation. Moreover, the amount of heterogeneity in the distribution of selected subgroup features can help inform our degree of trust and guide selection for choosing the relevant tree depth(s).

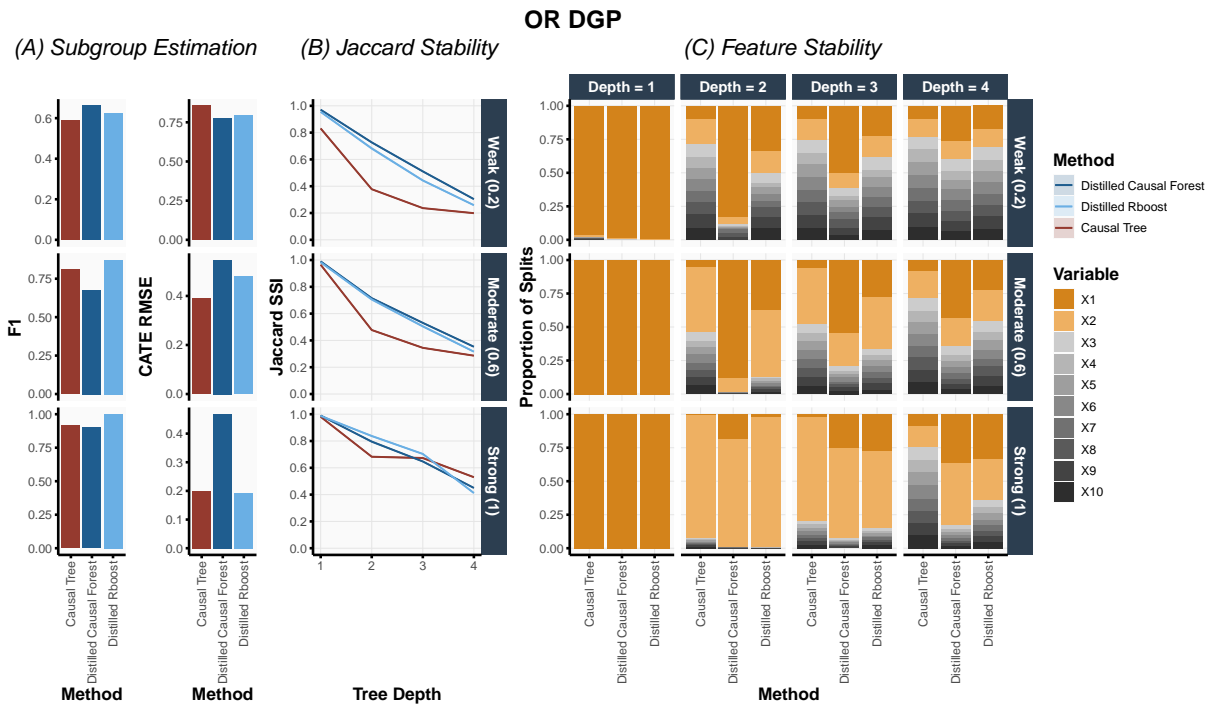


Figure A11: Under the ‘OR’ subgroup data-generating process (CATE-only), we examine (A) the subgroup estimation accuracy alongside (B) the Jaccard SSI for a range of tree depths and (C) the distribution of features selected at each tree depth across the 100 bootstraps. Results are shown for different subgroup estimation methods (colors) and treatment effect heterogeneity strengths (rows). Choosing the teacher model in CDT which leads to the highest Jaccard SSI generally corresponds to more accurate subgroup estimation. Moreover, the amount of heterogeneity in the distribution of selected subgroup features can help inform our degree of trust and guide selection for choosing the relevant tree depth(s).

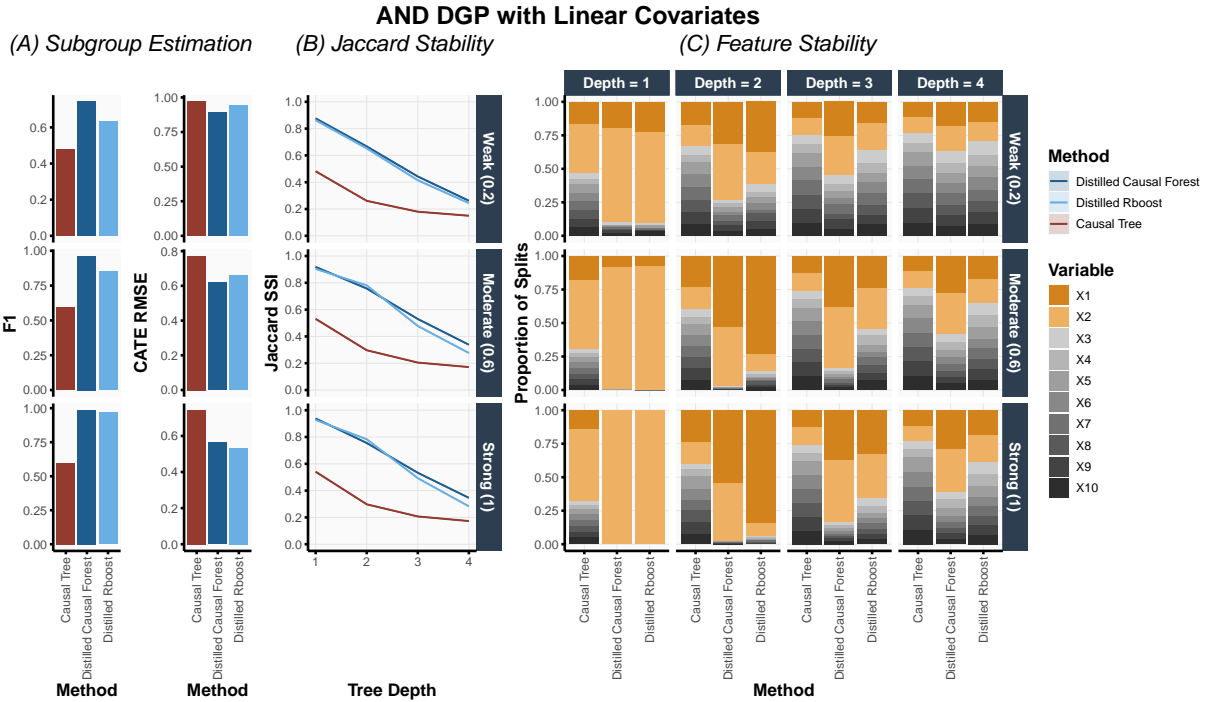


Figure A12: Under the ‘AND’ subgroup data-generating process with linear covariate effects, we examine (A) the subgroup estimation accuracy alongside (B) the Jaccard SSI for a range of tree depths and (C) the distribution of features selected at each tree depth across the 100 bootstraps. Results are shown for different subgroup estimation methods (colors) and treatment effect heterogeneity strengths (rows). Choosing the teacher model in CDT which leads to the highest Jaccard SSI generally corresponds to more accurate subgroup estimation. Moreover, the amount of heterogeneity in the distribution of selected subgroup features can help inform our degree of trust and guide selection for choosing the relevant tree depth(s).

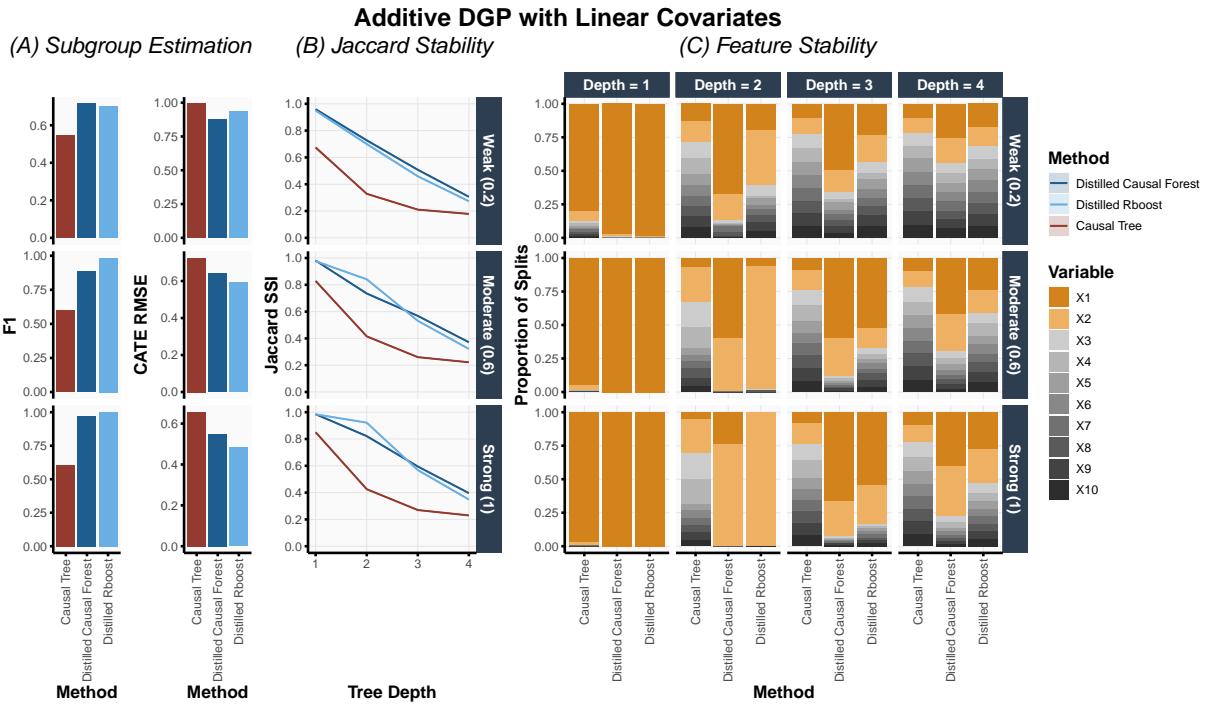


Figure A13: Under the ‘Additive’ subgroup data-generating process with linear covariate effects, we examine (A) the subgroup estimation accuracy alongside (B) the Jaccard SSI for a range of tree depths and (C) the distribution of features selected at each tree depth across the 100 bootstraps. Results are shown for different subgroup estimation methods (colors) and treatment effect heterogeneity strengths (rows). Choosing the teacher model in CDT which leads to the highest Jaccard SSI generally corresponds to more accurate subgroup estimation. Moreover, the amount of heterogeneity in the distribution of selected subgroup features can help inform our degree of trust and guide selection for choosing the relevant tree depth(s).

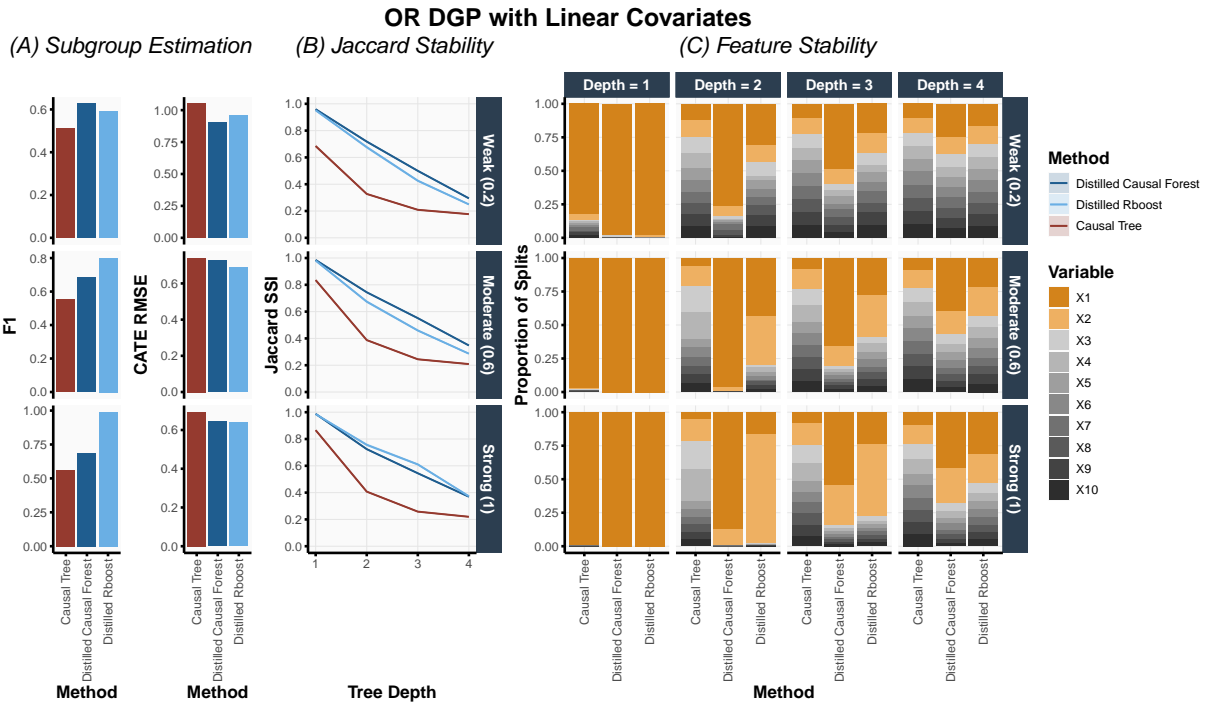


Figure A14: Under the ‘OR’ subgroup data-generating process with linear covariate effects, we examine (A) the subgroup estimation accuracy alongside (B) the Jaccard SSI for a range of tree depths and (C) the distribution of features selected at each tree depth across the 100 bootstraps. Results are shown for different subgroup estimation methods (colors) and treatment effect heterogeneity strengths (rows). Choosing the teacher model in CDT which leads to the highest Jaccard SSI generally corresponds to more accurate subgroup estimation. Moreover, the amount of heterogeneity in the distribution of selected subgroup features can help inform our degree of trust and guide selection for choosing the relevant tree depth(s).

F Extended Details of Case Study

While we presented the final subgroups and their estimated effects under Distilled Rboost in the main text, this is only after comparing our proposed Jaccard SSI on across two different teacher models. These were Causal Forest and Rboost. Figure A15 indicates that Distilled Rboost is consistently more stable across different tree depths.

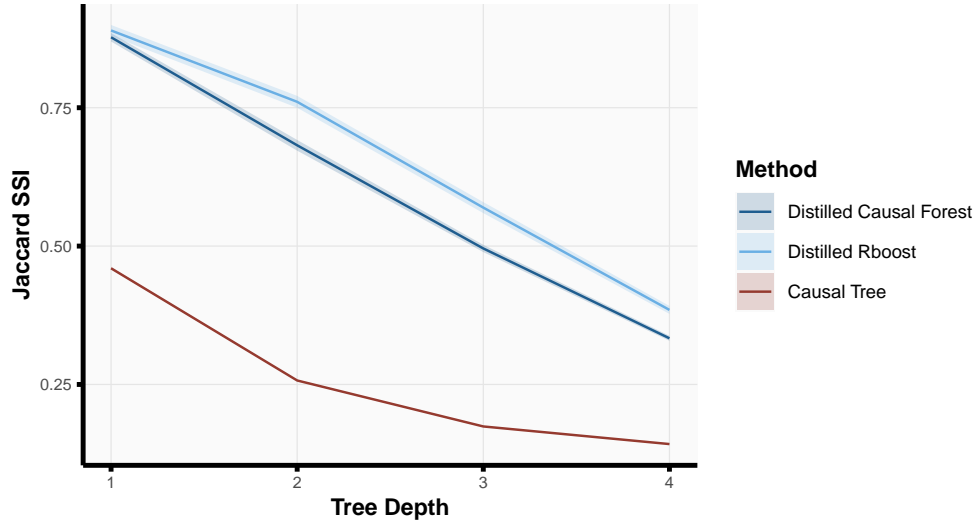


Figure A15: In our case study, we examine the the Jaccard SSI for a range of tree depths. Results are shown for different subgroup estimation methods (colors). Choosing the teacher model in CDT which leads to the highest Jaccard SSI generally corresponds to more accurate subgroup estimation.